

Methods for Quantitative Assessment of Dynamic Knee Joint Stability

by

Mark Sena

DISSERTATION

Submitted in partial satisfaction of the requirements for the degree of

DOCTOR OF PHILOSOPHY

in

Bioengineering

in the

GRADUATE DIVISION

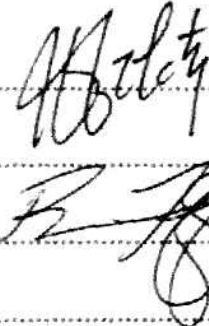
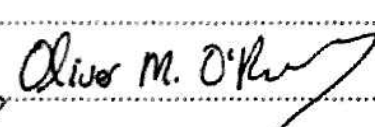
of the

UNIVERSITY OF CALIFORNIA, SAN FRANCISCO

AND

UNIVERSITY OF CALIFORNIA, BERKELEY

Approved:

Committee in Charge

Acknowledgments

First of all, I would like to acknowledge my advisors, Professor Jeffrey Lotz, Professor Oliver O'Reilly, and Dr. Brian Feeley, for giving me the opportunity to conduct research. I am extremely grateful that they also encouraged me to spin out my research into a company, which was probably the most valuable of my experiences during graduate school.

Jeff served as an incredible supervisor and mentor, helping me not only define the trajectory of my research at a high level, but also to troubleshoot problems with experiments. Despite the number and diversity of projects he manages, Jeff always seems to know the details and stumbling blocks of each one. Given any challenging situation, he always seems to have a relevant (and often comical) story that points out the silver lining. Jeff also treats his students more like families than employees, inviting us into his home for holiday parties, being flexible and supportive in times of need, and having genuine concern for our academic, professional, and emotional well-being.

Brian served as a fantastic clinical research advisor, helping me define and maintain the clinical relevance of my research. Brian was actually the first person I met associated with the Lotz lab. I initially met him at the Orthopaedic Institute to discuss what became my first project. Brian has a fantastic sense of humor, never failing to transform sentiments of dread, failure, and perfectionism into laughter. He also kept me motivated, applying just enough pressure to keep research projects moving forward.

Oliver served as a wonderful technical advisor and instructor, teaching me the mathematics needed to properly represent knee joint kinematics and kinetics. Oliver displays an incredible amount of dedication to, and patience for, his students. By the way he interacts with students, and the amount of time and effort he spends helping them with research and coursework, it is clear that Oliver prioritizes mentorship and teaching above all else. Oliver's

deep knowledge of rigid body dynamics is inspirational, as he can describe anything from a mechanical toy to a biomechanical joint with elegant equations. Oliver's attention to detail and consistency, especially when it comes to mathematics, is also worth noting.

I would also like to thank my many research collaborators who helped me collect the data presented in this dissertation.

Dr. Feeley's research fellows, including Dr. James Chen and Dr. Ryan Dellamaggiora, were critical in conducting knee studies using the mechanical pivot shift device. Both James and Ryan taught me a great deal of anatomy, how to wield a scalpel (and a bone saw), and essentially how to perform an ACL reconstruction on a cadaver knee.

Dr. Anthony Luke, Cynthia Conti, and Deepak Kumar of the UCSF Human Performance Laboratory helped me collect and analyze the Vicon data I needed to validate the Kinect as a marker-based motion capture tool.

Professor Richard Souza and Dr. Drew Landsdown of the Musculoskeletal Quantitative Imaging research group enabled me to collect MRI data (on my own knees, actually) for a pilot study on the use of a functional coordinate system to represent knee kinematics and kinetics.

Professor Ruzena Bajcsy's introductory robotics course was probably the most important one that I took at UC Berkeley, as it taught me the matrix math needed to analyze knee kinematics data. Ruzena also conducts research on upper extremity movement analysis using the Kinect. Although she was not a direct collaborator in my research, she and Professor Lotz may collaborate in the near future.

Next I would like to thank the members of the Lotz lab, who were always available and willing to lend a hand or an ear, helped break up the day with friendly conversation, and made the lab and (quite dingy) office feel like home.

Dezba Coughlin was responsible for getting me started on the right foot in the Lotz lab. She introduced me to the Optotrack equipment and helped me perform my first surgical knee experiments.

Julia Nichols was a fantastic comrade to have on the Kinect project. Due to the multidisciplinary nature of the project and the large number of stakeholders, working on this project was particularly challenging. It was great to have Julia in my corner.

Cory Laws was my fellow graduate student for the majority of the time in the Lotz lab. He welcomed me to the lab when I was a rotation student, and we shared many beers together while talking about biomechanics and entrepreneurship. Watching Cory graduate ahead of me was motivating and encouraging, giving me hope that I too could cross the finish line.

Jeannie, another Lotz lab veteran, never failed to provide an interesting (often evolutionary) perspective on biomechanics. Going out to lunch or grabbing coffee around Parnassus with her and Cory was always refreshing.

Aaron Fields, an experienced and knowledgeable postdoc in the lab, was a great sounding board. Thoughtful and meticulous, he always provided great feedback on figures and pieces of writing.

I would also like to thank my network of friends, colleagues, and professors in the joint Bioengineering program at UCSF and UC Berkeley. Whether at research seminars, on public transit between UCSF and Berkeley, or at the annual Bioengineering retreat, the sense of comradeship I developed with these individuals was priceless. Even after my fellow students and settled into our own labs, seeing each other less frequently, the occasional meeting over lunch or coffee was comforting, helping me remember that we are not alone in facing our personal challenges as graduate students.

A very special “thank you” goes to my great friends, Bertram and Lina. These two incredible human beings have been with me every step of the way throughout the program.

As talented scientists, they've provided advice and guidance on how to survive within academia. As mountain adventurers, Bertram and Lina introduced me to backcountry skiing, which has brought me a wealth of joy and adrenaline. As experienced world travelers knowledgeable in geopolitics, they've encouraged me to step out of my narrow world view and consider the impact that my own research (and science in general) could and should have on humanity.

Finally, and most importantly, I would like to thank my family for the love and emotional support they provided throughout my years as a graduate student.

My mom spent countless hours on the phone with me, sometimes listening to me talk about a recent achievement, brimming with excitement, but more often to me complaining about the challenges I was facing in my research and personal life. Regardless, she was always willing to listen and able to provide pertinent advice.

My dad has always been a role model for me. He is an incredibly hard worker, dedicated not only to 'doing things right' but also 'doing the right thing'. My dad is also a very generous person, always willing to donate his precious time and energy to help those in need.

My sister, an incredibly talented medical illustrator and tattooer has always been a source of love and admiration. Thinking about her always helps me appreciate how diverse the biomedical community is, and the many ways in which an individual can contribute to biomedical science or help improve the lives of recovering patients.

Last, I'd like to acknowledge my large extended family. All 60+ of my aunts, uncles, cousins, and now cousins' children have helped (and continue to help) me keep things in perspective. Family always comes first.

Abstract

Methods for Quantitative Assessment of Dynamic Knee Joint Stability

by

Mark Sena

The ability to quantitatively assess dynamic knee joint stability is a major need among biomechanics researchers, orthopaedic surgeons, and physical therapists. For example, following a tear of the anterior cruciate ligament (ACL), surgeons will often perform a manual examination called the pivot-shift test to evaluate the mechanical stability of the knee. Unfortunately the test qualitative, subjective, and difficult to reproduce. Biomechanics researchers have been developing ways to reproduce the pivot-shift in a laboratory setting. However, current approaches involve the application of mechanical loads that are either static or poorly defined. In addition to manual examinations, observational movement analysis is often used by physical therapists to assess the functional stability of the knee during tasks such as a single leg squat. However, the qualitative and subjective nature of observation makes it difficult to reliably document and monitor patient progress. Researchers can use multi-camera motion capture systems to extract quantitative information from functional tests in a laboratory setting. However, these systems are prohibitively expensive and cumbersome for routine use in the clinic.

In this dissertation we present novel techniques for quantitatively assessing dynamic knee joint stability in laboratory and clinical settings. First, we provide the mathematical foundation for describing knee joint motion (kinematics) and forces and moments (kinetics). This work extends the concept of a non-orthogonal joint coordinate system to include what's known as the dual Euler basis, which as we show, is particularly useful for representing

constraint moments acting at the knee. Next, we present a novel mechanical device for mimicking the pivot-shift test in a laboratory setting. Our device improves upon previous loading devices because it applies knee loads that are dynamic, well-defined, and reproducible to within a 10% tolerance. Using this device, we then compare the ability of several pediatric ACL reconstruction techniques to restore stability to the knee in a cadaveric model. Finally, we present a novel marker-based motion capture technique that leverages low-cost consumer 3D cameras like the Microsoft Kinect. We show that, using this technique, the position of markers placed on the body can be measured with 1-2 cm accuracy and precision. Hopefully the work presented in this dissertation will benefit biomechanics researchers, surgeons, and physical therapists who face the increasingly important problem of quantifying knee joint function and stability.

Dedication

I dedicate this dissertation to my loving mother, who provided moral and emotional support throughout my years as a graduate student.

Contents

Acknowledgments	iii
Abstract	vii
Dedication	ix
List of Figures	xiii
List of Tables	xv
1 Introduction	1
2 Clinical Background: Knee Joint Stability	6
2.1 Anatomy of the Knee	6
2.2 Knee Joint Stability	12
2.3 Anterior Cruciate Ligament Injury	21
3 Theoretical Background: Knee Joint Kinematics and Kinetics	25
3.1 Motivation	26
3.2 Coordinate Systems and Kinematics	28
3.3 Representing Forces and Moments	35

4 A Mechanical Pivot-Shift Device for Dynamically Loading Cadaveric Knees	44
4.1 Chapter Overview	44
4.2 Introduction	45
4.3 Methods	46
4.4 Results	53
4.5 Discussion	60
5 Evaluation of Physeal-Sparing Pediatric ACL Reconstruction Techniques	66
5.1 Chapter Overview	66
5.2 Introduction	67
5.3 Methods	69
5.4 Results	76
5.5 Discussion	79
6 3D Marker-based Motion Capture Using Inexpensive Depth Cameras	86
6.1 Chapter Overview	86
6.2 Introduction	87
6.3 Marker-based Motion Capture using the Microsoft Kinect	89
6.4 Markerless vs. Marker-based Kinect Motion Capture	93
6.5 Conclusion	100
7 Conclusion and Future Outlook	101
A Clinical Background: Supplemental Figures	107
B Theoretical Background: Supplemental Material	109
C Mechanical Pivot Shift Device: Supplemental Figures	114

D Marker-based Kinect Motion Capture: Supplemental Figures

117

Bibliography

121

List of Figures

2.1 Anatomy of the human knee joint	7
2.2 The stabilizing subsystems of the knee	14
2.3 Clinical knee-stability evaluations	19
3.1 Comparison of vector components using the Euler and dual-Euler bases	31
3.2 Bases associated with the knee joint	33
3.3 Three representative examples of moments	37
3.4 Joint contact forces and their moment at the knee	39
4.1 Working principle of the Mechanical Pivot-Shift Device	47
4.2 Dynamic forces and moments applied by the MPSD	54
4.3 Kinematic profiles and peak values	55
4.4 Test-method and inter-examiner agreement	59
5.1 Mechanical pivot-shift device and measurement coordinate system	72
5.2 Physeal-sparing reconstructions	75
5.3 Kinematic tracings for a knee	77
5.4 Mean kinematic peaks across 6 knees	79
6.1 Comparison of Kinect and Optotrack marker positions	90

6.2	Kinect marker position error	91
6.3	Comparison of markerless and marker-based measurement agreement with Vicon	95
6.4	Correlation between joint angles measured by Kinect and Vicon	96
6.5	Correlation between joint positions measured by Kinect and Vicon	97
A.1	Conceptual schematic for functional knee stability	107
A.2	Conceptual schematic for mechanical knee stability	108
B.1	Graphical representation of the dual-Euler and Euler basis vectors	111
C.1	Comparison of other pivot-shift devices	115
C.2	Proposed clinical version of the MPSD	116
D.1	Proposed clinical setup for Kinect motion capture	117
D.2	Flowchart for Kinect-based motion capture	118
D.3	Proposed method for static rigid body calibration	119
D.4	Proposed method for twist-based rigid body tracking	120

List of Tables

4.1 Effect of ACL transection on kinematic peaks measured by one examiner using MPSD and manual tests.	57
6.1 Kinect marker position error	91

Chapter 1

Introduction

The ability to quantitatively assess the dynamic function of the knee joint is a common need among biomechanics researchers, orthopaedic surgeons, and physical therapists. For example, when asking scientific questions about the effect of soft tissue damage on knee joint motion, biomechanics researchers require experimental setups that measure the joint's mechanical response to applied loads. Similarly, orthopaedic surgeons engaged in research may seek to compare different surgical techniques (e.g., anterior cruciate ligament reconstruction) in their ability to restore normal motion to the knee. In a clinical setting, surgeons routinely assess a patient's joint function after an injury and determine whether he or she is ready to return to normal activity. Physical therapists, while working with a patient recovering from a knee injury, need to assess knee function and monitor improvements over the course of therapy. Therapists may also seek to identify movement patterns associated with increased risk for knee injury, and prescribe preventative exercises.

Whether conducting experiments or working with patients, biomechanics researchers, surgeons, and therapists often face the same fundamental problem: that qualitative evaluation of dynamic knee joint stability is subjective and unreliable. In complex knee-loading

experiments that test joint stability, a major challenge for researchers is being able to apply forces and moments that are both reflective of physiological loads and also quantifiable and reproducible. When working with patients, a major challenge for surgeons and therapists is converting their observations of knee stability and function into clinical documentation that measures the patient's true functional status and progress towards recovery. To objectively and reliably assess dynamic knee joint stability in both a laboratory and clinical setting, quantitative experimental and analytical techniques are needed.

In this dissertation we present novel experimental and analytical techniques for quantitative assessment of dynamic knee joint stability. Specifically, we address the problems of 1) assessing knee stability in a laboratory setting under loading conditions that are both well-defined and dynamic, and 2) quantifying knee movement in a clinical setting using marker-based motion capture techniques and low-cost 3D cameras. Although the techniques presented may be applied to other biomechanical joints, we focus on the knee due to its high relevance across biomechanics, orthopedic surgery, and physical therapy; its biomechanical complexity; as well as the author's personal interest in the knee, having suffered from a traumatic knee injury in the past.

The knee is a complex and biomechanically interesting joint that is prone to injury due to the large loads it withstands. These loads are large due to the weight-bearing nature of the joint during ambulation and the long length of the femur and tibia bones, acting as lever arms. Functionally, while bearing body weight, the knee allows for a large range of rotational motion primarily in one direction (flexion and extension) while remaining stable against rotation and translation in the other directions. Stability is imparted by a combination of the joint's bony articular geometry, ligamentous restraints, and surrounding musculature. Injury to, or abnormal anatomy of, these structures may result in aberrant motions of the

knee joint in response to external loads. In a simplified sense, these motions and loads are what we wish to measure in order to quantify knee joint stability.

In the chapters that follow, we first provide the context necessary for understanding knee joint stability from a clinical and mechanical perspective. Then we tackle the problems of quantifying aspects of knee joint stability in laboratory and clinical settings.

Chapter 2 presents clinical background material relevant to knee joint stability. First we give a basic overview of the anatomy of the knee, describing the structure and function of the bones, ligaments, cartilage, and musculature. Then we introduce the concept of knee joint stability, defining it from a mechanics perspective, and discussing how clinicians evaluate it in practice. Last we discuss injury of the anterior cruciate ligament, surgical and nonsurgical treatment options, and clinical outcomes. The reader should take away a qualitative understanding of the stabilizing function of the individual anatomical structures of the knee, along with a conceptual framework for how these structures work synergistically in response to external loads.

Chapter 3 provides the mathematical background needed to quantitatively describe the motion of the knee joint (kinematics) and forces and moments it supports (kinetics). First we discuss the need for the specific mathematical formalisms we choose to employ when representing the kinematics and kinetics. Next we describe knee joint motion in terms of rotations and translations of the tibia relative to the femur, and introduce sets of basis vectors known as the Euler and dual Euler bases. Last we compare different representations of forces and moments in the knee, and argue that a representation featuring what is known as the dual Euler basis is ideal for describing the constraint moments acting within the knee. Although the reader need not master the mathematics presented in this chapter, he or she should understand the importance of using non-orthogonal basis vectors for representing knee joint kinematics and kinetics.

Chapters 4 and 5 present the development and application of a novel mechanical device for mimicking a clinical knee examination called the pivot shift test in a laboratory setting. The device is named the “mechanical pivot-shift device” (MPSD). First we describe the design of the device, how it works, and how it was validated by comparing it to the manual pivot-shift test. Unlike previous knee-loading devices that attempt to mimic the pivot-shift, the MPSD applies loads that are both dynamic and well-defined, using a simple apparatus accessible to other researchers. Then we use the device to compare the effectiveness of three different surgical techniques for reconstructing the ACL in children. Previous comparisons of these techniques performed in our laboratory were based on static rather than dynamic tests. The readers should understand the prior difficulty in evaluating dynamic knee stability using the pivot-shift test and appreciate the consistency with which dynamic knee loads can be reproduced using the MPSD.

Chapter 6 presents a novel marker-based motion capture technique that leverages low-cost consumer 3D cameras like the Microsoft Kinect. This technique enables one to measure the time-varying 3D position of individual retroreflective markers placed on the body using a single camera. Based on these marker positions a model of the body can be constructed. First we establish proof of concept for the technique and conduct a study to determine the accuracy and precision of measured marker positions. Then we compare the technique to a commercial markerless motion capture method that uses the same raw sensor data but employs a statistical approach (as opposed to direct marker-based measurements) to construct an anatomical ‘skeleton’ model of the body. The reader should realize that the new method presented represents an ideal intermediate between the expensive multi-camera motion capture systems used for research and the relatively inaccurate marker-less motion capture algorithms used for gesture-based video game control and computer interaction.

We conclude this dissertation in Chapter 7. First we discuss the need to quantify joint stability in a broader context and speculate as to how this need might evolve in the future. Then we summarize some of the critical findings and achievements from this work and how they are important within the broader context. We also propose new directions for future research, including additional studies that could be conducted as well as potential ways to improve the experimental and analytical methodologies, as presented.

Chapter 2

Clinical Background: Knee Joint Stability

2.1 Anatomy of the Knee

The knee is the largest and one of the most complex biomechanical joints in the human body. Structurally, the joint connects the thigh and the (lower) leg and comprises four bones, four primary ligaments, hyaline and fibrous cartilage, and over a dozen muscles. Functionally, the knee permits a broad range of motion during locomotion under extreme loads often greater than body weight.

To provide stability to the joint under dynamic motion, the anatomical structures of the knee support a variety of loads. The bones support the joint by bearing compressive loads. The elastic ligaments restrain excessive joint motion by withstanding tension. The articular and fibrous cartilage enable smooth joint motion and protect the bones by reducing frictional forces and distributing contact stresses. Finally, the muscles actuate the joint by producing contractile forces.

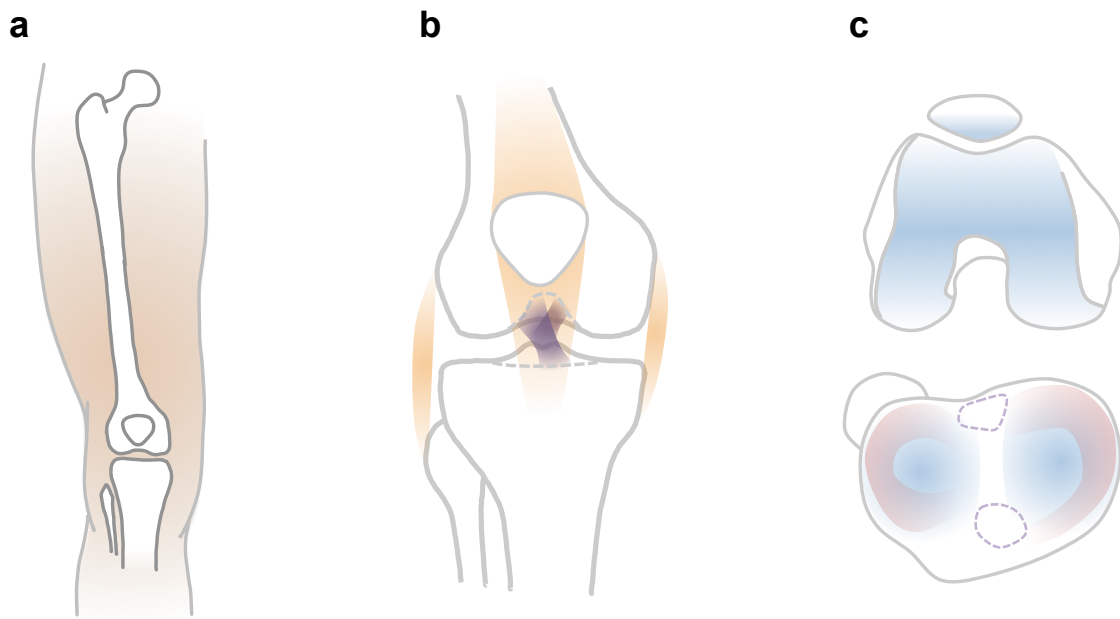


Figure 2.1: Anatomy of the human knee joint. **a)** From proximal (top) to distal (bottom), the femur bone of the thigh, the patella, and the tibia and fibula bones of the leg. **b)** The patellar tendon, medial and lateral collateral ligaments are extracapsular (orange). The anterior and posterior cruciate ligaments are intracapsular (purple). **c)** Hyaline cartilage (blue) covers the articular surfaces of the patella, femur, and tibia. The crescent-shaped menisci are composed of fibrocartilage (pink). The footprints of the anterior and posterior cruciate ligaments are indicated by a dashed purple line. The anterior direction is up for the femur and down for the tibia.

Bones

The bones of the knee include the femur, tibia, fibula, and patella (Fig. 2.1a). The femur and tibia bones support the body's weight, the patella facilitates knee extension, and the fibula helps stabilize the ankle. Interconnecting the hip and knee joints, the femur is the longest bone in the human body, and by some measures is the strongest as well. Proximally, the spherical femoral head articulates with the pelvis at the hip. Distally, the circular medial and lateral femoral condyles articulate with the tibia and patella at the knee.

The tibia and fibula interconnect the knee and ankle joints. The tibia transmits the majority of compressive loads from the ankle to the knee. Proximally the tibial plateau articulates with the femur. The medial plateau is concave while the lateral plateau is flat or slightly convex. Distally, the tibia articulates with the talus at the ankle. The fibula is slender and bears very little compressive load. It forms a semi-movable articulation with the tibia proximally and distally, and articulates with the talus, distally.

As the largest sesamoid bone in the body, the patella is tear-dropped in shape and rests in the trochlear groove of the femur. It is attached proximally to the quadriceps femoris muscle by the quadriceps tendon. Distally it is attached to the tibial tuberosity by the patellar ligament (also referred to as the "patellar tendon" due to its apparent continuity with the quadriceps tendon). The posterior surface is covered in smooth hyaline cartilage and articulates with the femur. The patella functions as a pulley and as a lever to aid knee extension, redirecting the contractile force generated by the quadriceps and providing a moment arm for that force.

Ligaments

The primary ligaments of the knee (not including the aforementioned patellar ligament) are the anterior and posterior cruciate ligaments and the medial and lateral collateral ligaments (Fig. 2.1b). These soft tissue structures passively stabilize the tibiofemoral joint so that a normal position of articular contact is maintained throughout the joint's range of motion. Exhibiting a nonlinear stress-strain profile, these ligaments allow free motion of the joint up to the point at which they begin to generate large restraining forces.

Within the joint capsule, the anterior and posterior cruciate ligaments attach between the intercondylar notch of the femur and the intercondylar area of the tibia. The anterior cruciate ligament (ACL) originates from the medial aspect of the lateral femoral condyle (within the notch) and inserts anteriorly onto the tibial plateau. Owing to its anteromedial orientation, the ACL is the primary restraint to anterior tibial translation (see 2.1). The fibers of the ACL are grouped into two bundles, which are often distinct but conjoined. The anteromedial bundle is oriented more horizontally and is taught in knee flexion. The posterolateral bundle is oriented more vertically and is taught in knee extension. The posterior cruciate ligament (PCL) originates from the lateral aspect of the medial femoral condyle and inserts posteriorly on the tibial plateau. Oriented posterolaterally, the PCL is the primary restraint to posterior tibial translation.

Outside the joint capsule, the medial collateral ligament (MCL) attaches between the medial condyles of the femur and tibia while the lateral collateral ligament (LCL) attaches between the lateral femoral condyle and the fibular head. The MCL is the primary restraint to valgus rotation while the LCL is the primary restraint to varus rotation.

In addition to the major ligaments mentioned above, other ligamentous soft tissue structures help stabilize the knee. The joint capsule itself contains layers of fibers oriented

in different directions to support loads. Some of these fiber bundles are more prominent than others such as the oblique popliteal ligament and the recently described anterolateral ligament. Although the origins and insertions of these structures are more difficult to define due to their contiguity with the capsule or with tendons, they serve an important role in stabilizing the knee, for example, against hyperextension.

Cartilage and Muscle

The knee contains articular and meniscal cartilage, which transmit and distribute the compressive loads in the joint (Fig. 2.1c). The articular surfaces of the tibia, femur, and patella are covered in a 2-4 mm thick layer of “articular” hyaline cartilage. Articular cartilage is avascular, composed mostly of type II collagen, and lubricates the joint under load. It forms a smooth bearing surface for the tibiofemoral and patellofemoral articulations.

In between the tibia and femur lie the “menisci”, two crescent-shaped pads of fibrocartilage that cushion the joint. Meniscal cartilage is vascularized at its periphery, is composed of both type I and type II collagen, and deforms somewhat elastically under load. It distributes contact stresses between the tibia and femur and also translates slightly to maintain congruous joint contact.

Over a dozen muscles cross the knee, both actuating and stabilizing the joint. Some of these also cross the hip or ankle, making them biarticular. These muscles insert into the bones of the (lower) leg including the tibia, femur, and calcaneous and can be classified broadly as either extensors or flexors of the joint. Simultaneous co-contraction of extensors and flexors generates compressive loads that stabilize the joint.

Knee Joint Motion

The knee joint consists of two articulations, or interfaces between bones, that have a geometry which facilitates movement. The tibiofemoral articulation allows rotation of the tibia relative to the femur (primarily in one degree of freedom) and also a small amount of translation. The patellofemoral articulation permits translation of the patella along the trochlear groove of the femur (by about 7 cm proximally in extension). A third articulation exists between the tibia and the fibula, however it permits only slight movement between the bones that does not contribute to the knee's primary function.

Of primary interest for the remainder of this thesis is the tibiofemoral articulation. Clinically, motion of the tibiofemoral joint is described in terms of the anatomical planes. The knee rotates primarily in flexion and extension, which is motion in the sagittal plane. Additionally, the knee rotates internally and externally by about 5-15° in the transverse plane. This axial rotation typically occurs about an axis passing through the concave medial tibial plateau. Rotation of the tibia with respect to the femur in the frontal plane is referred to as adduction and abduction or varus and valgus rotation. The terms varus and valgus also refers to the static alignment of the joint, which can vary according to gender and with bone deformity. As discussed in the following chapter, true abduction and adduction of the knee does not occur without liftoff of the femoral condyles.

Relative to the flexion-extension axis of the knee, the tibia normally translates very little. Motion of the knee was once described as a combination of a roll-back and anterior gliding of the femur on the tibia in the sagittal plane. However, more recent studies of knee kinematics have shown that the true three-dimensional motion can be described as nearly pure flexion about an axis fixed in the femur, passing between the epicondyles. Under an anterior or posterior shear, a healthy knee does indeed translate by as much as 1 cm. Some medial

lateral translation can occur as well, but is prevented by contact of the tibial tubercles (of the intercondylar eminence) with the femoral condyles within the intercondylar notch.

2.2 Knee Joint Stability

The term “joint stability” has many different definitions and interpretations within orthopaedic biomechanics and its sub-specialties, and the term’s correct usage is sometimes a matter of debate. However, in a mechanical sense “stability” can be defined more precisely and it is from a mechanics perspective that we seek to describe the behavior of the knee joint below and in the following chapter. One definition of joint stability put forth in an introductory biomechanics textbook is [Bartel *et al.*, 2006]:

the ability of a joint to maintain an appropriate functional position throughout its range of motion... A stable joint can move through a normal range of motion while carrying functional [or clinical] loads while producing contact forces of normal intensity between articular surfaces.

A defining characteristic of mechanical stability of a joint is that the joint must be able to maintain a configuration capable of supporting the applied load in question. Further, in order for the joint to function as intended (i.e. to move throughout a specified range of motion), it must be able to change configuration under load, without undergoing internal stresses that might damage the joint. Some specific criteria for a stable joint proposed by Bartel et al. [Bartel *et al.*, 2006] are that:

1. joint contact occurs between articular surfaces
2. peripheral loading (near the edge of the articular surface) does not occur

3. there exists a unique position of equilibrium for any loading
4. *small changes in either the magnitude or direction of the functional load do not lead to large changes in the position of joint contact*

A slightly revised definition of mechanical joint stability focusing on the fourth criterion is

the ability to support loads throughout a functional range of motion without large or sudden changes in the position of joint contact.

This proposed definition will be revisited in the following chapter, where we will consider joint loads and motions within a mathematical framework.

The Stabilizing System of the Knee

In discussing the concept of knee joint stability, it is instructive to consider the types of forces generated in the bones, ligaments, cartilage, and muscle of the knee, and how those forces act together in response to an external load. As emphasized early on by Noyes et al. [Noyes *et al.*, 1980], understanding the forces that each of these anatomical structures resist rather than the type of motion they prevent can provide insight as to their stabilizing function. In fact, it is useful to analyze the types of motions that these structures *allow* within a normal range of dynamic function; and how outside the normal range, the magnitude and suddenness of these motions can manifest as a kinematic instability of the knee.

In a framework similar to that described by Panjabi for the spine [Panjabi, 1992], the “stabilizing system” of the knee can be thought of as a collection of three cooperative “subsystems” which are either active or passive in nature. The muscles of the knee and their neural controllers are active, being responsible for actuating the joint. Unlike Panjabi,

we group these two components together as the “neuromuscular subsystem”, since in reality they are co-dependent. The connective tissues and articular geometry of the knee are passive, as they generate force only in response to an external or muscular load. Unlike Panjabi, we consider these to be separate subsystems since ligaments (“connective subsystem”) and bone (“articular subsystem”) stabilize the joint through drastically different mechanisms. The stabilizing subsystems of the knee act synergistically to provide a joint reaction force and moment that opposes external and inertial loads. The classification of the neuromuscular, connective tissue, and articular geometry subsystems is based on the types of forces they produce.

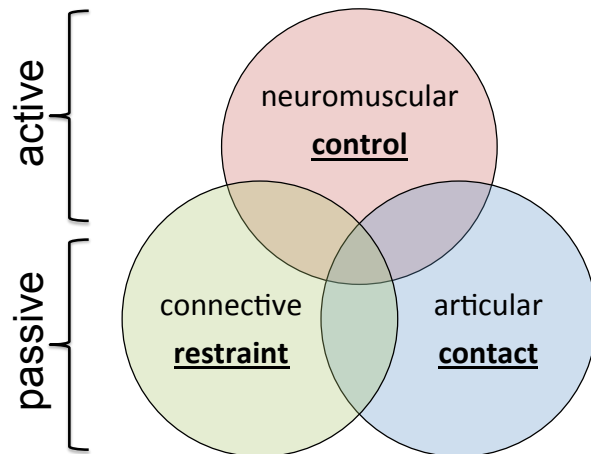


Figure 2.2: The stabilizing subsystems of the knee. The neuromuscular system actively generates *control* forces that actuate the knee joint. Compliant tissues passively generate *restraint* forces that limit joint motion. The articular geometry passively produces *contact* forces normal to the joint surfaces. These subsystems act synergistically to stabilize the knee joint through a functional range of motion.

The neuromuscular subsystem imposes *control* forces that actively change the knee's configuration and the position of joint contact. These tensile forces act at the point of attachment of the muscle tendon with the bone. The magnitude of these forces is dependent on the intensity of muscle contraction. In response to a perturbation of the joint, autonomic

or voluntary muscle contraction stabilizes the joint. For example, a rapid flexing of the knee will stretch the muscle spindles in the quadriceps, triggering the “knee jerk” reflex and resulting in contraction of the quadriceps. Alternatively, voluntary co-contraction of agonist and antagonist muscles (e.g. quadriceps and hamstrings) increases the magnitude of articular contact forces without necessarily altering the position of joint contact. In the case of a bicondylar joint, this increase enables the joint to resist an external moment that would otherwise result in condyle liftoff.

The connective subsystem passively generates *restraint* forces that limit the range of joint contact. These tensile forces act along the direction of the collagen fibers of the tissue, anchored between attachments. Due to the nonlinear loading characteristics of connective tissues, the magnitude of these forces remains low until the fibers become taught, and then increases as the fibers stretch elastically. A discrete ligament like the ACL is the best example of a connective tissue restraint. However, the joint capsule and even the meniscus, to some degree, can be thought of as functioning in this way.

The articular subsystem passively produces *contact* forces that rigidly support the joint by opposing both external loads and the internal tensile forces generated by muscles and connective tissue. These compressive forces act in a direction that is normal to the articulating surface at the point of joint contact possible. The magnitude of these forces is large and increases with external loading and muscle contraction. In response to a perturbation, the position of joint contact may shift slightly. Due to the curvature of the articular surface, the direction of the (normal) joint contact force also shifts, usually in a direction that opposes an external force (although if the articular geometry of the joint is suboptimal, this may not be the case, as discussed later). In the case of a bicondylar joint like the knee, which maintains two positions of joint contact, the distribution of compressive forces between the two condyles can also vary to oppose an external moment.

For the spine, Panjabi hypothesized that dysfunction of any one of the stabilizing subsystems can lead to a short-term compensatory response, a long-term adaptive response, or an injury [Panjabi, 1992]. Similarly, we can envision what happens to the knee when one or more of its stabilizing subsystems fails to function normally. Neuromuscular dysfunction results in an inability to generate appropriate control forces. This could happen as the result of an acute nerve injury or a neuromuscular disorder such as Cerebral Palsy, a deficit in strength and coordination, or simply during an unfamiliar motor task. In any case the inability to properly actuate the joint may be associated with unnatural postures, mistimed muscle activation, spastic or overly lax muscles.

Dysfunction or failure of connective tissues results in inadequate joint restraining forces and altered positions of joint contact. This could manifest simply as lax or hypermobile joints, which may not present a problem under appropriate muscle control. On the other hand, completely incompetent ligaments could be the cause of severe joint subluxations (e.g. dislocation of the shoulder or patella).

Abnormal articular geometry results in improper joint articulation, altered positions of joint contact, or limb malalignment. If the geometry isn't able to produce the appropriate reactive forces to external or internal loads, then the muscles and connective tissues must compensate and can potentially be overloaded. Additionally, due to extreme loading or joint contact near the edges of the articular surface, acute damage and/or gradual wear of the articular cartilage can result.

One may retain function despite deficiencies in any one of these subsystems, however failure or dysfunction of multiple subsystems could result in episodes of instability. For example, one might tear his or her ACL but have good neuromuscular function and stable articular geometry (e.g. a deeply concave medial tibial plateau and flat lateral plateau). As a result, he or she may be able to “cope” with ACL insufficiency and return to normal activities.

On the other hand, an individual with either poor neuromuscular control or weakness, or with suboptimal articular geometry (e.g. a flat medial tibial plateau and a posteriorly sloping lateral tibial plateau), might lose function entirely and require ACL reconstruction.

Clinical Evaluation of Joint Stability

A variety of manual and observational clinical evaluations are used to document the functional status of an individual's knee. In some cases the goal of these tests is to assess "joint stability", however that term has different interpretations in knee biomechanics and orthopaedics. One topic of controversy is the difference between "laxity" and "stability". In the context of manual examinations of the knee, these terms are sometimes used interchangeably.

On the other hand, in the context of functional movement, "instability" may be used to describe a patient reported symptom or an observation of a biomechanically poor movement pattern. A determination of "instability" may consist of the patient reporting symptoms of his or her knee buckling, giving way, or feeling loose or wobbly during every-day or sporting activities. The clinician might also ask the patient to perform a particular maneuver such as a one or two-legged squat or hop. Either an inability to perform the test, a visual observation of a compensatory movement pattern, or an exclamation of pain by the patient may indicate the presence of an instability. Some problems with observations of patient reports of functional instability is that they are qualitative and sometimes vague, and more importantly may be attributed to multiple biomechanical factors. For example, abnormal movement patterns and pain during a single leg squat could be the result of strength deficits and related adaptations, poor balance and coordination, or possibly joint injuries along with protective or compensatory strategies.

Another longstanding source of debate in the literature is the description of “static” versus “dynamic” stability during manual examinations. Static tests like the Lachman or Dial test evaluate the knee by applying a uniaxial force or moment in a fixed joint configuration. Such tests probe for deficiencies in the ability of connective tissues to mechanically resist translation or rotation of the joint. Despite the patient being relaxed (or at least instructed to relax) large motions of the joint are often classified as instabilities. However, research shows that many measures of laxity turn out not to be objective indicators of functional stability. Most notably, anterior-posterior laxity of the knee joint has been found not to correlate with functional outcomes following ACL reconstruction, including patient reported symptoms of “instability”.

On the other hand, dynamic tests like the pivot-shift test involve applying multiaxial forces and moments to the joint throughout a range of motion. In dynamic tests, the clinician looks or feels for kinematic instabilities that involve sudden motions of the joint under load. For example, a positive pivot-shift is characterized by an anterior and internal-rotary subluxation of the tibia on the femur, followed by a rapid posterior and external-rotary reduction. Originally the pivot-shift test was adopted because it seemed to mimic patient-reported symptoms of instability and the sensation of the knee giving way. Compared to static laxity tests, dynamic stability tests like the pivot-shift have been shown to be better indicators of functional stability [Kocher *et al.*, 2004]. Unfortunately, the pivot-shift involves a complex manual maneuver and is thus difficult to reproduce. Addressing this problem in particular is the focus of Chapter 4.

To summarize, by examining what manual and functional tests assess in terms of the components of the stabilizing system above, we can get a better idea of what aspects of joint stability each test is addressing (Fig. 2.3).

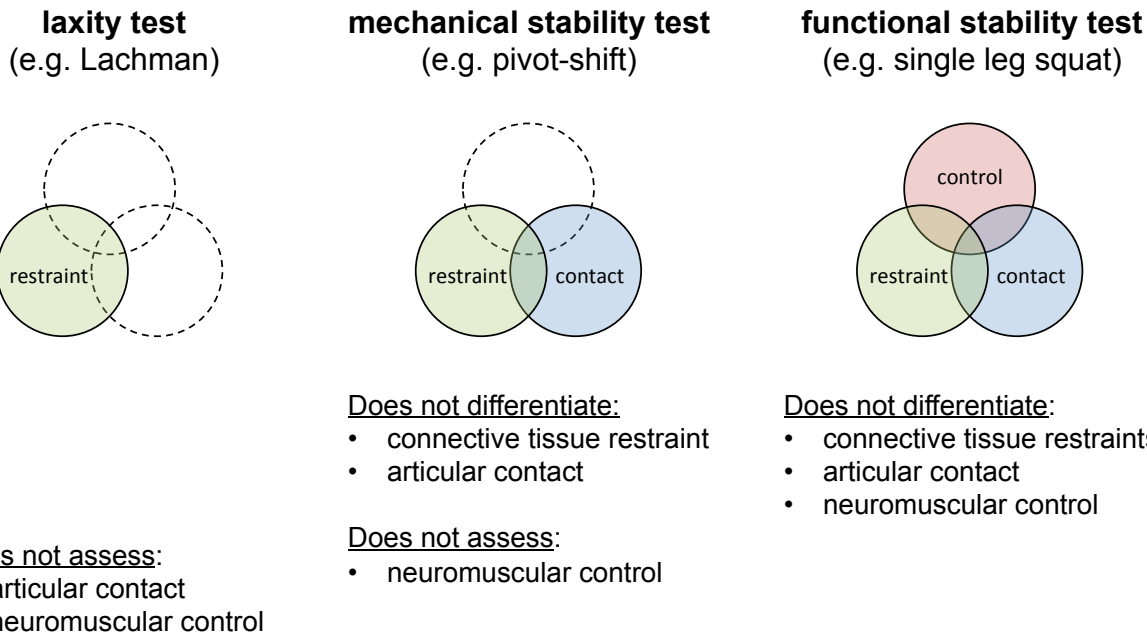


Figure 2.3: Clinical knee-stability evaluations assess and distinguish between the stabilizing subsystems of the knee. Static laxity tests directly assess connective tissue restraints in response to a static unidirectional load. Mechanical stability tests assess articular contact under dynamic multiaxial loads, in addition to connective tissue restraints. Functional stability tests assess the combined stabilizing system of the knee, but cannot necessarily distinguish between its components. Conducting multiple types of evaluations can help pinpoint which subsystems are deficient or dysfunctional in a patient.

Static laxity tests involve applying a uniaxial load to the joint and measuring displacement. Thus, they directly probe the soft tissue restraint force. However, such tests do not assess neuromuscular function or articular geometry.

Dynamic stability tests like the pivot-shift involve applying a combination of multiaxial loads to the joint throughout its range of motion. Such tests probe the *combination* of articular contact forces and connective tissue restraint forces to resist an applied load dynamically over a functional range of motion as the position of joint contact changes. (This meets our proposed definition of joint stability introduced at the beginning of this section). However, these tests do not *differentiate* between articular contact and ligamentous restraint forces. For example, a minor pivot-shift could be present in healthy knees that are slightly lax, or in ACL-injured knees (perhaps those of copers) that have ideal articular geometry.

Functional stability tests involve having the patient coordinate their neuromuscular system to perform a complex task. These tests probe the ability of neuromuscular control forces to actuate and stabilize the joint. However, functional stability tests actually assess the synergistic combination of the neuromuscular control, articular contact, and connective tissue restraint. Thus these tests cannot differentiate between these subsystems. For example, an inability to perform a single leg squat test could be due to muscle weakness and poor neuromuscular control, valgus knee alignment that puts the individual in an awkward posture, or incompetent ligaments that result in secondary compensatory movements.

Thus, there is clearly a need to perform all of these tests in order to construct a complete picture of the stabilizing system of the knee. Doing so enables a clinician to both probe and distinguish between the neuromuscular, articular, and connective stabilizing subsystems, and thus better understand where a patient stands in terms of the mechanical and functional stability of the joint.

2.3 Anterior Cruciate Ligament Injury

Injury of the anterior cruciate ligament (ACL) is the most common and well-studied cause of knee instability. The classic signs of mechanical instability of the joint and patient reports of the knee ‘giving way’ are reliable indicators of an ACL rupture. With an incidence of 1-10 ACL tears per 1000 people in the US, it is estimated that between 32,000-320,000 (and perhaps as many as 400,000) ACL tears happen each year [Vavken and Murray, 2013]. At about \$5,000-\$7000 per ACL reconstruction, that amounts to a cost of about \$2 billion per year, not including the cost of concomitant injuries, revision surgeries, and complications. ACL injuries are extremely common in sports, especially soccer, skiing, basketball, and football. Approximately 60-80% of all ACL injuries are “non-contact” injuries, occurring during cutting or pivoting motions. The mechanisms of injury vary from activity to activity and include extreme valgus, hyperextension, and tibial rotation.

Young women are at particularly high risk for ACL injury (4-6 times more likely than men), especially in the age range of 15-19. The cause of increased risk is not fully understood but is most likely multifactorial. Many gender-specific risk factors have been proposed including narrow intercondylar notch width, hormonal factors, and valgus knee alignment. Importantly, having torn one’s ACL increases their risk for injuring the same or contralateral ACL from less than 1% before injury to as high as 16% afterwards.

A number of injury prevention programs such as PEP and FIFA 11+ have been shown to decrease the risk of injury through neuromuscular training to improve strength, balance, coordination, landing mechanics, and general neuromuscular control of the lower extremity. However, the lack of accurate risk screening tools has made it difficult to perform targeted enrollment in these programs.

Surgical ACL Reconstruction

Early on it was recognized that a fully ruptured ACL does not heal on its own and that recurrent episodes or instability gradually destroy the meniscal and articular cartilage of the joint. This realization provided the impetus for inventing ACL reconstruction. Nowadays, between 100,000-400,000 ACL surgeries are performed each year in the US. In 2006, approximately 125,000 ACL reconstructions were performed and nearly 500,000 arthroscopic procedure for meniscal tears were performed [Kim *et al.*, 2011b]. Meniscal tears are common concomitant injuries, occurring in about two thirds of ACL patients.

Ernest Hey Groves reported the first ACL reconstruction using the iliotibial band in 1917. Since then a variety of techniques have been developed both for adults and children, with increasingly better results over the past several decades. The most common techniques currently utilize a hamstring or patellar tendon autograft with anatomical tunnels drilled in the tibia and femur. Allograft replacements are also common, but not in young active patients due to the longer healing time and potentially higher graft failure rates (20% vs 6% in the MOON study). Double-bundle ACL reconstruction has also been popularized, and is theoretically more anatomical than a traditional graft (since the two grafts and tunnels mimic the ACL's AM and PL bundles). However, clinical outcomes have not been shown to be any better and the procedure is significantly more expensive. For skeletally immature patients, other techniques have been developed that avoid drilling through the growth plates. Quantitatively evaluating the effectiveness of such techniques in a cadaver model is the focus of Chapter 5.

Conservative Treatment

Whether or not conservative treatment of ACL tears is an effective alternative to ACL reconstruction is debated. Frobell et al. [Frobell *et al.*, 2013] reported that at five years, patients assigned to rehabilitation plus early ACL reconstruction did not differ significantly in patient reported or radiographic outcomes from those assigned to initial rehabilitation with the option of delayed ACL reconstruction. In that study, optional/delayed ACL reconstruction was not any worse than early surgery with regard to outcomes. However 50% of the those in the optional group ended up getting ACL surgery. Within that group, 60% of patients had a positive pivot-shift at 5 year follow-up (82% of those patients who opted out of surgery had a positive pivot). In contrast, only 24% of patients who had early ACL reconstruction had a positive pivot-shift at 5-year follow-up. This may be acceptable depending on the level of desired function, and it is well known that many individuals can “cope” with ACL insufficiency without surgery and experience a minimal loss of function. However, it would be incredibly useful and cost-saving to be able to identify those who can cope based on objective tests and survey instruments.

Clinical Outcomes

Short term outcomes of early ACL reconstruction are good overall. Surgical outcomes have improved a great deal over time as a result of major studies discrediting suture-repair (rather than reconstruction) of a torn ACL and the use of synthetic grafts; as well as highlighting reductions in the rate of meniscal tears as a result of ACL reconstruction [Hettich and Spindler, 2013]. Revision rates for ACL surgery are low, at about 10%, and post-surgical patient satisfaction is generally high, as measured by KOOS, WOMAC, SF-36, Marx Activity, and other instruments.

Only allografts have conclusively been shown to be associated with worse outcomes—especially in younger active patients. Irradiated allografts have been shown to have higher failure rates. Patellar tenon grafts appear work as well as hamstring grafts and heal faster. However, they are associated with more anterior knee pain, and may possibly lead to patellofemoral arthritis [Neuman *et al.*, 2009; Jrvel *et al.*, 2001]. Allografts, higher BMI, and smoking are generally associated with worse outcomes.

In the long term however, ACL injury (especially in conjunction with meniscus injury) dramatically raises the likelihood of osteoarthritis (OA) later in life. It has not yet been shown that ACL reconstruction is capable of reducing the risk of OA. However, it has been shown conclusively that ACL reconstruction reduces the risk of further joint damage and meniscal degradation, which is a strong predictor of OA later in life. Meta-analyses have shown prevalence of OA following isolated ACL injury to be as high as 13% at 10-year follow up. With a combined meniscus injury, prevalence may be as hight as 48%.

In summary short term outcomes of ACL reconstruction are good and current surgical techniques are highly successful in adults and children. However, more research needs to be done to pinpoint and address the causes of the development of OA following ACL injury. More importantly, screening tools that can identify those at risk for ACL injury may help prevent injuries in the first place by enabling targeting of ACL prevention programs that currently work on a non-targeted basis.

Chapter 3

Theoretical Background: Knee Joint Kinematics and Kinetics

Acute injury and chronic pain of the knee place a tremendous burden on the US health care system. For example, more than 400,000 ACL injuries occur in the US each year at a cost of over \$2 billion [Vavken and Murray, 2013]. It is expected that 1.3-1.7 million total knee replacements will be performed annually by 2020 as a result of degenerative knee arthritis [Kurtz *et al.*, 2014]. To determine ways of preventing injury and chronic disease, and measuring the effectiveness of different treatments, there is a need to quantitatively characterize knee joint stability and overall function. A critical prerequisite to developing quantitative metrics of stability (such as joint stiffnesses) is the accurate representation of knee joint kinematics (motion) and kinetics (forces and moments). In this chapter we provide a mathematical framework, based largely on [O'Reilly, 2008; O'Reilly *et al.*, 2013], for describing knee kinematics and kinetics in a manner that is both clinically interpretable and representative of the unique biomechanical constraints of the bicondylar knee joint.

3.1 Motivation

A good joint coordinate system enables expression of joint kinematics and kinetics in a manner that's both biomechanically realistic (in terms of the allowed motions) and is easy to interpret clinically. As described in Chapter 2, clinical descriptions of knee joint motion include three rotations: extension-flexion, adduction-abduction, and internal-external rotation; and three translations: compression-distraction, lateral-medial translation, and anterior-posterior translation.¹ Seminal work by Grood and Suntay [Grood and Suntay, 1983a] provided the first widely adopted coordinate system for representing the three-dimensional motions of the knee joint. These authors used a 1-2-3 set of Euler angles to describe the rotational motion and used the axes associated with the three individual rotations of the Euler angles to describe a set of joint translations. We denote these axes by $\{\mathbf{g}_1, \mathbf{g}_2, \mathbf{g}_3\}$ in this chapter. Grood and Suntay's parameterizations of the rotational kinematics of the knee joint were quickly accepted. Significant progress towards a useful description of knee kinetics was later made by [Fujie *et al.*, 1996a].

In practice, one challenge in defining a “good” joint coordinate system for the knee is that although the motion of the tibia relative to the femur is governed by the intra-articular geometry, the axes of the joint are typically prescribed based on extra-articular anatomical landmarks. As a result, kinematic quantities measured in the anatomical frames may not be accurately represented. For example, a poorly-defined femoral axis may produce an apparent adduction-abduction of the knee when in fact the motion is pure flexion-extension. This “crosstalk” between joint angles is sometimes misunderstood as motion “coupling”, when in fact it is simply the result of non-physiological joint axes. To address this problem, investigators have proposed various “functional” coordinate systems, which impose kinematic

¹While the knee joint consists of the tibiofemoral articulation and the patellofemoral articulation, for the purposes of the present paper, attention will be focused on the former.

constraints on joint motion and rely less heavily on anatomical landmarks than do traditional joint coordinate systems. However, the mathematics behind these functional coordinate systems have not been rigorously connected to the contact forces and moments responsible for those constraints.

Another difficulty in accurately representing knee kinematics and kinetics can be traced to the fact that the axes of rotation for the knee joint are not necessarily orthogonal (i.e. $\mathbf{g}_1 \not\perp \mathbf{g}_3$). It can be difficult to find clinically relevant descriptions for the forces and moments at the knee joint since the standard convention of adding up vector components along axes does not hold in the case of non-orthogonal axes (i.e. $\sum_{i=1}^3 (\mathbf{M} \cdot \mathbf{g}_i) \mathbf{g}_i \neq \mathbf{M}$). This fact is often overlooked, and it is assumed that the projections of force and moment vectors onto the joint axes are equivalent to the force and moment components that act along those axes. As we show in Section 3.2, this is in fact not the case.

Fortunately, there exists another set of axes $\{\mathbf{g}^1, \mathbf{g}^2, \mathbf{g}^3\}$, dual to $\{\mathbf{g}_1, \mathbf{g}_2, \mathbf{g}_3\}$, that aids in the expression of forces and moments in the joint coordinate system. Both sets form bases, known as the Euler basis \mathbf{g}_i and the dual-Euler basis \mathbf{g}^i , which provide distinct representations for any vector [O'Reilly, 2007; O'Reilly, 2008]. As we discuss in Section 3.3, the connection between \mathbf{g}_i and \mathbf{g}^i provides a mathematical framework that links joint forces and moments to the kinematic constraints utilized in a functional coordinate system [O'Reilly *et al.*, 2013]. Moreover, the Euler and dual-Euler bases shed light on classical works including [Grood and Suntay, 1983a] and [Fujie *et al.*, 1996a]. For example, examining [Fujie *et al.*, 1996a] in light of works on dual basis vectors [Metzger *et al.*, 2010; O'Reilly, 2007; O'Reilly, 2008; Howard *et al.*, 1998; Žefran and Kumar, 2002], we found that the authors used the dual-Euler basis \mathbf{g}^i to represent forces and moments applied to the knee by a robotic testing system. However, they were not aware of the existence of this basis and misinterpreted these components as acting along \mathbf{g}_i rather than \mathbf{g}^i .

We have found that representations using both the Euler and dual-Euler bases are used in the literature on joint mechanics and are, with some exceptions [Desroches *et al.*, 2010; O'Reilly, 2008], not clearly distinguished. Preference for a representation of vectors featuring one basis over the other is problem dependent. For instance in classical mechanics, a representation of moments featuring the dual-Euler basis is particularly suited to describing mechanical power, conservative moments, and constraint (reaction) moments. In joint biomechanics, as we shall demonstrate from a discussion of the knee joint, it is also preferable to use a representation using the dual-Euler basis if joint stiffnesses are being computed. This recommendation is in conflict with that of others, however [Desroches *et al.*, 2010].

The remainder of this chapter is organized as follows: In Section 3.2, we discuss a range of frames associated with describing the relative motion of the tibia and femur. Related developments for forces and moments are collected in Section 3.3. For convenience, the chapter has an appendix (see Appendix B) which present explicit details on several matrices and vectors that feature prominently in the chapter. We also refer the interested reader to [Metzger *et al.*, 2010; O'Reilly, 2007; O'Reilly, 2008] for additional background on the dual-Euler basis and its applications to conservative moments and constraint moments. The dual-Euler basis is also related to the dual basis used in the screw motion descriptions of rigid body motions in [Howard *et al.*, 1998; Žefran and Kumar, 2002].

3.2 Coordinate Systems and Kinematics

In the analysis of biomechanical joints, it is standard to employ three coordinate frames: \mathbb{L} , \mathbb{P} , \mathbb{D} . The first of these frames, which is often known as a laboratory frame, is an inertial reference frame which is associated with a fixed point O . The second frame, is attached at a point O_P to the proximal anatomical segment and co-rotates with this body.

Correspondingly, the third frame is attached at a point O_D to the distal anatomical segment and co-rotates with the distal segment. The 4 components of these respective frames are denoted by

$$\begin{aligned}\mathbb{L} &= \{O, \mathbf{E}_1, \mathbf{E}_2, \mathbf{E}_3\}, \quad \mathbb{P} = \{O_P, \mathbf{p}_1, \mathbf{p}_2, \mathbf{p}_3\}, \\ \mathbb{D} &= \{O_D, \mathbf{d}_1, \mathbf{d}_2, \mathbf{d}_3\}.\end{aligned}\tag{3.1}$$

Here, $\{\mathbf{E}_1, \mathbf{E}_2, \mathbf{E}_3\}$, $\{\mathbf{p}_1, \mathbf{p}_2, \mathbf{p}_3\}$, and $\{\mathbf{d}_1, \mathbf{d}_2, \mathbf{d}_3\}$ are right-handed set of orthonormal vectors.

Of particular interest is the rotation of the distal anatomical segment \mathcal{S}_D with respect to the proximal anatomical segment \mathcal{S}_P . The rotation can be characterized by a rotation matrix R :

$$\begin{bmatrix} \mathbf{d}_1 \\ \mathbf{d}_2 \\ \mathbf{d}_3 \end{bmatrix} = \begin{bmatrix} R_{11} & R_{12} & R_{13} \\ R_{21} & R_{22} & R_{23} \\ R_{31} & R_{32} & R_{33} \end{bmatrix} \begin{bmatrix} \mathbf{p}_1 \\ \mathbf{p}_2 \\ \mathbf{p}_3 \end{bmatrix}.\tag{3.2}$$

Here, R_{ik} are the components of R . We also use the compact notation

$$\mathbf{d}_k = \mathsf{R}\mathbf{p}_k, \quad (k = 1, 2, 3).\tag{3.3}$$

In this chapter, R is parameterized by a set of Euler angles ψ , θ , and ϕ . Thus, R is decomposed into the product of a rotation ψ about a unit vector \mathbf{g}_1 followed by a rotation θ about a unit vector \mathbf{g}_2 and, finally, a rotation ϕ about a unit vector \mathbf{g}_3 . There are 12 possible sets of Euler angles, and, for each set, the first and third angles range from 0 to 2π . Depending on the specific set of Euler angles, the range of the second angle is restricted. For the 1-2-3 set of Euler angles used in this chapter

$$\theta \in \left(-\frac{\pi}{2}, \frac{\pi}{2}\right).\tag{3.4}$$

For each of the 12 sets, the three vectors $\{\mathbf{g}_1, \mathbf{g}_2, \mathbf{g}_3\}$ form a fourth set of basis vectors which is known as the Euler basis. This set of basis vectors is not orthogonal (nor is it necessarily right-handed). However, \mathbf{g}_2 is always perpendicular to the plane formed by \mathbf{g}_1 and \mathbf{g}_3 .

The Dual-Euler Basis

A fifth set of basis vectors, which is known as the dual (or reciprocal) Euler basis $\{\mathbf{g}^1, \mathbf{g}^2, \mathbf{g}^3\}$, plays a key role in expressing joint moments. Given a specific choice of Euler angles, one is able to define the Euler basis $\{\mathbf{g}_1, \mathbf{g}_2, \mathbf{g}_3\}$. The dual-Euler basis is then defined by the following 9 identities:

$$\mathbf{g}^i \cdot \mathbf{g}_k = \begin{cases} 1 & \text{when } i = k \\ 0 & \text{when } i \neq k \end{cases}, \quad (i = 1, 2, 3, k = 1, 2, 3). \quad (3.5)$$

It is known (see, e.g., [Simmonds, 1994]) that the solutions \mathbf{g}^i to these equations can be represented as follows:

$$\begin{aligned} \mathbf{g}^1 &= \frac{1}{g} (\mathbf{g}_2 \times \mathbf{g}_3), & \mathbf{g}^2 &= \frac{1}{g} (\mathbf{g}_3 \times \mathbf{g}_1) = \mathbf{g}_2, \\ \mathbf{g}^3 &= \frac{1}{g} (\mathbf{g}_1 \times \mathbf{g}_2). \end{aligned} \quad (3.6)$$

where $g = (\mathbf{g}_1 \times \mathbf{g}_2) \cdot \mathbf{g}_3$.² It is important to note that although \mathbf{g}_i are of unit length by definition, \mathbf{g}^i are not necessarily of unit length. As discussed in [O'Reilly, 2007; O'Reilly, 2008], the dual-Euler basis plays a key role in establishing transparent expressions for conservative moments and constraint moments. For instance, if one wishes the restrict

²For the 1-2-3 set of Euler angles used later in this chapter $g = \cos(\theta)$.

the rotation ϕ about \mathbf{g}_3 , then a constraint moment $M\mathbf{g}^3$ needs to be applied. This moment has no components in the \mathbf{g}_1 or \mathbf{g}_2 directions and so does not affect these rotations.

A vector \mathbf{b} has several distinct representations with respect to the aforementioned bases:

$$\mathbf{b} = \sum_{k=1}^3 B_k \mathbf{E}_k = \sum_{k=1}^3 b_{p_k} \mathbf{p}_k = \sum_{k=1}^3 b_{d_k} \mathbf{d}_k = \sum_{k=1}^3 b^k \mathbf{g}_k = \sum_{k=1}^3 b_k \mathbf{g}^k. \quad (3.7)$$

These representations are all valid, and the components can be obtained by taking the dot product of the vector \mathbf{b} with the appropriate basis vector. For example,

$$B_k = \mathbf{b} \cdot \mathbf{E}_k, \quad b^k = \mathbf{b} \cdot \mathbf{g}^k, \quad b_k = \mathbf{b} \cdot \mathbf{g}_k. \quad (3.8)$$

However, it is important to distinguish how one computes the component b^k along the basis vector \mathbf{g}^k , because in this case, the dot product $\mathbf{b} \cdot \mathbf{g}^k$ is not equivalent to the projection of \mathbf{b} onto \mathbf{g}^k (Fig. 3.1b). This is due to the fact that \mathbf{g}^k are not necessarily of unit length, unless $b_i = b^k$.

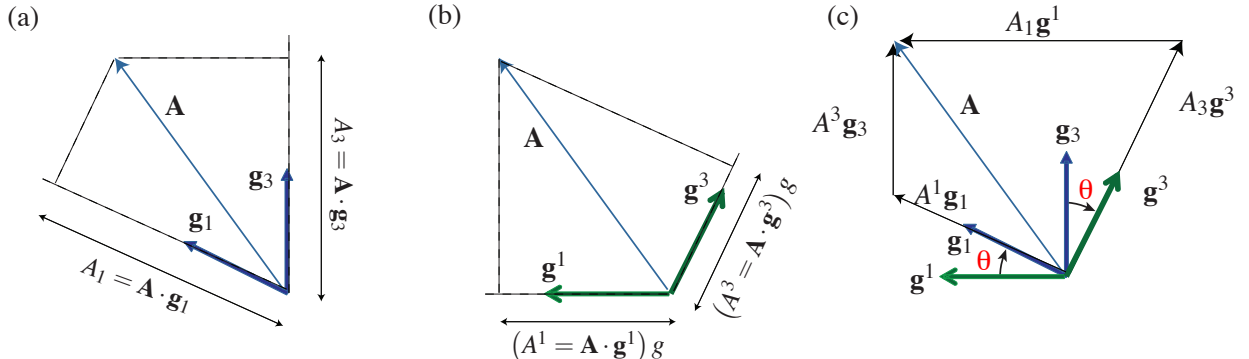


Figure 3.1: Comparison of the components of a vector $\mathbf{A} = A^1 \mathbf{g}_1 + A^3 \mathbf{g}_3 = A_1 \mathbf{g}^1 + A_3 \mathbf{g}^3$. In the interests of clarity, the $A^2 = A_2$ components are assumed to be zero. a) The components $A_{1,3}$ are equivalent to the projections of \mathbf{A} onto $\mathbf{g}_{1,3}$. b) The components $A^{1,3}$ must be scaled by g to obtain the projections of \mathbf{A} onto $\mathbf{g}^{1,3}$, because $\mathbf{g}^{1,3}$ have a magnitude g^{-1} . For the 1-2-3 set of Euler angles $g = \cos(\theta)$. c) To reconstruct the vector \mathbf{A} , the components $A_{1,3}$ are added up along $\mathbf{g}^{1,3}$, or the components $A^{1,3}$ are added up along $\mathbf{g}_{1,3}$.

More commonly in the biomechanics literature, the components b_k are calculated by projecting \mathbf{b} onto \mathbf{g}_k (Fig. 3.1a), for example in the case of joint moments. However it is not always understood that b_k do not add up along \mathbf{g}_k to produce \mathbf{b} , as they would in the case of an orthogonal basis. It should be apparent from Figure 3.1c that, in fact, the components b_k add up along the dual-Euler basis vectors \mathbf{g}^k to produce \mathbf{b} (the same can be said for b^k along \mathbf{g}_k).

A Joint Coordinate System for the Knee

To construct a joint coordinate system for the knee, we identify the proximal segment \mathcal{S}_P with the femur and the distal segment \mathcal{S}_D with the tibia. We follow [Grood and Suntay, 1983a] and use a set of 1-2-3 Euler angles to describe the rotation \mathbf{R} of the tibia relative to the femur. For convenience, explicit details on the Euler and dual-Euler basis vectors for this choice of Euler angles are contained in Appendix B.0.1.³

The three Euler angles that parameterize this rotation are identified with the three rotational degrees of freedom of the knee joint:

$$\text{extension-flexion rotation} \quad \theta_{EF} = \psi,$$

$$\text{varus-valgus angle} \quad \theta_{VV} = \theta,$$

$$\text{internal-external rotation} \quad \theta_{IE} = \phi.$$

Commensurate with the choice of Euler angles, the basis $\{\mathbf{g}_1, \mathbf{g}_2, \mathbf{g}_3\}$ is defined, where the vector $\mathbf{g}_1 = \mathbf{p}_1$ is taken to be aligned with the femur-fixed extension-flexion axis, and the vector $\mathbf{g}_3 = \mathbf{d}_3$ is aligned with the tibia-fixed internal-external rotation axis (Fig. 3.2a).

³In particular, expressions for, and graphical representations of, the Euler and dual-Euler basis vectors for the 1-2-3 set of Euler angles are presented in (B.3) and in Figure B.1.

A key feature of these axes is that the angle subtended by them is $\frac{\pi}{2}$ minus the varus-valgus rotation angle θ_{VV} (which is negative in Figure 3.2b). The axis \mathbf{g}_2 associated with the latter angle of rotation points along the varus-valgus axis, which is both parallel to the tibial plateau and perpendicular to the line connecting the two points of contact between the femoral condyles and the tibial plateau.

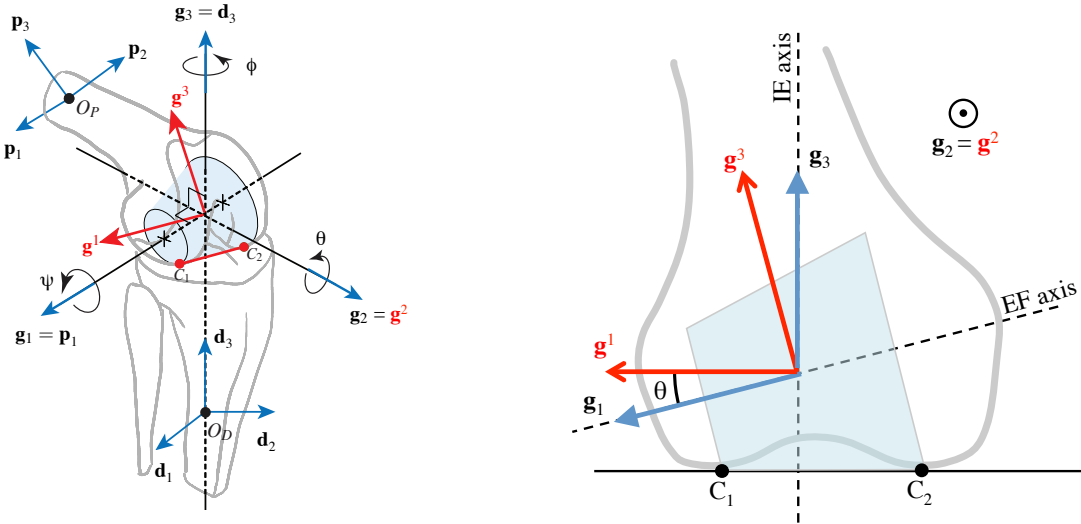


Figure 3.2: Bases associated with the knee joint, which is modeled as a truncated cone (femur) and plane (tibia). a) Proximal and distal frames of the femur and tibia, the Euler basis $\{\mathbf{g}_1, \mathbf{g}_2, \mathbf{g}_3\}$ associated with rotational motions of this joint, and the dual-Euler basis $\{\mathbf{g}^1, \mathbf{g}^2, \mathbf{g}^3\}$. b) Frontal plane view of the femoral condyles. The extension-flexion (EF) axis \mathbf{g}_1 is aligned with the axis of the truncated cone representing the femur. The internal-external (IE) rotation axis \mathbf{g}_3 is aligned with the normal of the plane representing the tibia. Note that in this figure, $\theta_{VV} < 0$.

We model the tibia as a rigid body with a planar articular surface and the femur as a rigid body with a conical articular surface. The knee joint is assumed to be under compression, so both condyles are engaged and the angle θ is constrained: $\theta = \theta_0$. Superimposing the Euler basis vectors and dual-Euler basis vectors on an image of the knee joint leads to several interesting observations. First, the angle θ is constant when both condyles are in contact with the tibial plateau. Second, under the condition of contact by both condyles with the tibial plateau, a contact moment in the \mathbf{g}_2 direction is present. This situation is similar to

the sliding cylinder discussed in [O'Reilly, 2007]. Our final observation is that the vector \mathbf{g}^1 is parallel to the line segment $\overline{C_1C_2}$ connecting the two points of contact between the femur and tibia.

Others have modeled the two primary rotational degrees of freedom see of the knee using variations of a compound hinge model, [Churchill *et al.*, 1998; Hollister *et al.*, 1993; Asano *et al.*, 2005]. However, to the author's knowledge, the cone and plane model featured here is the first to describe the two rotation axes along with additional degrees of translational freedom along the plane.

In practice the femoral and tibial axes \mathbf{g}_1 and \mathbf{g}_3 can be defined using bony landmarks, and the axis \mathbf{g}_2 can then be defined as the unit vector perpendicular to the plane formed by \mathbf{g}_1 and \mathbf{g}_3 . For example, it is well-accepted [Grood and Suntay, 1983a] that the extension-flexion (EF) axis is fixed to the femur and passes through its lateral and medial epicondyles, the internal-external rotation axis is fixed to the tibia and is parallel to its longitudinal axis, and the varus-valgus rotation axis is floating and is perpendicular to both the extension-flexion and internal-external rotation axes. However, for a given motion, it is well-known that the choice of the femoral and tibial axes effects the resulting values of the three angles θ_{EF} , θ_{VV} , and θ_{IE} (see, e.g., [Most *et al.*, 2004]).

To eliminate some of this variability, optimization schemes have been proposed with the aim of specifying \mathbf{g}_1 and/or \mathbf{g}_3 on the basis of functional motion rather than anatomical landmarks (see [Ehrig *et al.*, 2007; Reichl *et al.*, 2010] and references therein). These schemes seek to minimize some objective quantity (e.g., varus-valgus rotation and/or net tibial translation) under a particular set of assumptions (e.g., a compound pinned hinge model, or a shape function for the Euler angles) for a given motion of interest (e.g., flexion within the range of 40°-80°, or constrained tibial rotation). Motivated by the contact constraint force \mathbf{F}_c and moment \mathbf{M}_c described next in Section 3.3, we suggest that an optimization scheme

be chosen to minimize incremental varus-valgus rotations $\delta\theta_{VV}$ and compression-distraction translations δd^{CD} . Such an optimization scheme would be valid for any knee joint motion during which \mathbf{F}_c and \mathbf{M}_c do not perform work.

3.3 Representing Forces and Moments

It is possible to represent the forces and moments acting on the knee joint using any of the seven sets of basis vectors discussed in Section 3.2. It is particularly convenient to represent forces with respect to the orthogonal distal frame of the tibia $\{\mathbf{p}_1, \mathbf{p}_2, \mathbf{p}_3\}$ due to the mutually perpendicular orientations of the lateral-medial, anterior-posterior, and compression-distraction axes. However the corresponding representations for moments on the distal and proximal frames of the tibia and femur are often inconvenient. For the moments acting on the knee joint, of particular interest here are the representations

$$\begin{aligned}\mathbf{M} &= M^1\mathbf{g}_1 + M^2\mathbf{g}_2 + M^3\mathbf{g}_3, \\ \mathbf{M} &= M_1\mathbf{g}^1 + M_2\mathbf{g}^2 + M_3\mathbf{g}^3.\end{aligned}\tag{3.9}$$

As discussed in Section 3.2, the components M_k are computed by projecting \mathbf{M} onto the Euler basis vectors, while the components M^k are computed by taking the dot product of \mathbf{M} with the dual-Euler basis vectors. Both representations are equally valid, but it is imperative when presenting moment components for a given joint coordinate system to specify which representation one is using.

The relationship between the components M_k and M^i can be found with the help of (B.7) or, equivalently, by computing $\mathbf{g}_i \cdot \mathbf{g}_k$:

$$\begin{aligned} \begin{bmatrix} M^1 \\ M^2 \\ M^3 \end{bmatrix} &= \begin{bmatrix} \sec^2(\theta_{VV}) & 0 & -\frac{\sin(\theta_{VV})}{\cos^2(\theta_{VV})} \\ 0 & 1 & 0 \\ -\frac{\sin(\theta_{VV})}{\cos^2(\theta_{VV})} & 0 & \sec^2(\theta_{VV}) \end{bmatrix} \begin{bmatrix} M_1 \\ M_2 \\ M_3 \end{bmatrix}, \\ \begin{bmatrix} M_1 \\ M_2 \\ M_3 \end{bmatrix} &= \begin{bmatrix} 1 & 0 & \sin(\theta_{VV}) \\ 0 & 1 & 0 \\ \sin(\theta_{VV}) & 0 & 1 \end{bmatrix} \begin{bmatrix} M^1 \\ M^2 \\ M^3 \end{bmatrix}. \end{aligned} \quad (3.10)$$

A key feature of these identities is that $M_{1,3}$ and $M^{1,3}$ are simply related by the second Euler angle θ_{VV} . For instance, as $|\theta_{VV}|$ increases from 0, then the components M_1 and M_3 become increasingly distinct from M^1 and M^3 . Some examples of these relations are shown in Figure 3.3.

Expressing Joint Moments with the Dual-Euler Basis

Expressing force vectors and moment vectors as linear combinations of contravariant basis vectors and dual-Euler basis vectors has a long and illustrious history. However, the basis vectors are often not explicitly mentioned in classical texts and this can often be a source of confusion. In the biomechanics literature specifically, the components M_k acting along the dual-Euler basis vectors \mathbf{g}^k are usually computed, but the basis vectors themselves are often ignored. Rather, the Euler basis vectors are emphasized since they correspond to the axes of rotation of the joint and are thus more intuitive and easier to visualize. However, as we shall see, consideration for the dual-Euler basis is important when describing the constraints that limit motion of the knee joint.

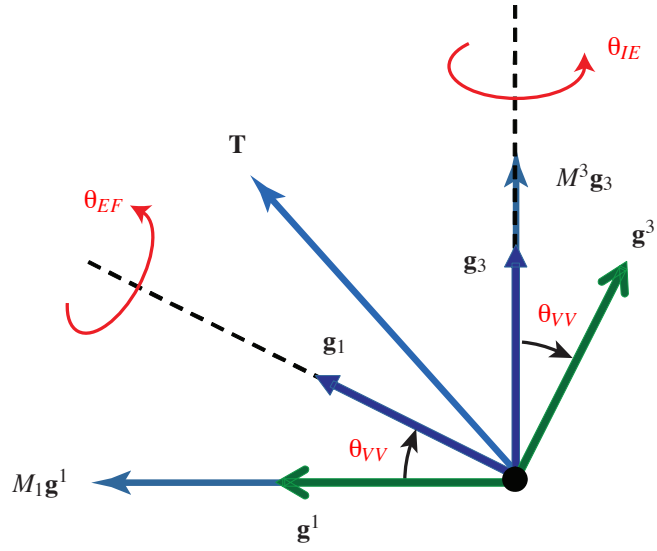


Figure 3.3: Three representative examples of moments: $M^3\mathbf{g}_3$, $M_1\mathbf{g}^1 = M_1 \sec^2(\theta_{VV})\mathbf{g}_1 - M_1 \sec^2(\theta_{VV}) \sin(\theta_{VV})\mathbf{g}_3$, and $\mathbf{T} = T^1\mathbf{g}_1 + T^3\mathbf{g}_3 = (T^1 + \sin(\theta_{VV})T^3)\mathbf{g}^1 + (T^3 + \sin(\theta_{VV})T^1)\mathbf{g}^3$. The different representations for the moments were obtained using (3.10).

To help illustrate the importance of the dual-Euler basis in expressing joint moments, suppose we wish to find the moment vector \mathbf{M} which will generate a rotation about \mathbf{g}_1 but not about \mathbf{g}_2 or \mathbf{g}_3 . It follows that \mathbf{M} must be in the direction of $\mathbf{g}_2 \times \mathbf{g}_3$. Consequently, the desired moment is in the direction of \mathbf{g}^1 . More generally, expressing a moment vector \mathbf{M} using the components M_k implies that \mathbf{M} is expressed in terms of the dual-Euler basis, i.e., $\mathbf{M} = M_1\mathbf{g}^1 + M_2\mathbf{g}^2 + M_3\mathbf{g}^3$. Each of the components M_k generates a rotation about a single \mathbf{g}_k .

As discussed in [O'Reilly, 2007; O'Reilly, 2008], $\mathbf{M} = \sum_{k=1}^3 M_k \mathbf{g}^k$ is also the most natural representation for expressing conservative moments and constraint (reaction) moments because $\mathbf{M} \cdot \boldsymbol{\omega} = M_1 \dot{\theta}_{EF} + M_2 \dot{\theta}_{VV} + M_3 \dot{\theta}_{IE}$.

Constraint Moments at the Knee Joint

One important implication of using the Euler and dual-Euler bases is that (if the axes are constructed properly) various components of joint forces and moments can be interpreted as being supplied by either the soft tissues or bony geometry of the knee. For example, the moment supplied by the knee joint in response to the applied moment \mathbf{M} can be decomposed into a conservative moment \mathbf{M}_{con} and a constraint moment $M_c \mathbf{g}_2$, provided by the soft tissues and femoral condyles, respectively: $\mathbf{M} = \mathbf{M}_{con} + M_c \mathbf{g}_2$. Here, the moment $M_c \mathbf{g}_2$ ensures that the varus-valgus angle θ_{VV} is constant, while the moment \mathbf{M}_{con} resists rotations about the two joint axes \mathbf{g}_1 and \mathbf{g}_3 to some degree.

The most important stabilizing feature of the knee joint is a pair of contact forces exerted by the condyles which prevents the tibial plateau from passing through them. These forces restrict varus-valgus rotation θ_{VV} and compression-distraction d^{CD} . Referring to Figure 3.4, the resultant of the pair of forces acts antiparallel to the \mathbf{g}_3 direction. The pair is equipollent to a resultant force \mathbf{F}_c and a resultant moment \mathbf{M}_c acting at point C :

$$\begin{aligned}\mathbf{F}_c &= \mu_1 \mathbf{a}^3 = \mathbf{F}_{c_1} + \mathbf{F}_{c_2}, \\ \mathbf{M}_c &= \mu_2 \mathbf{g}^2 = \boldsymbol{\pi}_1 \times \mathbf{F}_{c_1} + \boldsymbol{\pi}_2 \times \mathbf{F}_{c_2}.\end{aligned}\tag{3.11}$$

Here, $\boldsymbol{\pi}_1$ and $\boldsymbol{\pi}_2$ are the respective position vectors of the condyles C_1 and C_2 relative to C . The force \mathbf{F}_c is an example of a constraint (or normal) force, while \mathbf{M}_c is an example of a constraint moment. The latter serves to prevent rotation in the \mathbf{g}_2 direction. As the relative translational motion in the \mathbf{g}_3 and relative rotational motion in the \mathbf{g}_2 directions are assumed to be zero when both condyles are in contact with the tibia, \mathbf{F}_c and \mathbf{M}_c do no work.

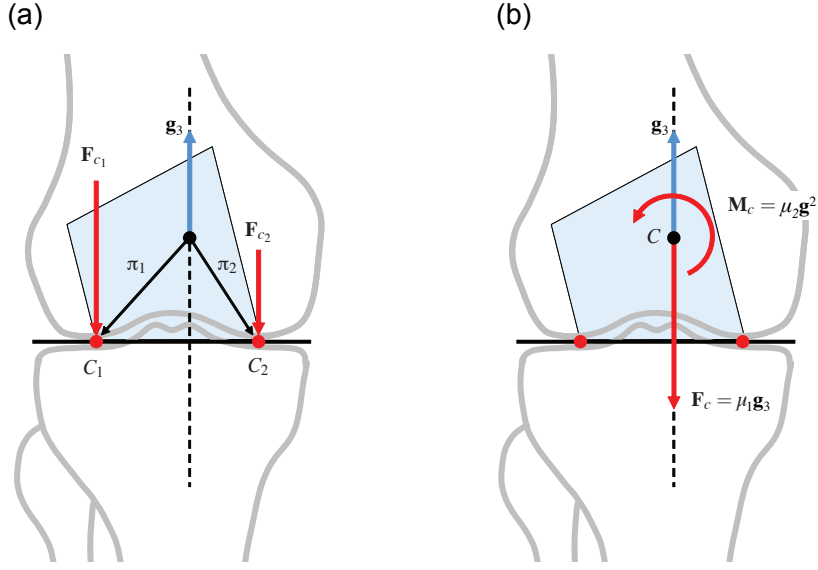


Figure 3.4: Joint contact forces and their moment at the knee. The reaction forces \mathbf{F}_{c_1} and \mathbf{F}_{c_2} acting at the condyles shown in (a) are equipollent to a moment $\mathbf{M}_c = \boldsymbol{\pi}_1 \times \mathbf{F}_{c_1} + \boldsymbol{\pi}_2 \times \mathbf{F}_{c_2}$ and a force $\mathbf{F}_c = \mu_1 \mathbf{g}_3$ where $\mu_1 = (\mathbf{F}_{c_1} + \mathbf{F}_{c_2}) \cdot \mathbf{g}_3$ acting at the point C .

Discussions of the stiffness of the knee joint can be found in the literature. For example, Cammarata and Dhaher [Cammarata and Dhaher, 2008] and Hsu et al. [Hsu *et al.*, 2006] present experimental measurements of the stiffness of the joint by comparing a varus-valgus rotation with the corresponding varus-valgus moment at 0° of flexion. Because of the multi-degree-of-freedom nature of the knee joint, this data constitutes one of the many components of the stiffness matrix of the knee joint and illuminates the difficulties in measuring a complete set of stiffness data for this joint.

To elaborate further, it is possible to construct a variety of stiffness matrices for the knee joint using the methods discussed in [Metzger *et al.*, 2010]. For instance, one such 6×6 matrix could relate the \mathbf{E}_i components of the increments in \mathbf{F} and \mathbf{M} to the increments $\delta\theta_{EF}$, $\delta\theta_{VV}$, $\delta\theta_{IE}$, δd^{LM} , δd^{AP} , δd^{CD} . Alternatively, another stiffness matrix could be constructed relating the \mathbf{d}_k components of the increments in \mathbf{F} and \mathbf{M} to the six increments $\delta\theta^j$ and

δd^i . In the interests of brevity we don't present the explicit details here as they are easily inferred from [Metzger *et al.*, 2010]. However, one important point to note is that if the knee is loaded so that increments to compression-distraction and varus-valgus rotation are not possible (i.e., $\delta d^{CD} = 0$ and $\delta\theta_{VV} = 0$), then it is possible to construct a 4×4 stiffness matrix relating the increments in $\mathbf{F} \cdot \mathbf{a}_1$, $\mathbf{F} \cdot \mathbf{a}_2$, $\mathbf{M} \cdot \mathbf{g}_1$ and $\mathbf{M} \cdot \mathbf{g}_2$ to $\delta\theta_{EF}$, $\delta\theta_{IE}$, δd^{LM} , and δd^{AP} . Such a stiffness matrix would not be dominated by the components of the reaction force $F_3\mathbf{a}^3$ and the reaction moment $M_2\mathbf{g}^2$ which ensure that the compression-distraction and varus-valgus rotation remain constrained. This is a unique feature of the coordinate system proposed in the present paper.

If the stiffness of the knee joint is modeled using a potential energy $U = U(\theta_{EF}, \theta_{IE})$, then it follows that the (conservative) moment \mathbf{M}_{con} produced by the knee joint has the representation [O'Reilly, 2007].

$$\mathbf{M}_{con} = -\frac{\partial U}{\partial \theta_{EF}}\mathbf{g}^1 - \frac{\partial U}{\partial \theta_{IE}}\mathbf{g}^3. \quad (3.12)$$

The second partial derivatives of U (e.g., $\frac{\partial^2 U}{\partial \theta_*^2}$) provide the three stiffnesses of the knee joint.

Assuming that $\mathbf{M}_{con} = 0$ when $\theta_{EF} = \theta_{IE} = 0$, we find the linear approximation

$$\mathbf{M}_{con} \approx -(k_{11}\theta_{EF} + k_{12}\theta_{IE})\mathbf{g}^1 - (k_{12}\theta_{EF} + k_{22}\theta_{IE})\mathbf{g}^3. \quad (3.13)$$

To measure the stiffnesses k_{11} , k_{12} , and k_{22} , it is thus necessary to measure θ_{EF} and θ_{IE} in addition to the applied moment \mathbf{M} . We also recall that $\mathbf{M} = \mathbf{M}_{con} + M_c\mathbf{g}_2$ and so the representation $\mathbf{M} = \sum_{k=1}^3 M_k\mathbf{g}^k$ is more convenient than $\mathbf{M} = \sum_{i=1}^3 M^i\mathbf{g}_i$.

Use of the Dual-Euler Basis in Other Works

It is instructive to compare our work with earlier works on the kinematics and kinetics of the knee joint. Starting with work in [Grood and Suntay, 1983a], two distinct types of displacements are discussed: clinical displacements q_i and joint translations S_i . Using the dual-Euler basis, it is straightforward to see that these displacements are simply related:⁴

$$q_1\mathbf{g}^1 + q_2\mathbf{g}^2 - q_3\mathbf{g}^3 = S_1\mathbf{g}_1 + S_2\mathbf{g}_2 + S_3\mathbf{g}_3. \quad (3.14)$$

Unfortunately, the magnitudes of \mathbf{g}^1 and \mathbf{g}^3 are $\sec(\theta_{VV})$ and so the magnitudes of the displacements q_1 and q_3 are difficult to interpret physically.

Furthermore, since \mathbf{g}^3 is not perpendicular to the tibial plateau when $\theta_{VV} \neq 0$, natural joint translations would produce nonzero displacements q_3 , which might be misinterpreted as unnatural joint compression or distraction.

The seminal work on forces and moments at the knee joint is Fujie et al. [Fujie *et al.*, 1996b]. In certain instances in this work, the forces and moments at the knee joint are expressed in terms of the \mathbf{g}^k basis. Specifically, examining (10) and (11) in [Fujie *et al.*, 1996b], one can interpret their components f_{LM} , f_{AP} , and f_{PD} as the force components $\mathbf{F} \cdot \mathbf{g}_k$, and their components m_{EF} , m_{VV} , and m_{IE} as the moment components $\mathbf{M} \cdot \mathbf{g}_k$, respectively. Here, \mathbf{g}_k are the Euler basis vectors for a 3-1-2 set of Euler angles. That is,

$$\begin{aligned} \mathbf{M} &= m_{EF}\mathbf{g}^1 + m_{VV}\mathbf{g}^2 + m_{IE}\mathbf{g}^3, \\ \mathbf{F} &= f_{LM}\mathbf{g}^1 + f_{AP}\mathbf{g}^2 + f_{PD}\mathbf{g}^3. \end{aligned} \quad (3.15)$$

Thus, for example, m_{EF} is obtained by projecting \mathbf{M} onto $\mathbf{g}_1 = \mathbf{p}_3$.

⁴See, in particular, equations (4c), (5a), ..., (7) in [Grood and Suntay, 1983a]. In their work, \mathbf{g}_i are denoted by \mathbf{e}_i and a dual-Euler basis is never mentioned.

Unfortunately, Fujie et al. [Fujie *et al.*, 1996b] did not explicitly mention the basis vectors they used when they described the aforementioned forces and moments which may cause confusion. For example, it was not clear that the “proximal-distal” force component f_{PD} acts in the \mathbf{g}^3 direction, which as mentioned earlier, is not necessarily perpendicular to the tibial plateau. Thus, $f_{PD}\mathbf{g}^3$ might be misinterpreted as a workless contact constraint force when in fact it would do work during natural joint translations. Further, Fujie et al. refer to the components M_k as “moments about the axes of the joint coordinate system”. If they were referring to $\{\mathbf{g}_1, \mathbf{g}_2, \mathbf{g}_3\}$, then this interpretation would be incorrect, because as we have shown, the components M_k are in fact the moments about the axes of the dual-Euler basis $\{\mathbf{g}^1, \mathbf{g}^2, \mathbf{g}^3\}$.

In [Desroches *et al.*, 2010], the components $M_k = \mathbf{M} \cdot \mathbf{g}_k$ are known as the “motor torques” or “orthogonal projections”, and are clearly distinguished from $M^i = \mathbf{M} \cdot \mathbf{g}^i$ which are referred to as the “nonorthogonal projections”. In this respect, Desroches et al. deserve credit for pointing out the distinction between the components $\mathbf{M} \cdot \mathbf{g}_k$ and $\mathbf{M} \cdot \mathbf{g}^k$. However, they champion the use of M^i without utilizing results from the literature on dual basis vectors applied to moment vectors—likely not realizing the usefulness of using the components M_k for describing constraint moments.

Closing Remarks

To summarize, we have introduced a coordinate system for describing knee joint kinematics and kinetics. Central to this coordinate system are two sets of basis vectors ($\{\mathbf{g}_1, \mathbf{g}_2, \mathbf{g}_3\}$ and $\{\mathbf{g}^1, \mathbf{g}^2, \mathbf{g}^3\}$) which are used to express joint rotations and joint moments in a manner consistent with [Grood and Suntay, 1983a; Fujie *et al.*, 1996b], and two analogous sets of basis vectors ($\{\mathbf{a}_1, \mathbf{a}_2, \mathbf{a}_3\}$ and $\{\mathbf{a}^1, \mathbf{a}^2, \mathbf{a}^3\}$) which are used to express joint translations and

joint forces. All four sets of basis vectors are related by the Euler angles θ_{IE} and θ_{VV} . Importantly, since $\mathbf{a}_3 = \mathbf{a}^3$ and $\mathbf{g}_2 = \mathbf{g}^2$, our coordinate system highlights the articular contact force $F_c \mathbf{a}^3$ and moment $M_c \mathbf{g}^2$, which prevent incremental compression-distraction translations along \mathbf{a}_3 and varus-valgus rotations about \mathbf{g}_2 , respectively. If aligned such that these incremental motions are minimal, our coordinate system simplifies the description of joint motions and also joint stiffnesses.

Chapter 4

A Mechanical Pivot-Shift Device for Dynamically Loading Cadaveric Knees

4.1 Chapter Overview

The pivot-shift is a manual examination of the knee used to evaluate joint stability following injury or reconstruction of the anterior cruciate ligament. Unlike other examinations such as the Lachman test, the pivot-shift involves taking the knee through a dynamic range of motion while applying a multi-planar combination of forces and moments. Because the pivot-shift is dynamic, it can induce the same mechanical joint instability that patients often experience when their knee “gives way”. Thus, a major focus of orthopaedic research has been to “simulate” the pivot-shift test in a laboratory setting so that investigators can study the effect of soft tissue injuries and surgical techniques on dynamic knee stability. However, current mechanical systems designed to mimic the pivot-shift are inadequate because they utilize either static or poorly-defined loads. In this study, we describe a novel mechanical pivot-shift device (MPSD) that applies dynamic, well-defined loads to cadaveric knees.

4.2 Introduction

The pivot-shift is a manual test for evaluating anterolateral rotary instability of the knee following injury or surgical reconstruction of the anterior cruciate ligament (ACL). Unlike tests like the Lachman that are performed by applying static unidirectional loads to the knee at fixed flexion angles, the pivot-shift test is performed by applying dynamic multi-directional loads throughout knee flexion [Bull and Amis, 1998a; Musahl *et al.*, 2012b]. These loads, including axial compression, valgus torque, and internal torque, induce a distinctive kinematic instability when applied to an ACL-deficient knee. This instability, often referred to as a “pivot-shift”, is characterized by an anterior and internal-rotary subluxation of the tibia on the femur followed by a rapid, posterior and external-rotary reduction between 30° and 40° of knee flexion [Galway and MacIntosh, 1980]. The clinical significance of a positive pivot-shift is that, in patients treated by ACL reconstruction, it is associated with poor outcomes and self-reported functional instability [Ayeni *et al.*, 2012; Kocher *et al.*, 2004; Leitze *et al.*, 2005; Jonsson *et al.*, 2004].

Owing to its functional relevance, the pivot-shift test is widely used in clinical and biomechanics studies as an objective indicator of joint instability. However, study results can be difficult to reproduce due to variability in the way the test is performed and interpreted. Patient guarding and the complexity of the maneuver itself can negatively affect intra-examiner reliability (repeatability) [Benjaminse *et al.*, 2006; Donaldson *et al.*, 1985]. Meanwhile, inconsistent descriptions of technique and grading criteria can contribute to poor inter-examiner reliability (reproducibility) [Jakob *et al.*, 1987; Noyes *et al.*, 1991; Bach *et al.*, 1988].

To improve the repeatability and reproducibility of the pivot-shift, recent research has focused on standardizing the manual application of loads to the knee [Hoshino *et al.*, 2012;

Musahl *et al.*, 2012a] and on quantifying pivot-shift kinematics using readily available technology [Kuroda *et al.*, 2012; Hoshino *et al.*, 2013; Labb *et al.*, 2014]. For use in an in-vitro setting, several investigators have developed mechanical systems that mimic pivot-shift loads [Kanamori *et al.*, 2000; Markolf *et al.*, 2008; Matsumoto, 1990]. However, these systems applied loads statically, at fixed knee flexion angles. Others have developed objective measurement and analysis techniques that quantify kinematic features of the pivot-shift [Musahl *et al.*, 2010c; Lane *et al.*, 2008b; Labbe *et al.*, 2010; Labbe *et al.*, 2011a]. However, in these studies, the loads applied to knees were not clearly defined. Static loads do not reflect the dynamic nature of the clinical pivot-shift test, and poorly-defined loads are not amenable to rigorous biomechanical testing. Therefore, a method is needed for applying both dynamic and well-defined pivot-shift loads to the knee.

Here we characterize and validate a previously reported mechanical pivot-shift device (MPSD) that induces a realistic pivot-shift by dynamically applying defined loads to ACL-transected cadaveric knees [Sena *et al.*, 2013]. Compared to the manual pivot-shift, the device is more repeatable within a given knee and more reproducible between knees and examiners. In addition, because the device is based on a simple mechanical design, it is readily accessible to biomechanics researchers.

4.3 Methods

Design

The key features of the MPSD are a constant-tension spring that generates force and an external fixation (ex-fix) unit that holds the spring in a predetermined position relative to

the tibia and femur. To generate the multi-planar loads required to induce a pivot-shift, the MPSD employs the principle of equivalent forces and moments [Bois, 1902], which states:

The resultant of a couple \vec{M} and a force \vec{F} in the plane of the couple is a single equal and parallel force in that plane at a distance $d = \|\vec{F}\|/\|\vec{M}\|$.

This principle implies that any combination of a torque and a perpendicular force can be produced by a single force, if its line of action is positioned appropriately. In the knee, components of valgus torque M_v and axial compression F_c can be produced by a line of action of force positioned laterally (Fig. 4.1b). Additional components of internal torque M_i and anterior shear F_a can be produced by orienting this line of action anteriorly (Fig. 4.1c).

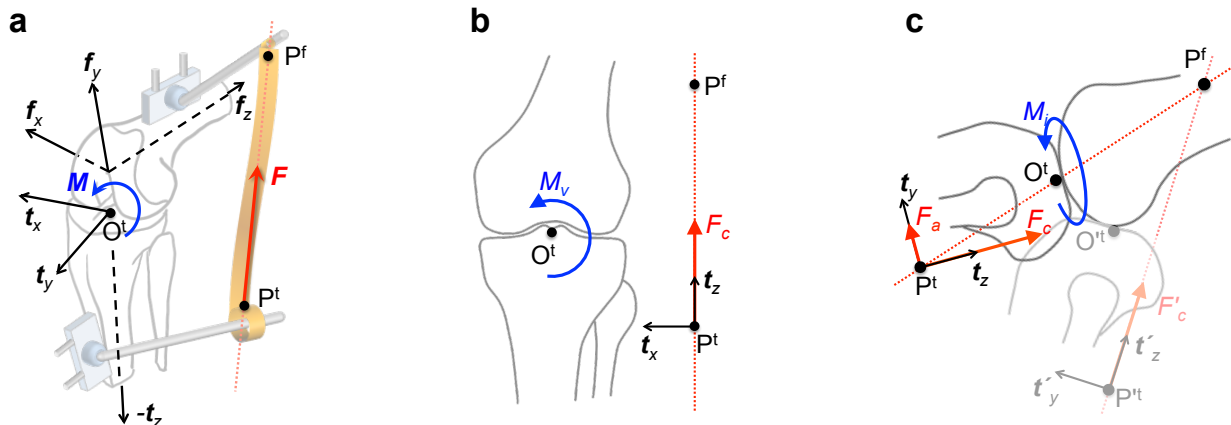


Figure 4.1: Working principle of the Mechanical Pivot-Shift Device. **a)** A spring attached between the points P^t and P^f produces a force \vec{F} and moment \vec{M} . An ex-fix unit holds the position of P^t and P^f fixed relative to the tibia and femur, respectively. **b)** In the frontal plane, \vec{F} and \vec{M} have compressive F_c and valgus M_v components. **c)** In the sagittal plane, \vec{F} and \vec{M} have anterior F_a and flexion (M_f , not shown) components. Additionally, in the transverse plane, \vec{M} has an internal-rotary component M_i . Near full extension, these forces and moments sublux an ACL-deficient knee. As the knee is flexed, F_a and M_i diminish in magnitude, allowing the knee to reduce (See also Fig. 4.2). The femoral and tibial coordinate systems are indicated by \vec{f}_i and \vec{t}_i . The line of action of the force \vec{F} is indicated by a dashed red line.

To produce these forces and moments experimentally, an ex-fix unit (Synthes, Paoli, PA) was used to position a 48 N constant-tension spring (McMaster Carr, Santa Fe Springs, CA) 15 cm lateral to the knee, oriented 20° anteriorly with respect to the tibia (Fig. 4.1a). Based on this approximate position, it was estimated that the spring would produce 7 N·m of valgus torque and 45 N of axial compression force throughout knee flexion, along with 2.5 N·m of internal torque and 16 N of anterior force that would diminish as a function of knee flexion. Prior to the present study, the position of the spring was fine-tuned so that it consistently induced a realistic pivot-shift in an ACL-transected cadaver knee. In the selected position, the coordinates of the spring endpoints were $P_t^t = (\pm 14.4, 1.7, -20.5)$ and $P_f^f = (\pm 15.7, 9.8, 15.9)$ (cm), measured in the tibia and femur coordinate frames, respectively (\pm : right/left legs).

To measure the loads generated by the MPSD, a small 6-axis load cell (AMTI, Watertown, MA) was attached to the femur between the ex-fix clamps and rods. Knee kinematics were measured using an Optotrak navigation system (NDI, Waterloo, Canada) consisting of a 3-aperture position sensor (accuracy: 0.1 mm, 0.1°), a handheld digital probe for registration of reference points, and 2 strobing infrared motion-tracking arrays attached to the tibia and femur. This system has been used previously for biomechanical studies in our laboratory [Kennedy *et al.*, 2011].

Knee Preparation

Six fresh-frozen human cadaveric knees (age: 46-64) were potted at the femur and mounted on a hinged testing base. The iliotibial band was dissected and attached to a 4.5 kg weight and pulley, which was used only during manual pivot-shift tests. A medial arthrotomy was performed to expose the ACL and intra-articular bony landmarks. All six knees demon-

strated full range of motion, no ligamentous laxity, and normal intra-articular anatomy. Two other knees were excluded from this study to due excessive AP joint laxity.

Motion-tracking arrays were fixed to the tibia and femur using Schantz screws. Anatomical coordinate systems were established by registering the intercondylar eminence, anterior crest, and distal shaft of the tibia; and the proximal shaft and epicondyles of the femur. Knees were fitted with the MPSD first by attaching ex-fix clamps to the tibia and femur using Schantz screws, and then by adjusting the ex-fix rods to properly position the spring. When the spring endpoints were within 1 cm of the desired coordinates P_t^t and P_t^f (as determined using the handheld probe) the rods were locked into place.

Testing Procedure

Using a fully-crossed experimental design, 5 repeated trials of MPSD tests and manual pivot-shift tests were performed by 2 different examiners before and after ACL-transection in six cadaveric knees. MPSD tests were conducted by supporting the ankle with an open palm and lowering the tibia until the knee surpassed $\sim 60^\circ$ of flexion. The femur remained fixed. Manual pivot-shift tests were performed using a technique consistent with the “standardized” description of Musahl et al. [Musahl *et al.*, 2012a], with the iliotibial band weight engaged. In this case the hinged testing base allowed flexion and extension of the femur.

First, each knee (in the ACL-intact condition) was passively flexed to establish a reference motion path. Then, each examiner conducted 5 MPSD trials, disengaged the spring, and conducted 5 manual pivot-shifts. These trials were repeated after surgically transecting the ACL. Finally, each knee was passively flexed again to ensure (by comparison to the reference motion) that the motion-tracking arrays had not accidentally moved. Tibiofemoral

kinematics were recorded for all trials, while load cell measurements were recorded only for MPSD trials.

Kinematics

Four kinematic variables were selected to characterize the pivot-shift. Anterior displacement, AD (mm), and internal-rotary displacement, IRD (°), quantified the magnitude of tibial subluxation. Posterior velocity, PV (mm/s), and external-rotary velocity, ERV (°/s), quantified the speed of tibial reduction. AD and IRD were extracted from the relative joint displacement matrix \mathbf{D} , while PV and ERV were extracted from the absolute joint velocity matrix $\hat{\mathbf{V}}$ [Murray *et al.*, 1994]:

$$\begin{aligned}\mathbf{D} &= \mathbf{T}_{\text{ref}}^{-1}(\psi) \mathbf{T}_{\text{trial}}(\psi) & \hat{\mathbf{V}} &= \mathbf{T}_{\text{trial}}^{-1} \dot{\mathbf{T}}_{\text{trial}} \\ &= \begin{bmatrix} \mathbf{Q} & \vec{d} \\ \vec{0}^\top & 1 \end{bmatrix} & &= \begin{bmatrix} \hat{\vec{\omega}} & \vec{v} \\ \vec{0}^\top & 0 \end{bmatrix} \\ \text{AD} &:= [0 \ 1 \ 0] \vec{d} & \text{PV} &:= [0 \ -1 \ 0] \vec{v} \\ \text{IRD} &:= \pm \tan_2^{-1}(Q_{12}, Q_{11}) & \text{ERV} &:= [0 \ 0 \ \mp 1] \vec{\omega}\end{aligned}$$

where $\mathbf{T} = \begin{bmatrix} \mathbf{R} & \vec{p} \\ \vec{0}^\top & 1 \end{bmatrix}$ is the homogeneous transformation matrix representing the motion of the tibia relative to the femur, and $\dot{\mathbf{T}}$ is the time derivative of \mathbf{T} . Motions during experimental trials $\mathbf{T}_{\text{trial}}$ and during intact passive flexion \mathbf{T}_{ref} were expressed as a function of the same knee flexion angle ψ . The Euler angles corresponding to knee flexion-extension (ψ), varus-valgus, and internal-external rotation were extracted from the rotation matrix \mathbf{R} following the convention of Grood and Suntay [Grood and Suntay, 1983b].

Kinetics

The loads acting on the tibia were both predicted based on the spring configuration and measured directly with a load cell. The force \vec{F} and moment \vec{M}^{O^t} applied to the tibia by the 48 N spring were predicted using the equations:

$$\begin{aligned}\vec{F} &= 48 \hat{\vec{u}} & \vec{M}^{O^t} &= \vec{r} \times \vec{F} \\ \hat{\vec{u}} &= \frac{P^f - P^t}{\|P^f - P^t\|} & \vec{r} &= P^t - O^t\end{aligned}$$

where $\hat{\vec{u}}$ is the unit vector directed along the line of action of spring force, and \vec{r} is the moment arm from the origin O^t of the tibia.

These predicted forces and moments were compared to measured ones by expressing both sets in the tibial coordinate frame. First the force \vec{F} and moment \vec{M}^{O^c} applied to the load cell by the spring were measured directly. These loads were then transformed to the tibial coordinate frame using the equation:

$$\begin{bmatrix} \vec{F}_t \\ \vec{M}_t^{O^t} \end{bmatrix} = \mathbf{A}_{(T_{trial})} \begin{bmatrix} \vec{F}_c \\ \vec{M}_c^{O^c} \end{bmatrix}$$

where $\mathbf{A}_{(T_{trial})}$ is the 6-by-6 adjoint matrix [Murray *et al.*, 1994] that varies as the tibia moves relative to the femur and load cell, and the subscripts t and c indicate that force and moment vectors are expressed in the coordinate frames of the tibia and the load cell, respectively.

Statistics

The reliability of knee kinetics and kinematics was assessed using average deviations, Analysis of Variance (ANOVA), and Bland-Altman statistics. The consistency with which loads were

applied by the MPSD was quantified by calculating the maximum deviation between a measured force (or moment) component F and its mean \bar{F} over a set of trials or knees, and then averaging it over N flexion angle increments ψ_j :

$$\overline{|\Delta F|}_{max} = 1/N \sum_j \max_i |F_i - \bar{F}|_{(\psi_j)}$$

A two-factor mixed model ANOVA with interaction [Burdick *et al.*, 2005] was used to assess the effects of ACL-transection (fixed effect) and knee-to-knee variability (random effect) on knee kinematics. Separate ANOVAs were conducted on MPSD and manual pivot-shift tests performed by each examiner. The ANOVA mean-squared error MSE was used to calculate the within-knee standard deviation ($s_w = \sqrt{MSE}$). Separate analyses were performed on the maxima of each kinematic variable, AD_{max} , IRD_{max} , PV_{max} , and ERV_{max} . Confidence intervals for the difference in values Δ between the ACL-severed and ACL-intact conditions were calculated from paired t-tests on the means of 5 trials for each knee. Effect sizes ($ES = \Delta/s_w$) and Repeatability Coefficients ($RC = 2.77s_w$) were calculated for MPSD and manual tests as measures of within-knee reliability.

Bland-Altman plots were used to assess agreement between the MPSD and manual test methods, and between the two raters. Pearson's correlation coefficients were calculated to determine whether there was a relationship between test methods or raters. The bias and 95% limits of agreement were calculated for each kinematic variable [Bland and Altman, 1999]. A three-factor mixed-model ANOVA was also performed on MPSD and manual pivot-shift tests conducted by both raters to assess the additional effect of inter-examiner variability on knee kinematics.

Unless otherwise noted, significance levels were set at $p<0.05$. Kinematic and kinematic calculations were performed using MATLAB (Mathworks, Natick, MA), and statistical analyses were performed using the MATLAB statistics toolbox.

4.4 Results

Applied Forces and Moments

The loads applied by the MPSD varied dynamically over 60° of knee flexion and were highly reproducible. On average, anterior shear F_a and internal torque M_i decreased from 16 N and 2.5 N·m to zero (Fig. 4.2). Axial compression F_c and valgus torque M_v remained relatively constant, ranging between 38-47 N and 5.5-7.4 N·m. Across all knees tested, the average deviation $|\bar{\Delta}|_{max}$ of measured loads from the mean was <5 N for forces and <1 N·m for moments (Fig. 4.2a). Within a given knee $|\bar{\Delta}|_{max}$ was <2 N and <0.3 N·m (Fig. 4.2b). Average measured load profiles differed from analytical predictions by less than 6 N and 0.7 N·m.

Pivot-shift Kinematics

MPSD and manual pivot-shift kinematics were qualitatively and quantitatively similar. For a representative knee (Fig. 4.3a), MPSD tests produced kinematic profiles that had the same basic shape as those of manual pivot-shift tests. Across all six knees tested (Fig. 4.3b), kinematic peaks always increased following ACL-transection when using the MPSD. The tibia subluxated by translating anteriorly and rotating internally by magnitudes of 6-13 mm AD_{max} and 16-25° IRD_{max} relative to its position during passive flexion. The tibia then rapidly reduced by translating posteriorly and rotating externally at speeds of 21-113 mm/s

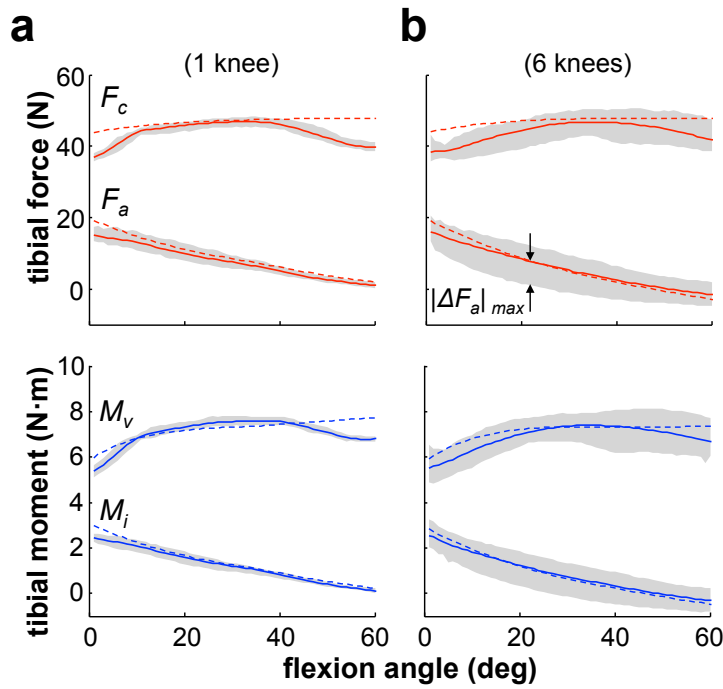


Figure 4.2: Dynamic forces and moments applied by the MPSD throughout knee flexion. Average applied forces (**top**) and moments (**bottom**) are shown for all tests conducted on one knee (**a**) and on six knees (**b**). Forces and moments were both directly measured (—), and were predicted (---) based on the predetermined spring position. Shaded areas indicate the maximum range of direct measurements. Forces: F_c =axial compression, F_a =anterior shear. Moments: M_v =valgus torque, M_i =internal torque. $|\Delta|_{max}$ =maximum deviation of measured loads from the mean.

PV_{max} and $65\text{--}267^\circ /s$ ERV_{max} . Peak subluxation magnitudes and reduction speeds were detected within $7\text{--}35^\circ$ and $29\text{--}54^\circ$ of knee flexion, respectively.

For both MPSD and manual pivot-shift tests conducted by one examiner, increases in AD_{max} , IRD_{max} , and PV_{max} (but not ERV_{max}) following ACL transection were significant (paired t-test and ANOVA). Increases ranged from 21-114% of ACL-intact values for MPSD tests and from 8-64% for manual tests. Peak values, effect sizes, repeatability coefficients, and their 95% confidence intervals are reported in Table 4.1.

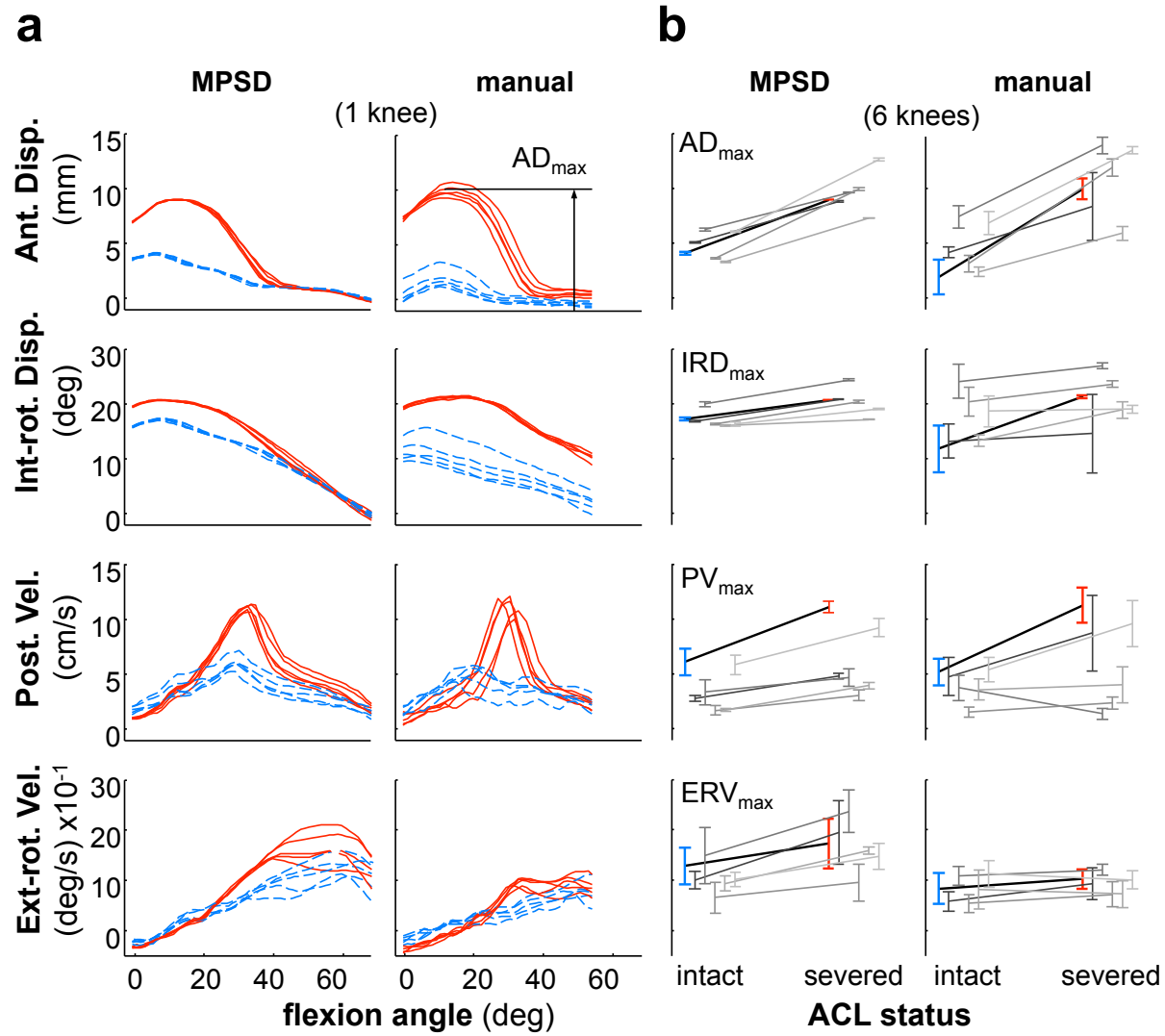


Figure 4.3: Kinematic profiles and peak values during MPSD and manual pivot-shift tests. **a)** Kinematic profiles throughout flexion are shown for five repeated trials performed on one knee before (—) and after (- -) ACL-transection. **b)** Peak values averaged across trials are shown for each of six knees before (intact) and after (severed) ACL-transection. Error bars represent $\pm 2\sigma$. AD=anterior displacement, IRD=internal-rotary displacement, PV=posterior velocity, ERV=external-rotary velocity.

The two-factor ANOVA indicated that knee-to-knee variability had a significant effect on IRD_{max} and PV_{max} for MPSD tests, and on all variables for manual tests. In both MPSD and manual tests, ACL-status by knee-specimen interaction was significant ($p \leq 0.01$). Residuals

from the ANOVA were normally distributed for all kinematic peaks except for ERV_{max} (Lilliefors test, p<0.01), in which case funneling [Burdick *et al.*, 2005] of peak values was observed with respect to ACL status.

Table 4.1: Effect of ACL transection on kinematic peaks measured by one examiner using MPSD and manual tests.

		ACL Intact		ACL Severed		Change		Effect Size		Repeatability Coef.	
		mean	(SD)	mean	(SD)	$\bar{\Delta}$	(95% CI)	$\bar{\Delta}/s_w$	(95% CI)	$2.77s_w$	(95% CI)
	AD_{max} (mm)	MPSD	4.4 (1.5)	9.4 (1.8)	5.0** (3.3, 6.7)	54.4 [†] (43.6, 65.3)	0.3 [†] (0.2, 0.3)				
		manual	4.4 (1.9)	7.2 (2.3)	2.9** (1.8, 4.0)	9.3 (7.4, 11.1)	0.9 (0.7, 1.1)				
	IRD_{max} (°)	MPSD	16.9 (1.4)	20.5 (2.5)	3.6** (1.9, 5.3)	24.3 [†] (19.5, 29.2)	0.4 [†] (0.3, 0.5)				
		manual	16.6 (3.2)	18.0 (2.9)	1.4* (0.3, 2.5)	1.5 (1.2, 1.8)	2.6 (2.1, 3.2)				
	PV_{max} (mm/s)	MPSD	23.8 (10.7)	48.9 (22.1)	25.1** (12.4, 37.8)	5.2 [†] (4.2, 6.2)	13.3 [†] (11.1, 16.7)				
		manual	73.6 (35.8)	111.8 (49.1)	38.2** (14.5, 61.9)	2.2 (1.7, 2.6)	48.4 (40.4, 60.5)				
	ERV_{max} (°/s)	MPSD	83.9 (16.2)	123.4 (44.1)	39.4 (-8.2, 87.1)	2.1 [†] (1.7, 2.5)	52.3 (43.6, 65.4)				
		manual	102.9 (38.8)	111.4 (24.4)	8.5 (-18.4, 35.5)	0.4 (0.3, 0.5)	59.0 (49.2, 73.7)				

* p<0.05 ACL intact vs. severed

** p<0.01 ACL intact vs. severed

† p<0.05 MPSD vs. manual pivot-shift

Test-method and Inter-examiner Agreement

MPSD and manual pivot-shift test methods were in good agreement with each other, and inter-examiner agreement was stronger for the MPSD than for the manual pivot-shift. Test-method agreement was assessed using data combined from both raters, averaged over 5 trials (Fig. 4.4a). Correlations between test methods ranged from $r=0.59-0.86$ ($p<0.005$) for all variables except ERV_{\max} ($r=0.12$). The mean difference between test methods (i.e. the bias) for AD_{\max} and IRD_{\max} was less than 1 mm and 1°. Only the bias in PV_{\max} was significant, and was non-constant with respect to the mean (regression: $\hat{\Delta}_{PV} = -0.7\mu + 0.8$). For all variables, the limits of agreement spanned $\pm 27-48\%$ of the overall range of measured values.

Inter-examiner agreement was assessed separately for manual and MPSD tests (Fig. 4.4b). Inter-examiner correlation coefficients ranged from 0.74-0.99 for MPSD tests and from 0.38-0.89 for manual tests. The correlation for IRD_{\max} using the manual test was not significant ($r=0.38$, $p=0.2$). The inter-examiner biases for AD_{\max} and IRD_{\max} were insignificant, at <1 mm and <1° for MPSD tests and <2 mm and <2° for manual tests. Significant bias was found for measurements of PV_{\max} and ERV_{\max} using the MPSD; and PV_{\max} using manual tests. For all variables, the limits of agreement spanned $\pm 7-38\%$ of the range of values measured using the MPSD and $\pm 27-43\%$ of the range using the manual test.

The 3-way ANOVA conducted separately on MPSD and manual datasets indicated that inter-examiner variability had a significant effect on PV_{\max} and ERV_{\max} for the MPSD, and on all variables for the manual pivot-shift.

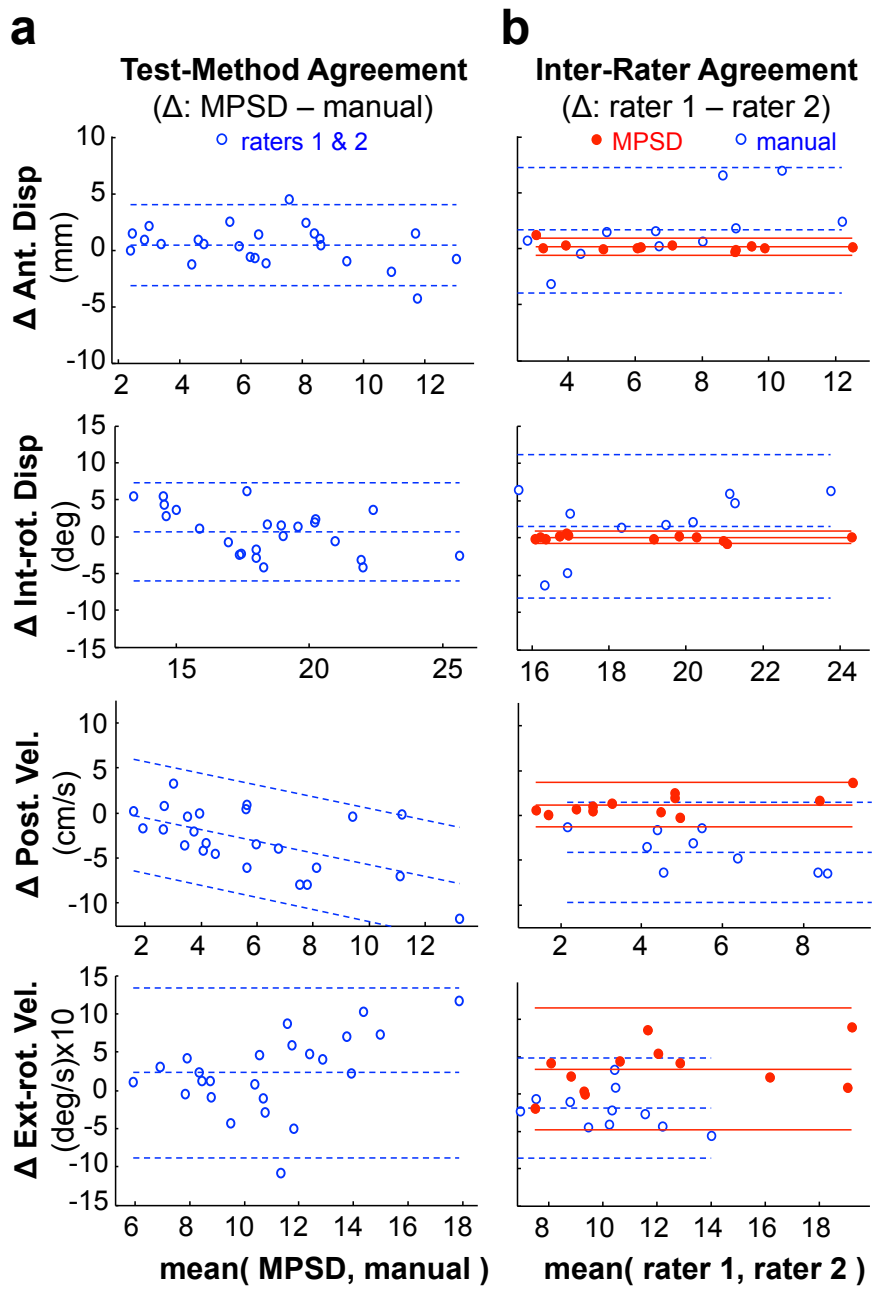


Figure 4.4: Bland-Altman plots of test-method and inter-examiner agreement. **a)** Test-method plots show the agreement between MPSD and manual measurements for tests pooled across the two raters (○). **b)** Inter-examiner plots show the agreement between two raters performing either the MPSD (●) or manual pivot-shift (○) tests. Scatter plots show the difference versus the mean for each pair of measurements, averaged across five trials. Parallel lines indicate the bias and limits of agreement.

4.5 Discussion

Key Findings

This study demonstrates that the MPSD reliably mimics the pivot-shift test by dynamically applying defined loads to cadaveric knees. The key features of the MPSD are a constant-tension spring that generates force and an ex-fix unit that holds the spring in a predetermined position relative to the tibia and femur.

In our experiments, the MPSD induced a realistic pivot-shift in knees following transection of the ACL. The overall shape of kinematic profiles was remarkably similar between MPSD and manual pivot-shift tests. Peaks in anterior and internal-rotary displacement were characteristic of tibial subluxation, while peaks in posterior and external-rotary velocity were characteristic of a sudden tibial reduction. MPSD and manual tests were in good overall agreement, as indicated by strong correlation coefficients ($r>0.5$, $p<0.005$) and small bias for all variables except for ERV_{max} . The limits of agreement were fairly broad relative to the range of values measured. However, broad limits can be attributed to variability in either of two test methods being compared [Bland and Altman, 1999].

The forces and moments applied by the MPSD were both dynamic and well-defined. At full knee extension, the line of action of the spring force was positioned laterally and oriented antero-proximally, producing an axial/anterior force and a valgus/internal torque that subluxated the tibia. Upon flexing the knee, the line of action became oriented more posteriorly, reducing the amount of anterior force and internal torque, and allowing the tibia to reduce spontaneously. Owing to the proximal orientation of the spring, it was not necessary to simulate an iliotibial band force when using the MPSD.

Because the line of action of force necessarily passes through the spring's endpoints, which were controlled experimentally, the resultant loads at the knee were well-defined. Precise positioning of the spring's endpoints within 1 cm of the predetermined locations made it possible to subject all knees to the same loading conditions within a 10% tolerance (relative to the maximum recorded force and moment components). Any given knee was subjected to the same loading conditions within a 4% tolerance.

Within knees, kinematic peak values were more repeatable for the MPSD than the manual pivot-shift test. The size of the effect of ACL-transection on kinematic peaks was 2-16 times larger for MPSD tests than for manual tests, indicating an enhanced ability to detect subtle changes in kinematics. The within-knee standard deviation of kinematic peak values was up to 7 times smaller for the MPSD than for the manual pivot-shift. The corresponding Repeatability Coefficients for AD_{max} and IRD_{max} were less than 1 mm and 1°. This measure, also known as the Smallest Real Difference, can be interpreted as “the value below which the absolute differences between two [repeated] measurements would lie with 0.95 probability” [Vaz *et al.*, 2013; Bland and Altman, 1999].

Both MPSD and manual tests exhibited good inter-examiner agreement overall, however MPSD tests were more reproducible. For both MPSD and manual tests, inter-examiner correlations were strong ($r>0.4$) or very strong ($r>0.7$) for all variables besides IRD_{max} for the manual test. We suspect that IRD_{max} values for manual tests were not correlated between raters due to differences in technique. Although AD_{max} and IRD_{max} were unbiased between raters, MPSD measurements of PV_{max} and IRD_{max} may have been biased due to differences in the speed at which the tibia was lowered. Importantly, the limits of agreement for all variables besides ERV_{max} were 2-12 times more narrow for the MPSD than for the manual test. The limits of AD_{max} and IRD_{max} spanned less than 1 mm and 1°, suggesting

that measurements between the two raters would differ by less than this amount 95% of the time.

Implications

Clinically, the pivot-shift is used to evaluate anterolateral rotational stability of the knee [Galway and MacIntosh, 1980]. Following ACL reconstruction, the presence of a positive pivot-shift is predictive of the development of osteoarthritis, failure to return to sport, patient-reported instability, and poor functional outcomes [Ayeni *et al.*, 2012; Kocher *et al.*, 2004; Leitze *et al.*, 2005]. Unfortunately, the pivot-shift maneuver is highly technique-dependent and variable among practitioners. Noyes, et al. analyzed the pivot-shift techniques of 11 surgeons and found significant differences in tibial translation and rotation [Noyes *et al.*, 1991]. Musahl et al. evaluated 12 expert surgeons and observed variations in technique, the amount of force used, and clinical grade [Musahl *et al.*, 2012a]. Thus there is a need for an ability to study pivot-shift kinematics under specified loading conditions.

Quantitative measurement tools have been used to study the pivot-shift for over 30 years [Allum *et al.*, 1984]. Anterior tibial translation is the most commonly reported kinematic variable in both static and dynamic evaluations of knee stability. Tibial rotation is also commonly reported, but has been recognized as a less reliable indicator of pivot-shift grade [Bull *et al.*, 2002; Yamamoto *et al.*, 2010; Kubo *et al.*, 2007]. Variability in tibial rotation might be due to differing amounts of internal-rotary torque applied during the pivot-shift [Bach *et al.*, 1988; Noyes *et al.*, 1991]. We measured the anterior and internal-rotary displacement of the tibia relative to its position during passive flexion. In agreement with prior studies, we observed that IRD_{max} was not correlated between raters performing the manual pivot-shift. For MPSD tests, however, IRD_{max} exhibited a strong inter-examiner

correlation, no detectable inter-examiner bias, and a significant increase following ACL transection. Thus, under consistent loading conditions, both anterior translation and internal rotation may be reliable kinematic variables.

Only under dynamic loading conditions can kinematic measures such as tibial velocity and acceleration be measured. Labbe et al. found that tibial accelerations and velocities best explained variability in manual pivot-shift recordings [Labbe *et al.*, 2010]. Translational, but not rotational components were correlated with pivot-shift grade. Many other investigators have since focused on quantifying dynamic aspects of the pivot-shift [Kuroda *et al.*, 2012; Ahldn *et al.*, 2012; Hoshino *et al.*, 2013; Labb *et al.*, 2014]. In both MPSD and manual pivot-shift tests we found that changes in posterior translational velocity (but not external-rotary velocity) following transection of the ACL were significant. MPSD measurements of PV_{max} were more repeatable within knees and more reproducible between raters than manual measurements. To the authors' knowledge, this is the first pivot-shift study employing mechanical, rather than manual, loads to report dynamic variables such as posterior translational velocity.

Other mechanical systems have been used to mimic the pivot-shift in cadaver knees. However, to the authors' knowledge, the MPSD is the first to consistently apply loads that are fully-defined in three dimensions, and vary dynamically throughout knee flexion. Early pivot-shift devices consisted of weights and pulleys that applied a laterally-directed force to the tibial shaft and a tensile force to the IT-band at either fixed or continuous degrees of knee flexion [Matsumoto, 1990; Bull *et al.*, 1999; Markolf *et al.*, 2008]. However, the combination of lateral force and IT-band tension required to produce a pivot-shift varied substantially and in some cases had to be "determined by trial and error" [Markolf *et al.*, 2008]. In contrast, the MPSD applied forces and moments to the tibia consistently between experiments without the need to simulate IT-band tension. Musahl et al. modified a continuous passive motion

machine to apply axial compression, valgus and internal torque throughout knee flexion [Musahl *et al.*, 2010c]. However, the device was originally limited by an “inability to apply known forces and moments”. It has since been improved to include a uniaxial force sensor [Petrigliano *et al.*, 2012], but the resultant forces and moments generated at the knee were not reported. In this study, the forces and moments generated by the MPSD at the knee were directly measured using a 6-axis load cell, and could also be reliably predicted without the use of a load cell. Kanamori et al. used a robotic/force-moment sensor testing system to simulate the pivot-shift by applying constant valgus and internal moments to the knee [Kanamori *et al.*, 2000]. However, these moments were applied statically “at fixed knee flexion angles”. Further, robotic systems are costly and require a dedicated laboratory space. On the other hand, the MPSD applies loads dynamically throughout knee flexion using an easily-obtainable constant-tension spring and ex-fix unit.

Static loads are not representative of a clinical pivot-shift, while poorly-defined or difficult-to-reproduce loads are not amenable to rigorous biomechanical testing. Since the MPSD meets these challenges it represents a significant advance in the ability to study the pivot-shift in a laboratory setting.

The limitations of this study include the fact that we did not control for the rate at which the knee was flexed when using the MPSD. This resulted in higher variability in PV and ERV compared to AD and IRD measurements. Flexion velocity could easily be standardized in future studies using a timer or metronome. Also, we did not measure tibial accelerations due to an inadequate sampling rate of the optical position sensor. As the MPSD is a dynamic test, we expect that tibial accelerations would help quantify the reduction phase of the pivot-shift. In our calculations we did not account for either inertial forces or the manual support load applied by the examiner. These loads were small relative to the 48 N force applied by the spring and likely contributed little to loading variability. Due to the invasive

nature of the ex-fix for attaching the spring, the MPSD is likely limited to use in cadavers. However it is conceivable that a clinical version could be designed using other means to fix a spring between the tibia and femur. Finally, manual pivot-shift tests were performed by two raters who used slightly different techniques. A standardized technique may have reduced variability in knee kinematics.

In summary, we have developed a novel mechanical device that is capable of inducing a realistic pivot-shift in cadaver knees. To the authors' knowledge this mechanical pivot-shift device (MPSD) is the first to consistently apply forces and moments that are both fully-defined and dynamic. As a result, the MPSD is highly repeatable within knees and reproducible between raters. Moreover, since the device is based on a simple mechanical principle and designed using easily obtainable components, it is readily accessible to other investigators. Thus the MPSD represents a significant advance in the ability to simulate and quantitatively study the pivot-shift as an objective indicator of joint instability.

Chapter 5

Evaluation of Physeal-Sparing Pediatric ACL Reconstruction Techniques

5.1 Chapter Overview

Conventional transphyseal anterior cruciate ligament (ACL) reconstruction techniques in skeletally immature patients have been questioned due to their potential to damage tibial and femoral growth plates (physes). Consequently, multiple alternative reconstruction options have been described to restore stability while sparing the physes. However, the degree to which these ‘physeal-sparing’ reconstruction techniques restore joint stability is poorly understood. Previously, we compared the effectiveness of different pediatric ACL reconstruction techniques under static loading conditions [Kennedy *et al.*, 2011]. However, static loads assess knee joint laxity, a measure which is poorly correlated with functional joint stability. In this study, to quantify the effect of pediatric ACL reconstructions on kinematic variables indicative of knee joint stability, we utilize the mechanical pivot-shift device to apply dynamic loads to cadaveric knees.

5.2 Introduction

Injury to the anterior cruciate ligament (ACL) is common in many sports, especially in soccer, football, basketball, and skiing. In the United States alone, over 125,000 ACL reconstructions are performed annually [Kim *et al.*, 2011b]. The incidence of ACL injuries is increasing with a more active population involved in sports and high-risk activities. As the success of ACL reconstruction has grown, the number of ACL reconstructions in skeletally immature patients has increased as well. Delay in reconstruction until skeletal maturity is often not an appropriate option, as persistent knee instability has been shown to increase the rate of meniscal injury and chondral damage [Dumont *et al.*, 2012; Graf *et al.*, 1992; Lawrence *et al.*, 2011; Millett *et al.*, 2002].

Conventional transphyseal ACL reconstruction has been questioned because of potential growth arrest and angular deformities caused by physeal damage from tunnel drilling [Kocher *et al.*, 2002]. To avoid this potential complication, multiple reconstruction options have been described to restore stability in the skeletally immature patient. All-epiphyseal (AE), transtibial over-the-top (TT), and iliotibial band (ITB) types of ACL reconstruction are the 3 most popular alternatives to the traditional transphyseal technique. Selection of the proper reconstruction technique is made more challenging by the lack of clinical evidence supporting any of the reconstruction types. Recent reviews of outcomes after ACL reconstruction for children concluded that the overall evidence supporting management options for pediatric ACL reconstructions is low [Mohtadi and Grant, 2006; Moksnes *et al.*, 2012] with no consensus on the preferred treatment option (surgical or nonsurgical) or reconstruction type.

We have previously investigated the effect of different pediatric ACL reconstruction techniques on static knee stability under uniaxial loading [Kennedy *et al.*, 2011]. In this

prior study, we found that static rotational and translational laxity were reduced by the AE and TT reconstructions to near intact levels and that internal rotation was overconstrained by the ITB reconstruction at greater than 30° of flexion. However, our loads were applied statically at fixed flexion angles; thus, it was not possible to evaluate the effect of pediatric ACL reconstructions on dynamic knee stability.

Dynamic instability of the knee is difficult to quantify and may not always be eliminated by ACL reconstructions employing traditional techniques [Markolf *et al.*, 2010b]. In a clinical setting, dynamic instability is evaluated using the pivot-shift maneuver [Lane *et al.*, 2008a]. The presence of a positive pivot shift is more predictive (than anteroposterior instability, as assessed by the Lachman test) of the development of osteoarthritis, failure to return to previous level of play, patient-reported instability, and poor subjective and objective outcomes after ACL reconstruction [Kocher *et al.*, 2004; Leitze *et al.*, 2005; Lie *et al.*, 2007]. Unfortunately, the pivotshift maneuver is highly technique dependent and variable among practitioners. Consequently, it has poor sensitivity [Bull and Amis, 1998b; Bach *et al.*, 1988] and is difficult to reproduce in a clinical or laboratory setting [Noyes *et al.*, 1991]. Past biomechanical studies have employed various instrumented devices designed to mimic the rotational instability observed in ACL-deficient knees [Bedi *et al.*, 2011; Markolf *et al.*, 2010a; Markolf *et al.*, 2008; Musahl *et al.*, 2011; Musahl *et al.*, 2010b; Musahl *et al.*, 2010c; Kanamori *et al.*, 2000]. However, in these studies, knee loads were either unknown or applied statically. Because different joint loading combinations induce distinctive kinematic behaviors, the results and their interpretation are difficult to compare between studies [Markolf *et al.*, 2010b; Musahl *et al.*, 2010a; Musahl *et al.*, 2010c; Pearle *et al.*, 2009].

To overcome these limitations, we have recently developed a mechanical pivot-shift device (MPSD) for consistently applying known dynamic forces and moments to the knee [Sena *et al.*, 2011]. The objective of the present study was to use the MPSD to extend our prior

findings with regard to pediatric ACL reconstruction to include measures of dynamic stability that may be more reflective of clinical outcomes. Further, we sought to develop a novel knee stability index (KSI) that combines the multiple MPSD outcome measures into a single continuous value between 0 (intact) and 100 (deficient). We hypothesized that all pediatric reconstructions would restore individual knee stability measures to intact levels and that the KSI would discriminate stability patterns between reconstruction techniques.

5.3 Methods

Specimen Preparation

Six fresh-frozen left and right human cadaveric knees were used (4 female, 2 male; average age, 54 years). Legs with major structural bony and ligamentous abnormalities were not considered. Specimens were stored at 50°C and thawed at room temperature for 12 hours before testing. The tibia and fibula were cut 3 cm proximal to the tibiotalar joint so that the longitudinal axis of the tibia could be accurately localized, and the femur was cut at the neck so that it could be properly potted. Soft tissue was stripped from the proximal femur, leaving intact tissue 20 cm proximal to the joint line. The proximal femur was then secured in a custom-made cylindrical container with Smooth Cast 300 (Smooth-On Inc, Easton, Pennsylvania). The potted specimens were mounted on a base plate that was securely attached to the rigid platform.

Application of MPSD

The MPSD consists of a single constant-tension spring (48 N) that crosses the knee along the lateral aspect of the leg and applies a reproducible combination of axial compression,

valgus torque, and internal torque throughout manual knee flexion (Figure 5.1) [Sena *et al.*, 2011]. This spring ends are rigidly attached to the femur and tibia using an external fixation system (Synthes, Paoli, Pennsylvania), which allows for precise positioning of the line of force acting across the knee. With the knee extended, the constant tension spring initially produces an internal rotatory torque of 2.5 N·m, valgus torque of 5.5 N·m, and axial compression of 38 N. As the knee is flexed to 60°, the spring approaches the mid-portion of the knee (from anterior to posterior), reducing the internal torque to approximately 0 N·m while maintaining the valgus and axial loads.

During testing, knee kinematics were recorded using the Optotrak (NDI Inc, Waterloo, Canada) navigation system that consists of a 3-aperture position sensor (accuracy, 0.1 mm and 0.1°), 2 infrared strobing marker clusters attached to the tibia and femur using Schanz screws (Synthes), and a handheld digital probe for registration of reference points. This system has been previously validated and used in biomechanical studies by our laboratory [Kennedy *et al.*, 2011]. Femoral and tibial origins were defined at the femoral intercondylar notch and center of the tibial plateau; *x*-axes coincided with the longitudinal bone axes; and points on the medial epicondylar eminence and proximal tibial ridge defined the *xz* and *xy* planes of the femur and tibia, respectively (Figure 5.1, inset). The points at which the constant-tension spring attaches to the tibial and femoral rods were registered to ensure consistent spring placement between each specimen.

To facilitate proper positioning of the constant-tension spring, a series of clamps and rods were attached separately to the lateral side of the tibia and femur using a surgical external fixation system. Pin clamps with outrigger posts were rigidly secured to the bone using Schanz screws. Carbon fiber rods were then mounted on the posts using small swivel clamps, which allowed the rods to be positioned freely in space. Finally, the constant-tension spring was attached to the tibial and femoral rods. Before the experiment, the 3-dimensional

coordinates of the spring attachment points between the rods were digitally registered using the Optotrak handheld probe. This step was essential, as it allowed for positioning of the spring attachments within 1 cm of a chosen location relative to the tibia and femur. Precise placement of the spring ensured that forces and moments were applied consistently between tests.

Measurement of Knee Kinematics

As each knee was taken through a range of flexion, ψ , the joint configuration was represented as a set of tibial translations $T(\psi) = \{T_x, T_y, T_z\}$ and rotations $R(\psi) = \{R_\theta, R_\phi\}$ of the tibia relative to a full-extension reference configuration, where θ and ϕ were the abduction/adduction and internal/external rotation angles, respectively. To quantify the magnitude of the subluxation phase of the pivot-shift event during MPSD loading, anterior displacement (AD) and internal rotation (IR) of the tibia were calculated relative to intact passive flexion. To quantify the speed of the reduction phase, posterior translational velocity (PTV) and external rotational velocity (ERV) were calculated relative to the femur. Data were recorded using the Optotrak and processed using custom MATLAB code (MathWorks, Natick, Massachusetts).

The primary outcome variables were maximum AD (AD_{max}), maximum IR (IR_{max}), maximum PTV (PTV_{max}), and maximum ERV (ERV_{max}). The MPSD tests were performed in triplicate for each knee, with the reconstruction and testing order randomized between knees to eliminate bias. In addition, between each reconstruction and at the end of testing, knees were taken through passive flexion to ensure that the measured motions in the ACL-deficient knee state were consistent (i.e. that the markers were not bumped during the reconstruction procedure).

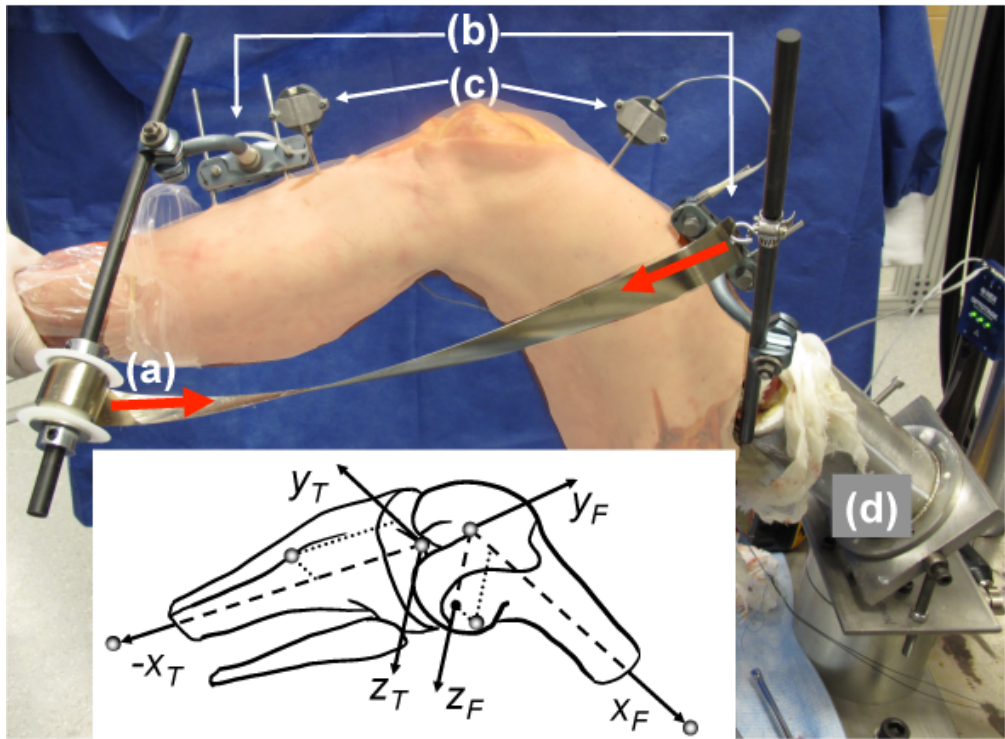


Figure 5.1: Mechanical pivot-shift device and measurement coordinate system. A constant-tension spring (**a**) was held rigidly in a predetermined position relative to the tibia and femur by external fixators (**b**). Optotrak smart markers (**c**) attached to the tibia and femur enabled the tracking of tibiofemoral motion. Potted specimens were mounted on a hinged testing base (**d**) to allow for free rotation in the sagittal plane during manual testing. Inset: Coordinate systems (tibia/femur) were constructed by defining an origin (center of tibial plateau/top of intercondylar notch), a long axis (distal tibial shaft/proximal femoral shaft), and a plane point (anterior tibial ridge/lateral femoral epicondyle). Using a Z_F - Y - X_T Euler angle convention, rotations are defined about the fixed Z_F (flexion), floating Y (valgus), and fixed X_T (external) axes for a left knee.

Surgical Technique

A medial arthrotomy was made to expose the tibiofemoral joint for digitization of landmarks and for surgical transection of the ACL. After the MPSD data in the intact state were collected, the ACL was transected and removed from the notch to reduce the chance of

impingement. Care was taken to preserve the posterior cruciate ligament attachments. Then, after data were collected in the ACL-deficient state, tunnels for each of the reconstructions were drilled in each knee so that only graft fixation needed to be performed between repeated MPSD measurements on each knee.

The all-epiphyseal (AE) and transtibial over-the-top (TT) reconstructions were performed using an autogenous doubled hamstring tendon graft as described previously [Kennedy *et al.*, 2011]. The semitendinosus tendon was deemed to be of adequate quality and size for solitary use. The average graft size was 8 mm (range: 7-9 mm). The grafts were prepared by removing excess muscle, placing over a continuous-loop EndoButton (Smith & Nephew, Andover, Massachusetts), and whip-stitching the proximal ends with free suture. The iliotibial band (ITB) reconstruction was performed using autogenous iliotibial band tissue [Kocher *et al.*, 2005]. In all cases, graft fixations were backed up with a post, and grafts were marked with a tissue-marking pen to check against slipping.

The AE reconstruction (Figure 5.2a) was performed by drilling epiphyseal tunnels into both the femoral and tibial sides [Anderson, 2003]. The femoral tunnel was positioned at the anterior aspect of the ACL footprint, and a guide wire was placed using an ACL aiming guide (Arthrex, Naples, Florida) set at 75°. Fluoroscopy was used to confirm tunnel position. Upon confirmation of adequate positioning in the femoral epiphysis, an appropriately sized reamer was used to overream the tunnel. Tibial tunnel placement was accomplished with a tibial guide positioned with one end centrally in the ACL tibial footprint and the other end in the tibial epiphysis 12 mm distal to the joint line and 15 mm medial to the medial border of the patellar tendon. Satisfactory positioning was confirmed with a guide wire, and an 8-mm tunnel was reamed. The EndoButton and graft were passed, and the EndoButton was flipped. The knee was then flexed to 30° and the graft cycled, tensioned, and secured

distally to the tibial metaphysis with a staple (Arthrex) before tying over a post as back-up fixation.

The TT reconstruction (Figure 5.2b) utilized a tunnel on the tibial side with an over-the-top configuration on the femoral side [Andrews *et al.*, 1994; Kim *et al.*, 1999]. The tibial tunnel was placed using a tibial aiming guide set at 50° and positioned in the central portion of the ACLs tibial footprint and at a point 3 cm distal to the joint line and 6.5 mm medial to the medial border of the patellar tendon. After correct positioning was confirmed with a guide wire, an 8-mm reamer was used to drill the tunnel. Careful soft tissue dissection was performed on the femoral side to prepare it for an over-the-top graft position. The graft was passed through the tibial tunnel to the appropriate overthe-top position, where it was secured on the lateral aspect of the femur with a staple and back-up fxiation with the sutures tied over a post. The knee was then flexed to 30°, and the graft was tensioned and fixed to the tibial metaphysis with a staple and then tied over a post.

The ITB reconstruction utilized autologous iliotibial band tissue (Figure 5.2c) as a physeal-sparing technique as described by Kocher et al [Kocher *et al.*, 2005]. Using an oblique incision centered over the lateral joint line, the iliotibial band was dissected free proximally and distally, maintaining its attachment at Gerdy's tubercle. An anterior and posterior incision were made in the iliotibial band at the joint line and extended proximally to the desired graft length. Graft preparation was completed with a whip-stitch at the free end. With the knee in 90° of flexion, the graft was secured to the lateral femoral condyle with a staple and then passed into the joint under the intermeniscal ligament. The graft was then pulled through the notch and placed in an over-the-top position. The knee was positioned in 20° of flexion, and the graft was secured to the tibia just distal and medial to the tibial tubercle with a staple and tied over an adjacent post for back-up fixation.

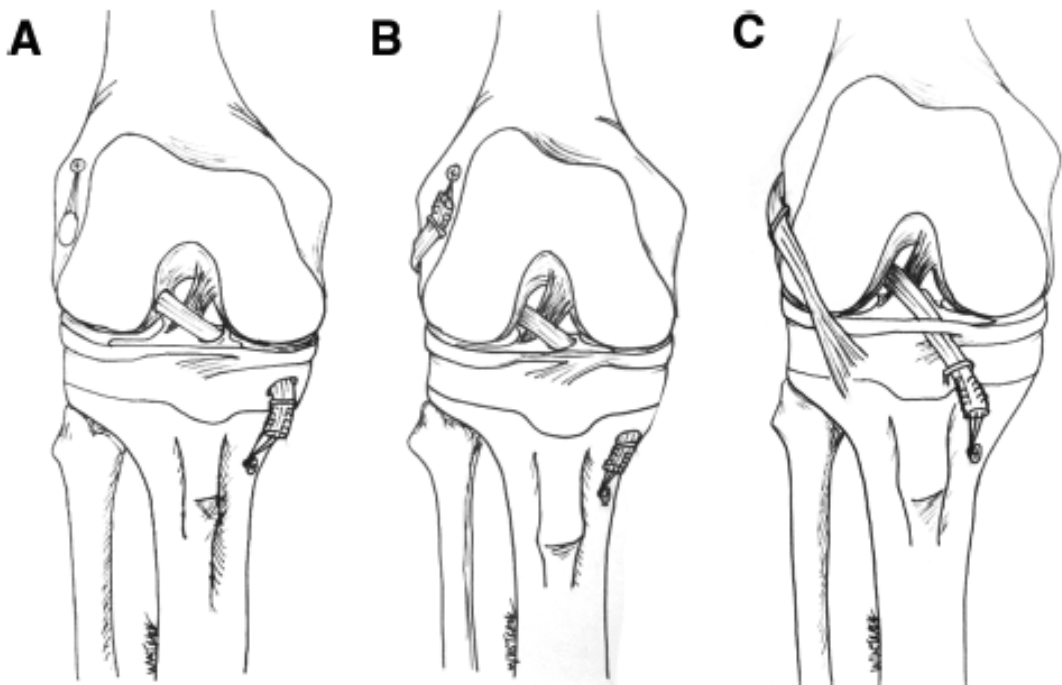


Figure 5.2: Physeal-sparing ACL reconstruction techniques. (A) All-epiphyseal reconstruction. The tunnels were placed in the femoral and tibial anterior cruciate ligament (ACL) attachments and drilled to stay within the epiphysis. The graft was secured on the femur with an EndoButton and post and on the tibial side with a staple and post. (B) Transtibial over-the-top ACL reconstruction. The graft was secured on the femoral and tibial sides with a staple and post. (C) Iliotibial band ACL reconstruction. The graft was secured first on the femur with a staple and then tensioned appropriately and secured to the tibia with a staple and post. Figure reprinted with permission from Kennedy et al. [Kennedy et al., 2011] *Am J Sports Med.* ©2011 AOSSM.

Determination of KSI

The KSI is an algebraic formula that combines weighted MPSD outcome measures into a single numeric value. Logistic regression procedures in JMP (version 10, SAS Institute, Cary, North Carolina) were used to calculate probabilities for the categorical response (intact vs ACL injured) as predicted by the set of continuous measurement variables (AD_{max} , IR_{max} , PTV_{max} , and ERV_{max}). The logistic regression output provides weighting coefficients for each measurement variable plus an intercept term. The resulting algebraic formula comprises the

KSI algorithm, which maps kinematic peak values to a single continuous number between 0 and 100 for knee-assessing stability. The value 0 corresponds to the intact knee with the lowest kinematic peak values, while 100 corresponds to the deficient knee with the largest kinematic peak values. The KSI was applied to the outcome measurements obtained from each of the ACL-reconstructed legs to quantify which procedure best matched the intact state.

Statistical Analysis

An a priori power analysis was performed with a 10% difference in AD_{max} as a primary outcome variable. With type-I and type-II error rates of 5% and 10%, 5 knees were calculated to be necessary to determine a statistically significant difference between testing states based on previous data. Statistical analysis was performed using the MATLAB Statistics Toolbox (version 2009a, MathWorks) and JMP. A repeated-measures analysis of variance (ANOVA) without knee-by-state interaction was used to determine the effects of the different reconstruction techniques on knee kinematics. Significance was set at $p<0.01$. Data are presented as the mean \pm standard deviation. Repeatability and reproducibility were quantified by calculating the maximum absolute deviations of measured values from trial means and knee means, respectively.

5.4 Results

There were no graft failures or failure of fixation during the testing. One of the 6 knees was not fully included in the analysis because the Optotrak markers were bumped during the TT reconstruction procedure. After ACL transection, the MPSD produced a pivot-shift event characterized by an anterior and internal rotatory subluxation (AD and IR peaks) observed

between 10° and 30° of flexion, followed by a posterior and external rotatory reduction (PTV and ERV peaks) between 40° and 60° of flexion (Figure 5.3). The ACL reconstruction reduced the magnitude of the tracings for each kinematic variable compared with the ACLdeficient tracings.

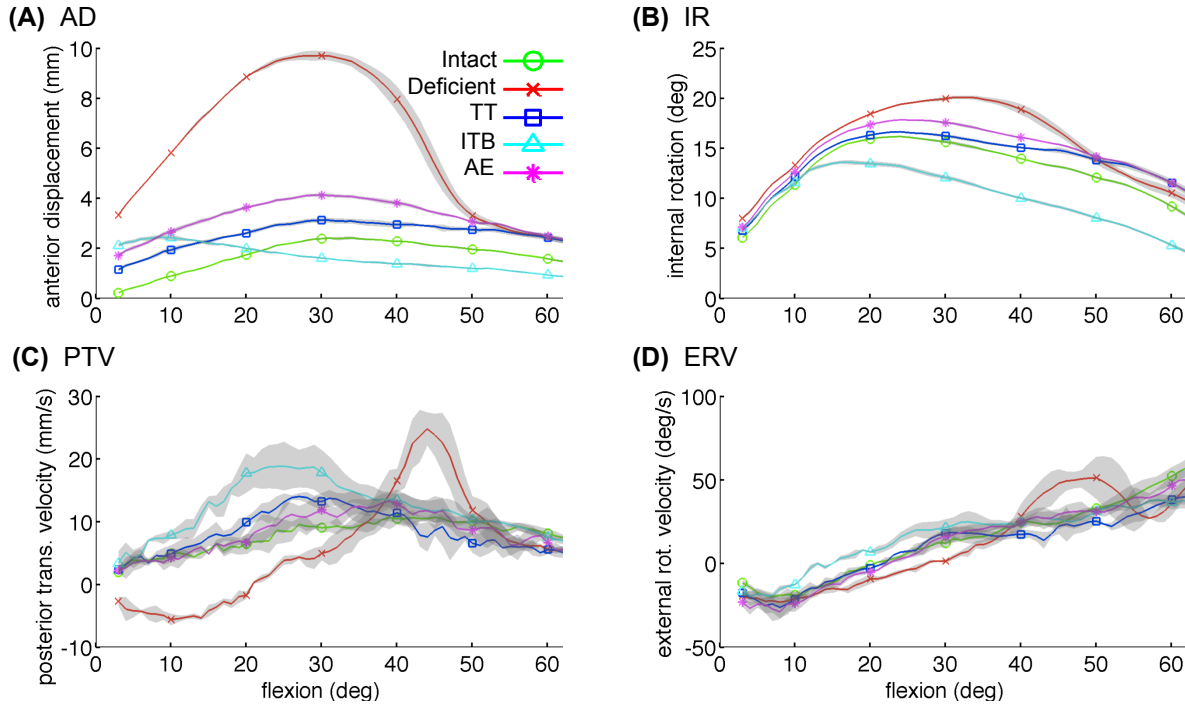


Figure 5.3: Kinematic tracings for a single knee under continuous mechanical pivot-shift device loading before and after anterior cruciate ligament (ACL) transection and after pediatric reconstruction. Representative tracings of anterior displacement (**A**) and internal rotation (**B**) of the tibia relative to intact passive flexion and posterior translational velocity (**C**) and external rotational velocity (**D**) of the tibia relative to the femur. In the ACL-deficient state (-×-), the pivot-reduction event can be seen between 40° and 50°. Lines and shaded areas represent the mean±standard deviation for 3 repeated tests in each of the 5 knee states. Line symbols are drawn at 10° intervals for clarity.

Knee kinematic tracings under MPSD loading were highly repeatable within knees. For the representative tracings in Figure 5.3, the maximum deviations from the mean of 3 repeated trials (% range) were 0.7 mm (9%) AD; 0.7° (6%) IR; 5.8 mm/s (17%) PTV; and

$19.0^\circ/\text{s}$ (21%) ERV. Kinematic peak values were fairly reproducible between knees as well. Across 5 knees, the maximum deviations from the mean peak value (% overall maximum) were 3.5 mm (28%) AD_{\max} ; 7.0° (28%) IR_{\max} ; 27.3 mm/s (36%) PTV_{\max} ; and $63.5^\circ/\text{s}$ (34%) ERV_{\max} .

The ACL transection increased kinematic peak values from intact levels by a magnitude (% change from intact) of 5.0 mm (113%) AD_{\max} , 3.6° (21%) IR_{\max} , $25.1^\circ/\text{s}$ (104%) PTV_{\max} , and 40.1 mm/s (48%) ERV_{\max} (Figure 5.4). With respect to the deficient state, all reconstructions significantly reduced kinematic peak values, except for ERV_{\max} for the TT reconstruction ($p<0.05$). Only the ITB reconstruction significantly reduced AD_{\max} and IR_{\max} beyond intact levels by 2.3 mm (52%) and 6.4° (38%), respectively. On average, the TT reconstruction most closely restored AD_{\max} and IR_{\max} relative to intact levels to within 0.2 mm (5%) and 1.1° (6%). Additionally, the TT reconstruction restored PTV_{\max} and ERV_{\max} to within 3.9 mm/s (16%) and $17.8^\circ/\text{s}$ (21%). On the other hand, the AE reconstruction most closely restored PTV_{\max} and ERV_{\max} to within 2.1 mm/s (9%) and $0.8^\circ/\text{s}$ (1%), respectively.

The logistic model for the KSI fit the data well ($R^2 = 1.0$; $p = 0.002$):

$$KSI = -2.28IR' + 4.00AD' - 0.30ERV' + 2.46PTV'$$

where IR' , AD' , ERV' , and PTV' were the differences between the treated and intact tests for each knee. The mean KSI for the ACL-deficient state was 61.7 ± 22.2 (range: 47-100), while the ITB reconstruction had a mean KSI of 0.82 ± 24.0 (range: 24 to 35), the TT reconstruction had a mean KSI of 13.3 ± 8.9 (range: 0.3-23), and the AE reconstruction had a mean KSI of 4.0 ± 15.2 (range: 24 to 14). The KSI was not different between reconstructions, and all were significantly lower than the ACL-deficient state ($p<0.0001$).

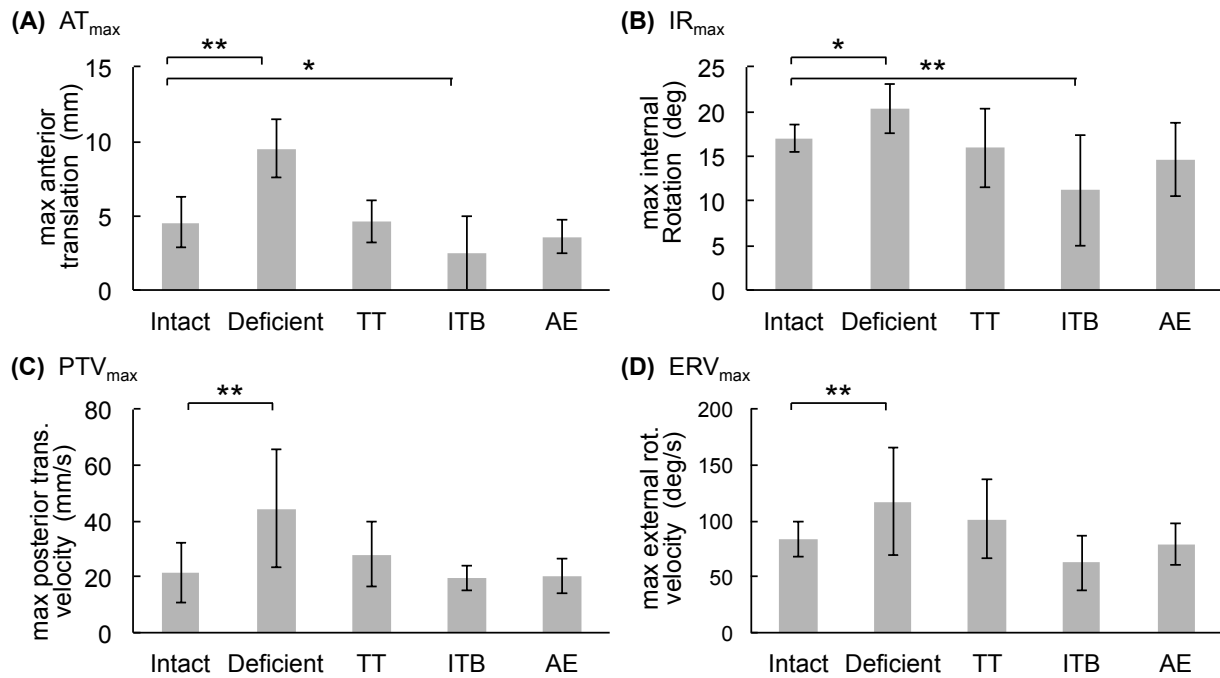


Figure 5.4: Mean kinematic peaks across 6 knees before and after anterior cruciate ligament (ACL) transection and after pediatric reconstruction. AD_{\max} (**A**) and IR_{\max} (**B**) were significantly lower for the iliotibial band reconstruction versus the intact state. AD_{\max} , IR_{\max} , and also PTV_{\max} (**C**) were significantly lower in all reconstructed states versus the deficient state. ERV_{\max} (**D**) for the transtibial over-the-top reconstruction was lower but not significantly ($p<0.05$). All kinematic variables were significantly higher in the ACLdeficient knee state versus the intact state. Repeated-measures ANOVA, Bonferroni adjustment for multiple comparisons. * $p<0.01$. ** $p<0.001$.

5.5 Discussion

The purpose of this study was to biomechanically evaluate the stabilizing effect of several pediatric ACL reconstruction techniques using a novel MPSD, which reproducibly mimics a pivot shift through the application of standardized dynamic loads. All reconstruction techniques tested were able to improve stability measures relative to the ACL deficient state by some degree. Consistent with our previous findings [Kennedy *et al.*, 2011], the ITB reconstruction was found to overconstrain AD_{\max} and IR_{\max} . On average, the TT

reconstruction most closely restored AD_{max} and IR_{max} toward intact levels. However, the TT reconstruction did not significantly reduce ERV_{max} from deficient levels. On the other hand, the AE reconstruction restored AD_{max} and IR_{max} and also most closely restored PTV_{max} and ERV_{max} toward intact levels. Further, the AE reconstruction exhibited the lowest KSI, a logistic regressionbased linear combination of all 4 measured dynamic knee stability metrics.

Over the previous 2 decades, a strong emphasis has been placed on the benefits of youth participation in sports. However, with an increase in youth participation, the rate of ACL injury is expected to grow. In skeletally immature patients, nonoperative management leads to an increased risk of meniscus and cartilage injuries [Dumont *et al.*, 2012; Graf *et al.*, 1992], and therefore, surgical reconstruction is often recommended for those patients who wish to remain active in sports. Although it has not been proven that drilling across the physis will result in angular growth deformities or growth arrest, many surgeons opt for techniques to avoid this potential complication, especially in younger patients [Kocher *et al.*, 2002]. The best techniques for pediatric ACL reconstruction, from a biomechanical standpoint, should restore dynamic stability of the knee and limit the risk of further injury.

We found that the AE, TT, and ITB physeal-sparing reconstructions were each able to improve kinematic measures of rotational and translational stability relative to ACL-deficient knees under dynamic MPSD loading. Thus, each reconstruction type may successfully restore dynamic stability to some degree. However, the ITB reconstruction significantly reduced AD and IR beyond intact levels. The implications of overconstraining the knee in a juvenile population require further study. These two findings were consistent with our previous evaluation of static knee stability under uniaxial loading conditions [Kennedy *et al.*, 2011]. Another finding was that, although the TT reconstruction most closely restored AD_{max} and IR_{max} toward intact levels, it did not restore PTV_{max} and ERV_{max} by the same degree (to within 6% vs to within 21%). Correspondingly, 4 of the 6 TT-reconstructed knees included

in this study exhibited noticeable spikes in PTV and ERV between 35° and 60° of flexion. The dynamic KSI reflects the above findings, as the KSI for the TT reconstruction was highest (13.3, where 0 = intact and 100 = deficient) of the 3 reconstructions evaluated.

Unlike the TT reconstruction, the AE reconstruction closely restored PTV_{max} and ERV_{max} to within 9% of intact levels in addition to restoring AD_{max} and IR_{max}. Accordingly, the KSI value for the AE reconstruction was the lowest (4.0). The AE reconstruction is the most anatomically correct in terms of restoring the ACL footprint anatomy and has been shown recently to improve tibiofemoral contact in a cadaveric study [Stonestreet *et al.*, 2012]. As the most anatomic reconstruction, it makes sense in a biomechanical context that the AE reconstruction would restore dynamic knee stability. This conclusion is supported by previous adult ACL reconstruction studies in which anatomic reconstructions were found to better restore knee stability compared with nonanatomic reconstructions [Kim *et al.*, 2011a; Sohn and Garrett, 2009].

Defining clinically relevant and reproducible measures of dynamic knee stability is a major challenge in orthopaedic research. Clinically, the pivot shift is utilized to assess dynamic stability. Although it has been correlated with clinical outcomes in multiple studies [Kim *et al.*, 2011a; Ochiai *et al.*, 2012], the test is poorly sensitive and variable among practitioners [Bull and Amis, 1998b]. In an effort to make the pivot shift more reliable, researchers have developed various instrumented devices that either mimic the test or produce quantitative outputs [Bedi *et al.*, 2011; Markolf *et al.*, 2010a; Markolf *et al.*, 2008; Musahl *et al.*, 2011; Musahl *et al.*, 2010b; Musahl *et al.*, 2010c; Kanamori *et al.*, 2000]. However, in these studies, knee loads were either applied statically, or they are unknown. Static loads do not reflect the dynamic nature of the manual pivot-shift test, and unknown loads are not amenable to biomechanical testing. Therefore, there has been a need for a simple laboratory tool that

applies both dynamic and known pivot-shift loads to the knee over a continuous range of flexion angles.

The MPSD is a simple mechanical device composed of 2 external fixation units and a constant-tension spring. It applies known and reproducible loads that reproduce the complex kinematics of a pivot shift in an ACL-deficient knee [Sena *et al.*, 2011]. In this study, the MPSD was able to elucidate differences in clinically relevant kinematics between pediatric ACL reconstruction techniques. We chose 4 primary variables as our key parameters to study rotational and translational kinematics of the knee. Two variables quantified displacements of the tibia (AD_{max} and IR_{max}), which characterize the subluxation phase of the pivot shift. Two variables also quantified velocities of the tibia relative to the femur (PTV_{max} and ERV_{max}), which characterize the reduction phase of the pivot shift. The choice of these primary outcome variables was based on recent studies that evaluated different components of the pivot shift to determine the factors that are responsible for the instability. Rotational and translational tibial displacements have been consistently described in other studies of pivot-shift kinematics. Lane *et al.* [Lane *et al.*, 2008b] found that anterior tibial translation and tibial rotation had a high correlation between examiners and the ACL state in a clinical study of the pivot shift. Similarly, Yamamoto *et al.* [Yamamoto *et al.*, 2010] found a high degree of anteroposterior displacement and pivot-shift grade in a clinical study. On the basis of these results, we used both AD_{max} and IR_{max} to quantify displacements. We found that the MPSD was able to induce AD and IR repeatability between trials (within 9% of trial means) and reproducibly between knees (within 28% of knee means). Labbe *et al.* [Labbe *et al.*, 2010] performed a principal component analysis on manually applied pivot-shift tests and found that angular velocity accounted for the most variability. We found that PTV_{max} in the ACL-deficient knee increased more than 2-fold compared with the intact state. Similarly, ERV_{max} increased significantly in the ACL-deficient state compared with the intact state,

although not by such a high amount (48%). Although Labbe et al. [Labbe *et al.*, 2010] and others [Ahldn *et al.*, 2012; Lopomo *et al.*, 2010] suggest that acceleration be evaluated as well, we did not analyze accelerations in this study. Future studies will explore the ability to use acceleration as an additional outcome variable.

A primary limitation of many of the biomechanics studies of knee kinematics is that they take a complex motion such as the pivot shift and analyze the components separately rather than as part of a composite kinematic signature. A composite signature could provide a better framework for understanding how multiple kinematic variables contribute to overall knee stability. The algorithm based approach to combine multiple joint motions into a comprehensive score has been described previously in the knee, albeit with different input variables than the ones we used [Labbe *et al.*, 2011b]. In this study, we introduced the KSI as a novel method to quantify a complex kinematic motion such as the pivot shift. The premise behind the KSI is that MPSD measurements provide independently valuable information regarding knee stability. To form the KSI, stability measurements were weighted (because their discriminatory value is likely not equivalent) and combined into an algebraic formula that produced a single quantitative stability metric that distinguishes the intact knee state from the deficient state. Although we obtained the best discrimination between intact and deficient states when all 4 kinematic variables were included in the model, we observed a degree of multicollinearity between our 4 kinematic variables. Additionally, because of the small sample size, the KSI values for the TT, ITB, and AE reconstructions were not significantly different from each other. Nonetheless, the KSI results were consistent with those from the 4 independent stability measures. The AE reconstruction appeared to best restore knee stability to the intact state, as it had the lowest KSI value and most closely restored PTV_{max} and ERV_{max} . In contrast, the TT reconstruction had the highest KSI value and was the least effective in reducing PTV_{max} and ERV_{max} from deficient levels. Clearly,

more studies are needed to confirm the validity of the KSI in a clinical population. However, we anticipate that it will be a powerful tool for objectively quantifying dynamic knee stability in the future.

There were several limitations to this study. We used adult specimens to study a pediatric reconstruction technique because of restrictions in obtaining young cadaveric specimens. There are likely important differences in kinematics between skeletally immature and mature specimens that we could not assess in this study. However, we hypothesize that the overall kinematic responses to ACL transection and reconstruction are the same in both groups. Nonetheless, the present results may not be generalizable to all pediatric patients, especially very young patients. Further study is merited. Next, we performed time-zero tests that do not take into account factors such as graft changes during healing or secondary stabilizers of the knee. This is particularly important when considering the ITB reconstruction, which requires a significant amount of soft tissue healing on the surfaces of the tibia and femur. Another limitation was that the MPSD is a novel technique that has been studied in our laboratory but has not been validated across multiple investigators. This limitation is true of many of the other current techniques used to study instability of the knee [Markolf *et al.*, 2010a; Musahl *et al.*, 2010c]. The primary functional limitation of the MPSD is that knee flexion is manual, and thus, the flexion rate is not inherently standardized. As a result, PTV and ERV were more variable than AD and IR. As PTV and ERV are directly dependent on flexion rate, we will attempt to standardize it in future studies. Kinematic data were collected at 50 Hz, which is also a minor weakness of this study. Increasing the sampling rate will improve future velocity estimates and allow us to calculate accelerations. Graft fixation can be problematic during biomechanical testing. However, in this study, we used the MPSD to apply less than physiological loads (50 N, 10 N·m). In addition, we doubly fixed the grafts on either side of the knee. Thus, we saw no evidence of graft loosening or failure during the

experimental procedure. Despite these limitations, the biomechanical results of this study confirm several characteristics of the pediatric ACL reconstruction techniques that have been reported clinically but never tested biomechanically.

In summary, we used a novel MPSD to evaluate the dynamic stability provided by 3 common physeal-sparing ACL reconstruction techniques. The MPSD applies dynamic forces and moments to cadaveric knees in a reproducible manner. While all techniques improved knee stability, our data suggest that the AE technique best restores dynamic stability of an ACL-deficient knee. Although this is an important first step in determining the best treatment option for pediatric ACL reconstruction, the decision is multifactorial and must be based on age, anatomic considerations, and desire to return to play. Objective clinical outcomes following these reconstruction techniques will help determine the optimal treatment strategy.

Chapter 6

3D Marker-based Motion Capture Using Inexpensive Depth Cameras

6.1 Chapter Overview

New consumer 3D-camera technology like the Microsoft Kinect™ has made realistic-looking markerless motion capture widely accessible. However, since markerless motion-tracking was designed to be robust (for gaming) rather than accurate, it may not be suitable for clinical use. The majority of published clinical movement analysis research is based on the paradigm of marker-based motion capture. However, research-grade camera systems are difficult to use and prohibitively expensive for routine clinical use. To enable routine 3D clinical motion capture, there is a need to bridge the gap between consumer 3D cameras and research-grade multi-camera systems. In the following two studies we present a promising intermediate approach that combines a Kinect camera and marker-based motion capture techniques. Using research-grade motion capture systems as a reference, we then compare this approach to markerless motion capture.

6.2 Introduction

Clinical assessments of joint function and injury risk that rely on observational or video-based movement analysis are qualitative and subjective. If used routinely in a clinical setting, a quantitative and objective movement analysis technology would have the potential to: deepen the scientific and clinical knowledge base of joint function and injury risk, help practitioners effectively communicate with patients regarding their functional status, and enable quantitative documentation of injury and recovery with respect to normative data.

Current technologies that enable quantitative movement analysis include marker-based, and more recently, markerless 3D motion capture. Marker-based 3D movement analysis systems are typically used in a laboratory setting for clinical and biomechanical research. These systems utilize multiple cameras to measure and track the 3D position of active strobing infrared LEDs or passive infrared reflectors placed on an individual's body. Although the research applications of marker-based movement analysis are broad, clinical applications are limited. The most common clinical indication for 3D movement analysis is Cerebral Palsy, for which its use is well supported [Wren *et al.*, 2011a]. For example, orthopaedic surgeons utilizing gait reports made significantly different treatment decisions than surgeons without such reports (by 20%, $p<0.01$), in terms of choosing whether or not to operate on children with cerebral palsy [Wren *et al.*, 2011b].

The emergence of inexpensive 3D-cameras like the Microsoft Kinect has recently made 3D motion capture more accessible. The Kinect and similar “depth” cameras use structured light, time-of-flight, or other range-imaging technology to reconstruct a 3D representation of an environment from a single viewpoint. Based on that representation, computer vision algorithms can recognize static 3D geometries and dynamic human body position. The applications of depth cameras are broad, ranging from computer animation to robotic feedback

and control [Han *et al.*, 2013]. This technology is highly accessible due to the fact that hardware is compact and inexpensive, and 3D recognition algorithms are fast and robust.

Unfortunately, marker-based and markerless 3D motion capture systems are either too expensive or inaccurate to use routinely in the clinic. Marker-based motion capture systems require multiple expensive cameras, a dedicated laboratory space, and trained personnel. Researchers today face many of the same challenges they did more than twenty years ago such as time-consuming camera calibration and manual marker labeling [Davis, 1988]. These difficulties have limited the number of patients that could potentially benefit from quantitative motion analysis.

Meanwhile, current markerless motion capture methods based on depth cameras do not meet the stringent requirements of clinical research. The human body models produced by this technology, while anatomically realistic, are not necessarily biomechanically accurate (especially for the lower extremity). More importantly, the algorithms used to generate such models are “black-box” in nature, and may mask important differences in kinematics between individuals. Thus, new movement analysis technologies that are both accessible (inexpensive and easy to use) and accurate (validated and tied to the literature) are needed.

We have developed a novel movement analysis technique that combines the accessibility of depth cameras with the accuracy of marker-based 3D motion capture. We use depth and infrared images from a Kinect sensor together with retroreflective markers to track the 3D position of specific anatomical landmarks. The key features of this approach are that in the infrared image, retroreflective markers are visible with high contrast; kinematic variables can be calculated from 3D marker coordinates using established methods; and markerless models of the human body from the same sensor can be used as a template to facilitate marker identification and tracking.

6.3 Marker-based Motion Capture using the Microsoft Kinect

The objective of this study was to determine the accuracy and precision of our a new marker-based Kinect motion capture technique during a two-legged squat task. The Optotrak Certus motion capture system was used as a standard for comparison.

Methods

A shared reference coordinate system was defined by placing three markers on a stationary object ~3 m in front of the Optotrak and Kinect (Figure 6.1b). Marker positions were registered using the Optotrak digitizing probe and a manual digitizing routine (Kinect). Thin plastic discs ($\phi 12$ cm) served as rigid bodies for attachment of an Optotrak optical tracking array and an marker (1 pair per disc). Marker positions on each disc were manually registered at the start of the experiment using the Optotrak probe. Markers were identified automatically by the Kinect using an algorithm developed by the authors. Since both active and passive markers were fixed on each disc, the tracking performance of the same rigid bodies could be compared between both systems.

A male subject facing 45° from the Kinect performed four squats within an 6 s time span. Discs were attached to a subjects right hip, knee, and ankle using velcro straps such that each marker was roughly aligned with the iliac crest, lateral epicondyle, and lateral malleolus, respectively. Data collected by the Optotrak at 100 Hz and by the Kinect at 30 Hz were temporally matched by manual alignment.

Error analysis was performed for the hip, knee, and ankle markers during the 4-squat experiment. Systematic error was defined as the raw difference between the Kinect and Optotrak 3D position data ($\vec{S} = \vec{p}_{\text{kin}} - \vec{p}_{\text{opt}}$). Random error was defined as the difference between Kinect and transformed-Optotrak data ($\vec{R} = \vec{p}_{\text{kin}} - \mathbf{G}\vec{p}_{\text{opt}}$), where \mathbf{G} is the single

constant 4-by-4 homogeneous transformation matrix that minimized $\|\vec{R}\|$ for the hip, knee, and ankle. The maximum absolute value of \vec{S} ($\max |\vec{S}|$) and root-mean-square of \vec{R} ($\text{RMS}[\vec{R}]$) were calculated, and an ANOVA with multiple comparisons and a Bonferroni adjustment were used to identify differences between their x , y , and z components. Overall accuracy and precision were defined as the norm $\|\cdot\|$ of \vec{S} and \vec{R} , respectively, averaged over N time points for which data could be compared (hip: $N=160$, knee: $N=96$, ankle: $N=63$).

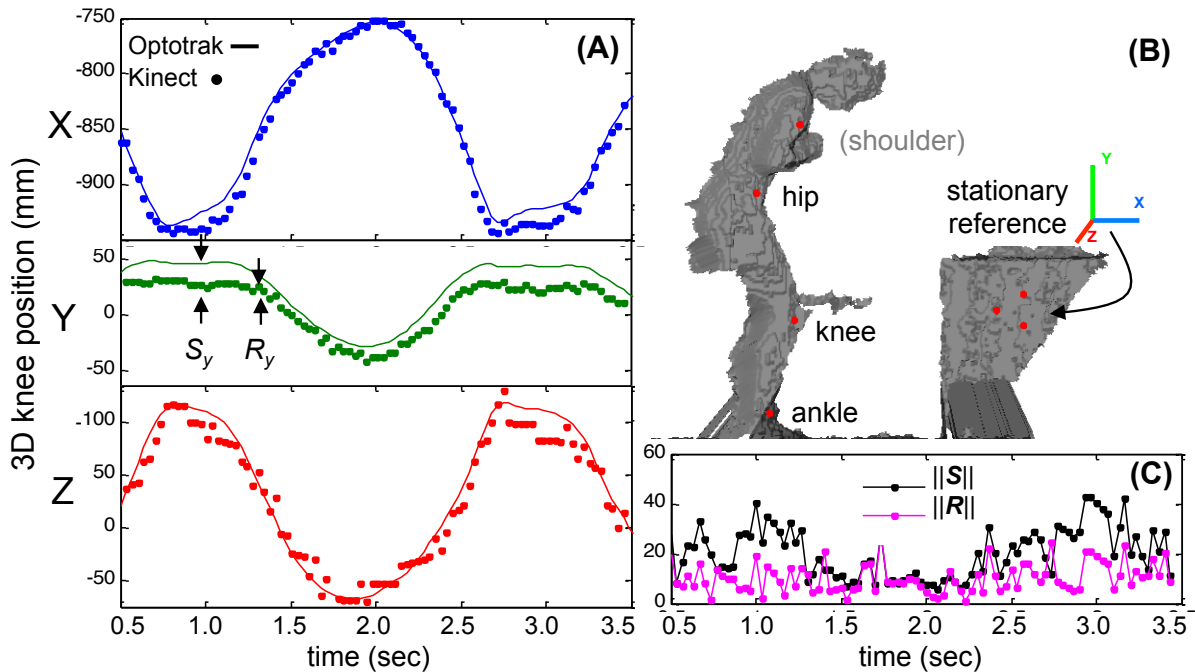


Figure 6.1: Comparison of Kinect and Optotrack marker positions. **A)** $x/y/z$ components of the subjects knee position over the course of a two-legged squat (Optotrack –, Kinect •). **B)** Raw 3D Kinect output with overlaid positions of anatomical and reference markers. **C)** Systematic (-•-) and random (-○-) error magnitudes versus time for the knee.

Results

Means and standard deviation across the hip, knee, and ankle for the following systematic and random error metrics are given in Table 6.1. The maximum absolute difference ($\max |\vec{S}|$) between $x/y/z$ values recorded by the Optotrak and Kinect ranged from 11-35 mm, and the time-averaged distance (time-avg: $\|\vec{S}\|$) between the apparent Optotrak and Kinect positions ranged from 18-23 mm. The RMS deviation of the Kinect $x/y/z$ data from the transformed-Optotrak data (RMS $[\vec{R}]$) ranged from 3-12 mm. RMS deviation in z was significantly greater than that of x and y ($p<0.005$). The time-averaged noise, or effective RMS distance between the Kinect and transformed Optotrak-data (time-avg: $\|\vec{R}\|$) ranged from 10-11 mm. Figure 6.1c shows a representative plot of $\|\vec{S}\|$ and $\|\vec{R}\|$ versus time for the knee.

Table 6.1: Error metrics (mm) averaged over the hip, knee, and ankle

component	Systematic Error		Random Error	
	$\max[\mathbf{S}]$	time-avg. $\ \mathbf{S}\ $	RMS $[\mathbf{R}]$	time-avg. $\ \mathbf{R}\ $
X	20.0 ± 8.5		4.8 ± 0.44	
Y	23.1 ± 2.6	20.3 ± 2.3	4.0 ± 1.2	10.3 ± 0.7
Z	$33.1 \pm 3.0^*$		$10.4 \pm 1.0^\dagger$	
mean \pm standard deviation		* $p > 0.05$	† $p < 0.005$	(Bonferroni adj.)

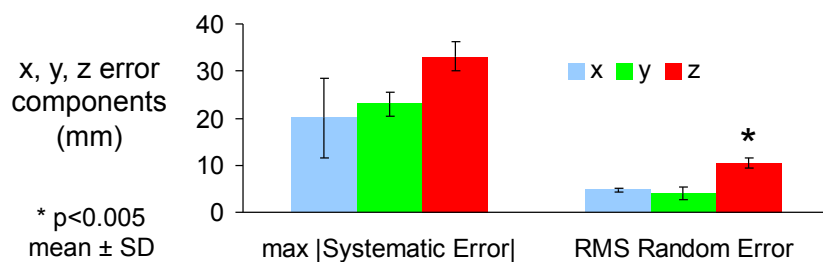


Figure 6.2: Systematic and random error for the x , y , and z components of measured marker positions. Error values were averaged over the hip, knee, and ankle. Error bars represent one standard deviation. p-value from ANOVA with Bonferroni adjustment for multiple comparisons.

Discussion

These results demonstrate that using our technique, it is possible to track markers placed on joints with an accuracy of 20 ± 2 mm and a precision of 10 ± 1 mm. These values are larger than commercial motion capture errors (<1 mm), however, they are comparable to the magnitude of soft tissue artifact (up to 30 mm) [Peters *et al.*, 2010]. The finding that random noise out of the camera plane was significantly larger than noise in the plane is consistent with the Kinect's lower depth resolution. Systematic error out of the camera plane was also larger, but the difference was not significant.

Other low-cost human motion tracking systems have been developed for clinical applications using the Kinect [Stone and Skubic, 2011] and the Nintendo WiiTM [Attygalle *et al.*, 2008]. Unlike our technique, however, these others require separate hardware, stationary camera positions, calibration, background subtraction, and data filtering before analysis of gait and hand motion were possible. To the authors' knowledge, the technique presented here is the first that permits automatic 3D tracking and identification of multiple anatomical markers using only the Kinect, retroreflective markers, and a laptop equipped with open-source Kinect libraries. Importantly, marker tracking was facilitated by using the Kinect skeleton as a template for identifying markers based on their nearest skeleton joint.

We acknowledge the relatively slow frame-capture rate (30 Hz), 11-65% marker occlusion, and the lack of rigid body rotation data. Hardware improvements, the use of multiple Kinect units, and additional markers will address these limitations.

6.4 Markerless vs. Marker-based Kinect Motion Capture

The objective of this study was to compare a new marker-based Kinect motion capture technique to the OpenNI markerless skeleton algorithm during a single-leg squat task. The Vicon Nexus motion capture system was used as a standard for comparison.

Methods

Three participants provided written and verbal consent to undergo motion analysis at the UCSF Human Performance Laboratory. Participants were instructed to perform five repeated single leg squats on their left and right legs.

Ground truth lower body kinematics were recorded using a 10-camera Vicon Nexus system (Vicon, Oxford Metrics LTD. Oxford, England). Marker position data was acquired at 250 Hz. Rigid retroreflective marker clusters were fastened to the left and right thigh, shank, and foot. Tracking markers for the pelvis were placed on the anterior/superior iliac spines (ASIS/PSIS) and iliac crests (IC). Calibration markers were placed on the greater trochanter, medial/lateral femoral epicondyles and malleoli, and the 1st/5th metatarsals, and were removed after a static trial. Following data collection, Visual 3D software (C-Motion, Rockville, MD) was used to extract joint center coordinates for the hips, knees, and ankle.

Simultaneously, marker-based and markerless motion capture was performed using a Microsoft Kinect camera (Microsoft, Redmond, WA) positioned 2 m anterior to each participant. OpenNI (PrimeSense, Israel) software were used to collect both raw and markerless ‘skeleton’ Kinect data at 30 Hz. Marker-based position measurements of the ‘hip’, ‘knee’, and ‘ankle’ were made by tracking retroreflective tape placed anteriorly on the ASIS, tibial tuberosity, and distal tibia. Marker detection and tracking were performed using custom

MATLAB code (Natick, MA) and the “Kinect Matlab” toolbox [Kroon, 2011]. First, infrared images were filtered and thresholded to segment retroreflective markers from the image background. Then, 3D coordinates of the points corresponding to segmented marker pixels were extracted from the depth map. Hip, knee, and ankle markers were tracked over time using a nearest-neighbor approach, and labeled manually. Markerless joint position measurements were extracted directly from the “skeleton” hip, knee, and ankle joints (provided by OpenNI) without post-processing.

Planar joint angles were calculated between pairs of unit vectors oriented along the hips \vec{u}_h , thigh \vec{u}_t , and shank \vec{u}_s (Figure 6.3a). Unit vectors were constructed from the positions of either Vicon joint centers, Kinect markers, or Kinect skeleton joints. Pelvic obliquity, hip flexion, hip adduction, knee flexion, ankle dorsiflexion, and apparent knee valgus were calculated using the equations:

Pelvic obliquity:	$\theta_p = \sin^{-1}(\vec{u}_h \cdot \vec{z})$
Hip flexion:	$\psi_h = \cos^{-1}(-\vec{z} \cdot \vec{u}_t)$
Hip adduction:	$\theta_h = -\sin^{-1}(\vec{u}_h \cdot \vec{u}_t)$
Knee flexion:	$\psi_k = \cos^{-1}(\vec{u}_t \cdot \vec{u}_s)$
Ankle dorsiflexion:	$\psi_a = \cos^{-1}(-\vec{z} \cdot \vec{u}_s)$
Apparent knee valgus:	$\theta_k = \sin^{-1}(\vec{u}_{\text{lat}} \cdot \vec{u}_s)$

where the the unit vector $\vec{u}_{\text{lat}} = \vec{z} \times (\vec{u}_h \times \vec{z})$ points laterally along the ground plane based on the orientation of the hips.

Discrete peak values for joint position and angles were extracted at the bottom of each squat, as determined by local minima in vertical knee position. Pearson's correlation coefficients and Bland-Altman statistics (bias, $|\bar{\Delta}|$ and limits of agreement, LOA) were used to compare marker-based or skeleton-based Kinect peak values to Vicon. Bias represents the mean difference between measurement techniques, whereas the limits of agreement represent the range within the differences between measurement techniques can be expected to lie with 95% probability.

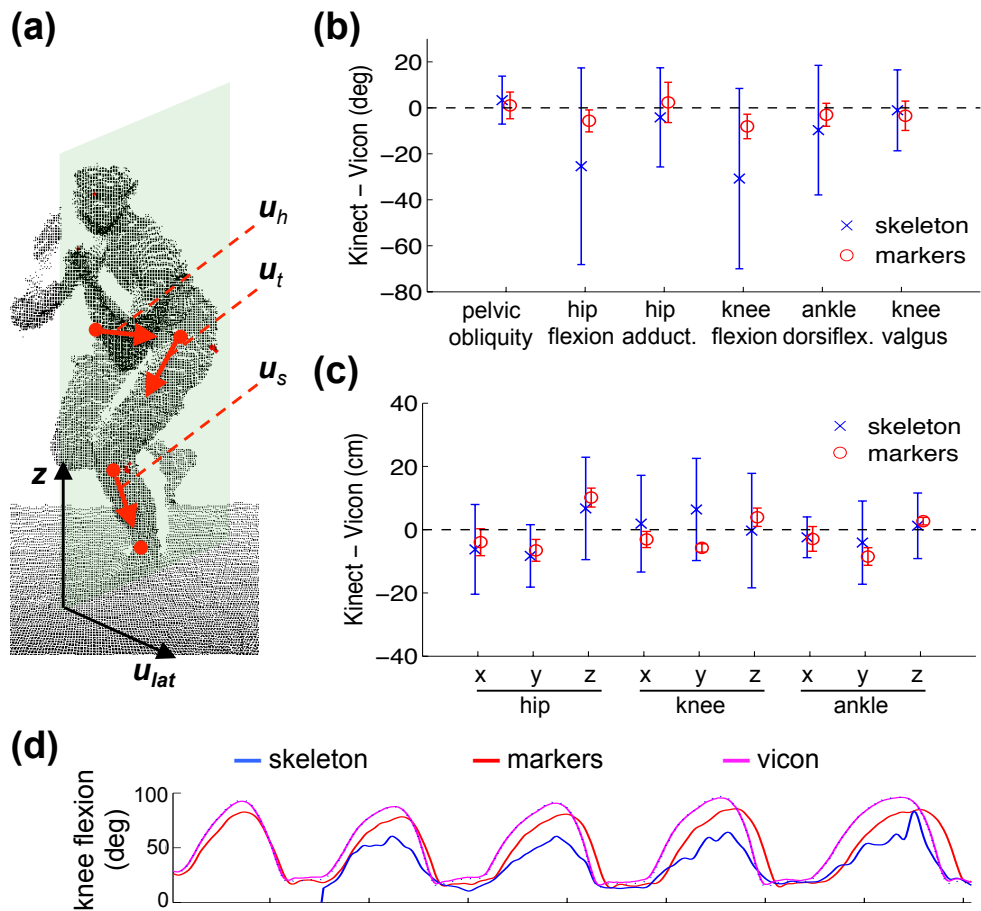


Figure 6.3: Comparison of markerless and marker-based measurement agreement with Vicon. **(a)** Raw 3D Kinect data and unit vectors for the hips, thigh, and shank. **(b, c)** Bland-Altman bias and limits of agreement (relative to Vicon) for joint angles and joint positions. **(d)** Continuous measurement of knee flexion.

Results

Compared to the Kinect skeleton, marker-based continuous measurements of joint positions and angles were more similar to Vicon. Skeleton-based joint angles varied erratically, while marker-based joint angles were continuous like Vicon (Figure 6.3d). Towards the bottom of each squat, both skeleton and marker measurements underestimated hip and knee flexion. A temporal offset between Kinect and Vicon measurements was observed for some subjects due to poor synchronization of the two data sources.

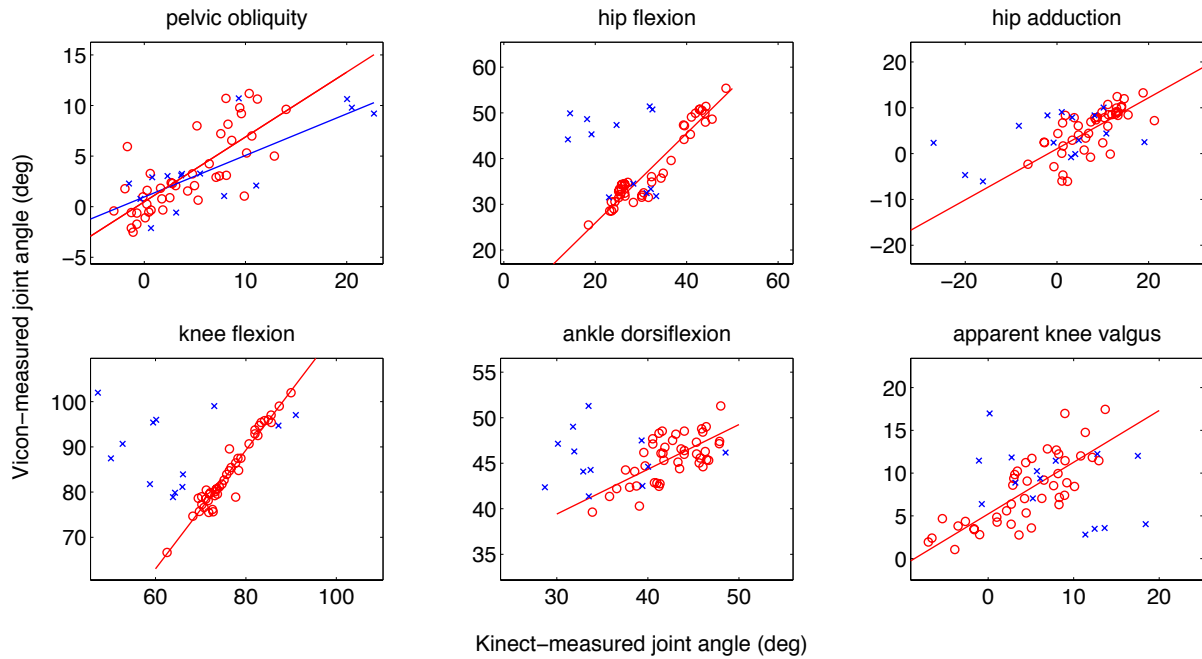


Figure 6.4: Correlation between relevant joint angles measured by Kinect and Vicon. Vicon-measured joint angles are plotted against angles from the Kinect skeleton (x) or Kinect markers (o). Regression lines are shown if the correlation was significant ($p < 0.01$).

Peak joint angles based on markers were less biased and had narrower limits of agreement than skeleton-based angles. All marker-based peak joint angles were strongly correlated with Vicon angles ($r > 0.6$, $p < 0.01$), whereas only skeleton-based pelvic obliquity was significantly correlated with Vicon ($r = 0.8$, $p < 0.01$). The bias for peak joint angles based on markers ($|\bar{\Delta}|$):

$1\text{--}8^\circ$) was up to 4.5 times lower than for skeleton-based angles ($|\bar{\Delta}|$: 1-31°). For example, marker-based peak knee and hip flexion angles were 6° and 8° smaller than Vicon, while skeleton-based angles were 25° and 31° smaller. The limits of agreement for markers (LOA: $\pm 5\text{--}9^\circ$) were up to 9 times more narrow than for the skeleton (LOA: $\pm 10\text{--}42^\circ$) (Figure 6.3b).

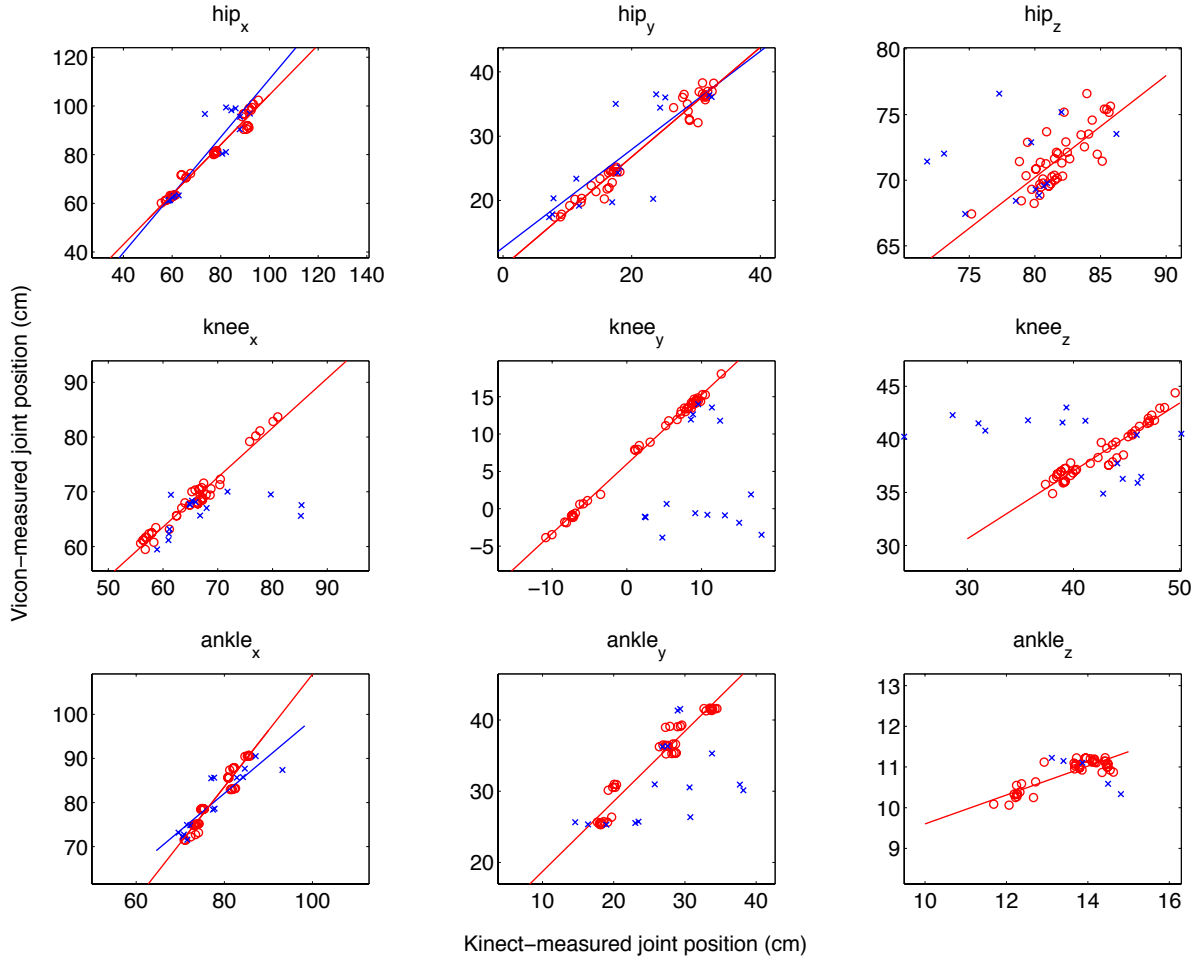


Figure 6.5: Correlation between joint positions measured by Kinect and Vicon. Vicon-measured joint positions are plotted against the positions of Kinect skeleton joints (blue 'x') or Kinect markers (red open circles). Regression lines are shown if the correlation was significant ($p < 0.01$).

Both marker- and skeleton-based joint positions were biased, however marker measurements have narrower limits of agreement. Marker position coordinates for all joints were strongly correlated with Vicon joint centers ($r > 0.7$, $p < 0.01$), whereas only the x and y

coordinates of the skeleton hip joint and the x coordinate of the ankle joint were significantly correlated. The biases for marker and skeleton joint coordinates were similar, ranging from 3-10 cm and 1-8 cm, respectively. The hip marker was consistently higher (larger z -coordinate) than the Vicon hip joint center. However, the limits of agreement for all marker coordinates (LOA: ± 1 -4 cm) were up to 12 times more narrow than for the skeleton (LOA: ± 6 -18 cm) (Figure 6.3c).

Discussion

Markerless measurements using the PrimeSense skeleton algorithm were noisy and erratic, while marker-based measurements closely followed Vicon. The anatomical models produced by these algorithms are not necessarily biomechanically accurate, and may mask important differences in kinematics between individuals. Both markerless and marker-based measurements of joint positions and joint angles were somewhat biased. Smaller marker-based hip and knee flexion angles could be explained by the more anterior positions of the markers relative to anatomical joint centers. Larger marker-based vertical (z -coordinate) hip positions could be explained by placement of markers on the ASIS. Marker-based measurements were more consistent than skeleton-based measurements, with narrower limits of agreement. The limits of agreement for skeleton measurements of hip and knee flexion were particularly wide (up to 43°), which can be interpreted as a high probability (95%) for observing errors of that magnitude.

Others have reported the accuracy and reliability of markerless motion capture using the Kinect. Obdrzalek et al. [Obdrzalek *et al.*, 2012] compared the Microsoft Kinect skeleton to PhaseSpace, an active LED-based system. They found variations in skeleton joint positions and limb lengths on the order of ~ 10 cm. Clark et al. [Clark *et al.*, 2012] compared the Kinect

Skeleton to Vicon using Pearson's correlations and Bland-Altman statistics. In contrast to our study, they found that Kinect measurements were strongly correlated with Vicon and had comparable inter-trail reliability. However, the authors reported relative displacements, not absolute positions, which are less prone to systematic error. Further, their measurements were averaged over multiple trials, which reduced random error.

We compared both marker-based and markerless Kinect measurement methods to gold standard Vicon. Thus, rather than reporting error metrics without context, we were able to quantify the relative improvement of our marker-based technique over the markerless PrimeSense skeleton. We showed that the use of markers, although prone to bias, provides a dramatic increase in reliability (narrower limits of agreement) compared to markerless measurements.

There were several limitations of this study. Kinect markers had to be placed anteriorly, instead of in standard anatomical positions, in order to be visible by the Kinect camera. An oblique or sagittal view would allow markers to be placed on lateral bony landmarks. Intersegmental (Euler) angles were not calculated from Vicon data. Planar joint angles derived from joint position data were used instead so that direct comparisons could be made between Vicon, Kinect markers, and the skeleton. Last, since we were using OpenNI software for data collection in this study, we could not test Microsoft's implementation of the markerless skeleton. Future studies should investigate the accuracy and reliability of Microsoft's skeleton, which is known to be more stable and realistic than the OpenNI skeleton.

6.5 Conclusion

These two studies demonstrate that retroreflective markers can be used in combination with a Kinect camera to measure the position of anatomical landmarks with 1-2 cm accuracy and precision; and that this marker-based method is more reliable than the OpenNI markerless ‘skeleton’ algorithm. Individual markers can be tracked during slow activities like a single-leg squat, and tracking is facilitated by using a markerless skeleton as a template. Joint positions and intersegmental angles can then be used to calculate important biomechanical measures of lower extremity function.

Multi-camera motion capture systems like Vicon are the gold standard for biomechanics research, however these systems cannot be used routinely. Markerless motion capture is accessible and easy to use, but not reliable or accurate enough for the clinic. Our approach is a promising intermediate between marker-based and markerless motion capture that may lead to both accurate and accessible 3D clinical movement analysis. The ability to perform accurate 3D movement analysis using low-cost cameras like the Microsoft Kinect may aid physicians and therapists in diagnosis, treatment, and monitoring of a range of musculoskeletal disorders.

Chapter 7

Conclusion and Future Outlook

Quantitative evaluation of musculoskeletal function is one of the most pressing needs in orthopaedic medicine and physical therapy. Health care policy changes, an increasingly active population, and the rise of personal health monitoring devices are all increasing the demand for and ability to produce quantitative metrics. Unfortunately, compared to measures of cardiovascular or metabolic health, measures of musculoskeletal health are far more qualitative and subjective. Thus, to maximize the value of musculoskeletal care in the future, there is a tremendous need for quantitative health metrics including measures of knee joint function and stability.

Recent changes in health care policy have created an increased demand for quantitative measures of health outcomes. For example, pay-for-performance policies are emphasizing effectiveness and accountability of care, penalizing errors and rewarding efficiency. To comply with these policies, health care providers must make an increased effort to record quantitative metrics for care quality and patient outcomes. Physical therapists who wish to bill Medicare are now required to use G-codes and G-code modifiers, respectively, to classify and quantify functional impairments. However, the tools needed to produce these

quantitative measures of impairment are lacking, so therapists must often resort to making estimates. Since insurance companies are now required to provide coverage to all individuals, they are experiencing increased pressure to stop paying for procedures that do not work. To identify such procedures (as well as to determine when a patient has returned to ‘normal’) insurance companies are becoming dependent on quantitative health metrics.

Both younger and older individuals are placing greater demands on their joints. Increasing numbers of children and adolescents are becoming susceptible to injury by participating in sports. The rate of ACL injury and reconstruction has been rising steadily over the past 15 years for individuals below the age of 20. However, according to the CDC, more than half of all sports injuries in children are preventable. Reliable identification of those who could benefit from preventative training will require better quantitative predictors of injury risk. Meanwhile, the number of hip and knee replacements is growing, and older individuals are demanding to be more active after surgery. Early identification of those at risk for degenerative osteoarthritis can dramatically reduce the impact of the disease. Doing so will require more sensitive indicators of declining joint function.

The hardware for performing quantitative movement analysis is becoming more pervasive, making it possible to collect musculoskeletal health data on an enormous scale. High performance cameras, accelerometers, and gyroscopes are becoming smaller, cheaper, and more integrated into everyday devices. For example, the iPhone 6 can natively capture video at frame rates as high as 240 frames per second. Smartphones and tablets are used regularly by physical therapists and sports trainers to record patient movements, however quantitative metrics are rarely extracted from the video data. Hardware from three-dimensional ‘depth’ cameras like the Microsoft Kinect is now being integrated into laptop computers. As studied in Chapter 6, these cameras are capable of tracking human movement without markers, albeit at a lower level of accuracy compared to marker-based

motion capture systems. Accelerometers and gyroscopes capable of recording 3D motions are appearing in the growing number of wearable devices and fitness trackers. Currently data from these sensors is processed to provide crude measures of physical activity such as step counts and sleep duration, but algorithms for calculating more relevant musculoskeletal health metrics will certainly appear in the near future. All these devices were once used exclusively in a laboratory setting for conducting movement analysis research. Now they are in the possession of everyday consumers. This presents in an incredible opportunity, and also a challenge, to make the applications useful to health consumers instead of just researchers.

Given the context of evolving health policy, an aging population, and advancements in consumer technology, the relevance of the work presented in this dissertation should be apparent. Hopefully the tools and techniques developed will not only aid researchers in answering questions about knee stability in the laboratory, but will also directly benefit clinicians and their patients suffering from knee injuries. The future development of quantitative outcome measures for musculoskeletal health using new sensor technology will be dependent on continued research on topics like the ones presented in the preceding chapters.

In Chapter 3, we emphasized the importance of biomechanically accurate descriptions of knee kinematics and kinetics. Proper representation of knee joint motion and loads serves as the foundation for quantitative analysis, and is critical for making valid clinical interpretations. For example, the Euler basis and dual Euler basis were useful for describing the rotations and moments of the knee joint. The relationship between these two bases provided a formal connection between the joint contact moment imposed by two femoral condyles and the kinematic constraint limiting varus valgus rotation. This formalism also allowed for a simplified representation of the stiffness matrix for the knee joint, eliminating potentially confounding contributions of the articular geometry to joint stiffness.

Future work should focus on making these mathematical developments clinically applicable. Experimental data are needed to show the benefits of using the Euler and dual Euler basis with joint axes defined using functional calibration approaches (rather than the axes being defined using anatomical landmarks). Clinical studies should also be performed to link quantitative metrics like varus-valgus angle and joint stiffness coefficients to clinical outcomes data.

In Chapter 4 we presented a new laboratory tool for quantitatively evaluating dynamic joint stability in cadaveric knees. This tool, called the Mechanical Pivot Shift Device (MPSD) applied knee loads that were both dynamic and well-defined to mimic a clinical examination called the pivot-shift test. Previous methods of quantifying the pivot-shift employed either poorly defined or static loads. In Chapter 5 we used this tool to compare the effectiveness of different pediatric ACL reconstruction techniques for restoring native knee kinematics. The sensitivity of the device made it straightforward to determine that all of the ACL-reconstruction techniques tested eliminated the pivot-shift, but that one in particular (the iliotibial band reconstruction) over-constrained the knee in axial rotation.

Future research should use the MPSD to study the effects of soft tissue damage and repair on knee kinematics, and also to improve the MPSD. In unpublished pilot studies, we found that the magnitude of the pivot-shift was particularly sensitive to damage of the lateral meniscus. We also found that different components of the pivot shift were sensitive to cutting either the anteromedial or posterolateral bundles of the ACL. We have also used the MPSD to investigate the effect of damaging capsular connective tissue structures like the anterolateral ligament on knee kinematics. Improvements to the MPSD can be made by fine tuning the loads applied by the device to better match those applied during the manual test, although these manual loads have yet to be measured experimentally. It might also be

possible to produce a clinical version of the MPSD that employs accelerometers and gyros instead of an optical tracking system.

In Chapter 6 we presented a new marker-based motion capture method that leverages consumer-available 3D cameras like the Microsoft Kinect. We demonstrated that, using this method, it was possible to measure the 3D position of landmarks with an accuracy and precision on the order of 1-3 cm, and to do so more reliably than a markerless tracking method. Unlike markerless methods, which have not been thoroughly evaluated, the new method presented can be directly compared to standard marker-based motion capture, which has been the paradigm for movement analysis for decades. The new method presented represents an ideal intermediate between the expensive multi-camera motion capture systems used for research and the relatively inaccurate marker-less motion capture algorithms used for gesture-based video game control and computer interaction.

Future work should focus on developing a software application for movement analysis that can be used easily by therapists and clinicians. The algorithms for extracting joint stability metrics from 3D motion data should be fine tuned and validated for specific functional tasks. More advanced modeling approaches for associating skin-mounted markers with rigid-body limb segments may also be employed. For example, in unpublished work, a linked kinematic chain model of the body was used to constrain the possible joint motions, and rigid body velocities were calculated using ‘twists’ to aid in tracking marker positions from frame to frame. Marker occlusion problems could potentially be solved by merging data from two different depth cameras recording from different angles. Last, the next generation Kinect sensor (v2) should be utilized for research. This sensor has a higher 2D and 3D resolution than the previous version and the included ‘skeleton’ provides a much more robust representation of human movement, which could benefit marker tracking. However, our

preliminary work with the Kinect v2 determined that tracking of the knee position using the skeleton is not smooth.

In closing, within this dissertation we have presented new experimental tools and analytical techniques for quantitative evaluation of knee joint stability. Mathematical techniques featuring the Euler and dual Euler bases enable representation of knee joint motion and loads within the context of the biomechanical constraints imposed by the femoral condyles and connective tissue structures. The mechanical pivot shift device enables one to quantitatively assess, with a high degree of reproducibility, the effects of soft tissue damage or repair on knee dynamic knee joint stability in a cadaveric knee model. Finally, marker-based motion capture using the Kinect sensor enables accurate and accessible 3D motion capture for lower extremity movement analysis. Hopefully, these contributions will benefit biomechanics researchers, surgeons, and physical therapists in both laboratory and clinical settings who face the increasingly important problem of quantifying knee joint function and stability.

Appendix A

Clinical Background: Supplemental Figures

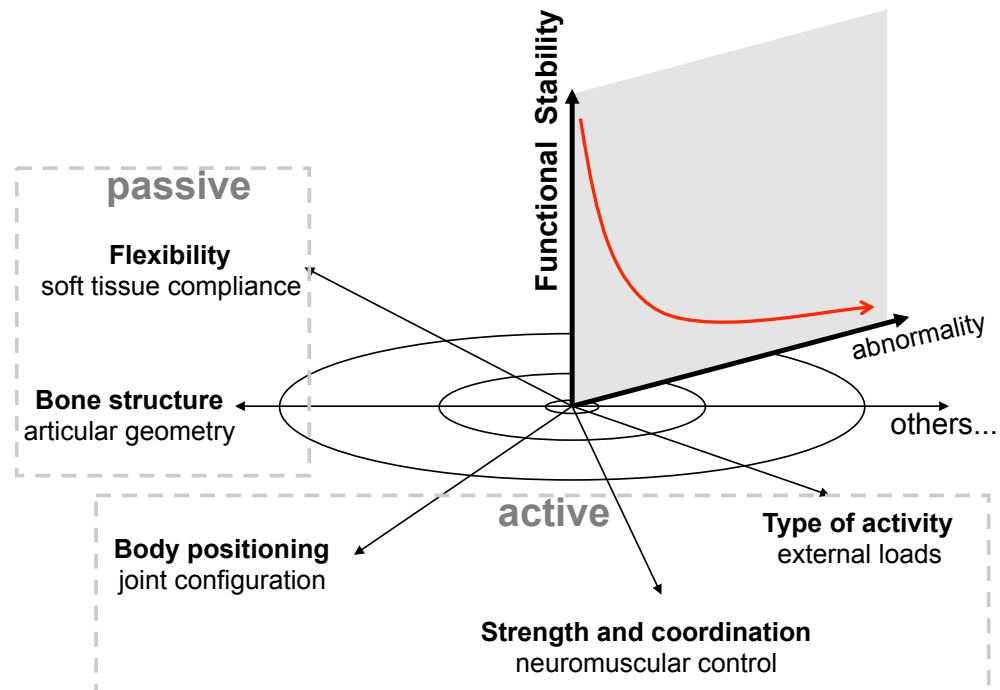


Figure A.1: Conceptual schematic for functional knee stability. A variety of passive and active factors contribute to the functional stability of the knee joint.

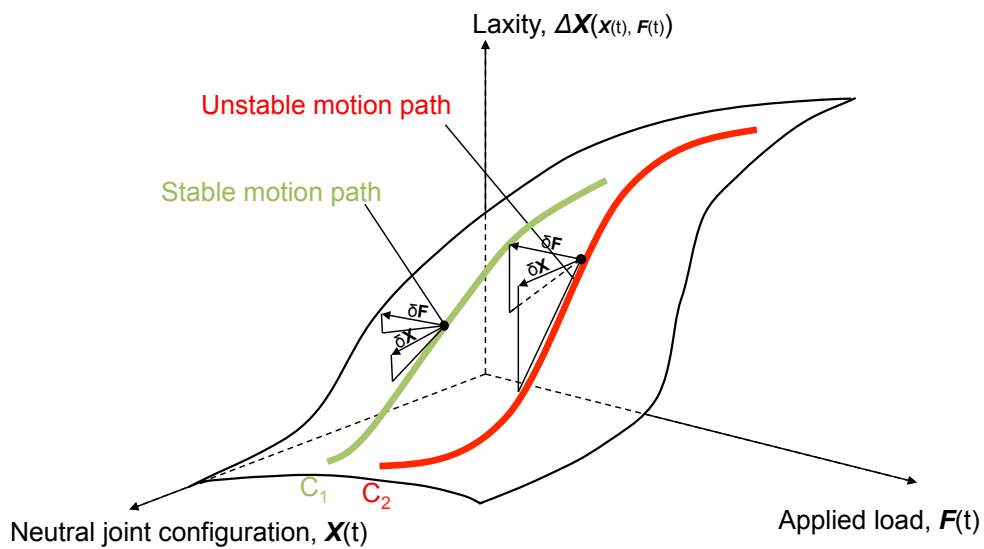


Figure A.2: The kinematic response of the knee joint is dependent on both the applied load and the configuration of the joint before loading. One combination may result in a stable motion path, while another may result in an unstable motion path.

Appendix B

Theoretical Background: Supplemental Material

B.0.1 Explicit expressions for the Euler and dual-Euler basis vectors for the 1-2-3 set of Euler angles

In the paper, we follow [Grood and Suntay, 1983a] and use a 1-2-3 set of Euler angles.

For the 1-2-3 set, the rotation R has the decomposition

$$R = CBA, \quad (B.1)$$

where A, B, and C are three rotation matrices:

$$\begin{aligned}
 A &= \begin{bmatrix} 1 & 0 & 0 \\ 0 & \cos(\psi) & \sin(\psi) \\ 0 & -\sin(\psi) & \cos(\psi) \end{bmatrix}, \\
 B &= \begin{bmatrix} \cos(\theta) & 0 & -\sin(\theta) \\ 0 & 1 & 0 \\ \sin(\theta) & 0 & \cos(\theta) \end{bmatrix}, \\
 C &= \begin{bmatrix} \cos(\phi) & \sin(\phi) & 0 \\ -\sin(\phi) & \cos(\phi) & 0 \\ 0 & 0 & 1 \end{bmatrix}.
 \end{aligned} \tag{B.2}$$

The most frequently used choice of Euler angles in biomechanics is the 3-2-1 set and the corresponding developments for this set can be found in [O'Reilly, 2007; O'Reilly, 2008].

The Euler basis and dual-Euler basis for the 1-2-3 set of Euler angles can be expressed in terms of the proximal basis vectors and the distal basis vectors:

$$\begin{aligned}
 \begin{bmatrix} \mathbf{g}_1 \\ \mathbf{g}_2 \\ \mathbf{g}_3 \end{bmatrix} &= \mathsf{E}_p \begin{bmatrix} \mathbf{p}_1 \\ \mathbf{p}_2 \\ \mathbf{p}_3 \end{bmatrix} = \mathsf{E}_d \begin{bmatrix} \mathbf{d}_1 \\ \mathbf{d}_2 \\ \mathbf{d}_3 \end{bmatrix}, \\
 \begin{bmatrix} \mathbf{g}^1 \\ \mathbf{g}^2 \\ \mathbf{g}^3 \end{bmatrix} &= \mathsf{G}_p \begin{bmatrix} \mathbf{p}_1 \\ \mathbf{p}_2 \\ \mathbf{p}_3 \end{bmatrix} = \mathsf{G}_d \begin{bmatrix} \mathbf{d}_1 \\ \mathbf{d}_2 \\ \mathbf{d}_3 \end{bmatrix}.
 \end{aligned} \tag{B.3}$$

The four matrices in these equations have the representations

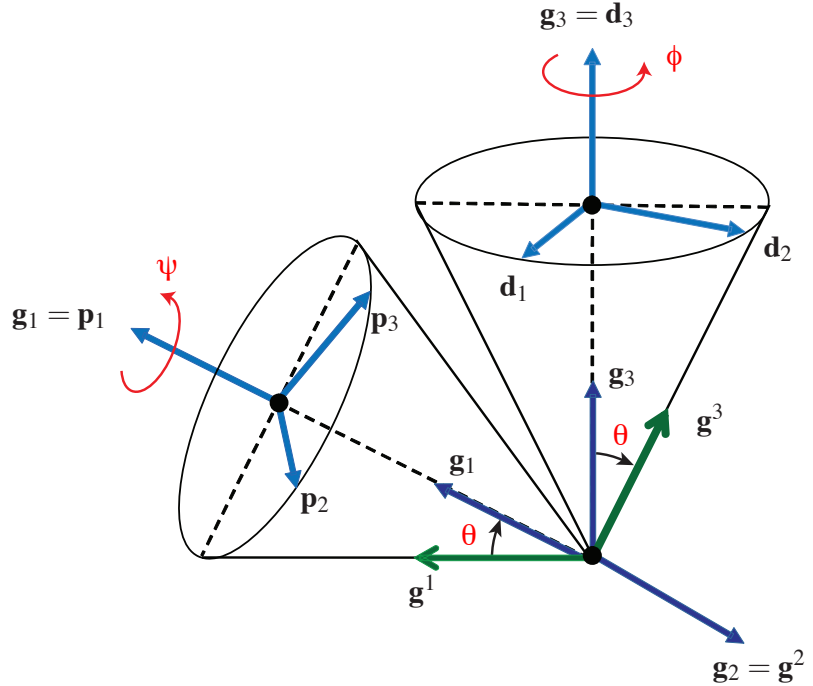


Figure B.1: Graphical representation of the dual-Euler and Euler basis vectors and their relationships with the proximal \mathbb{P} and distal \mathbb{D} frames. Explicit expressions for these vectors can be found in (B.3). In this figure $\theta > 0$.

$$\begin{aligned}
 E_p &= \begin{bmatrix} 1 & 0 & 0 \\ 0 & \cos(\psi) & \sin(\psi) \\ \sin(\theta) & -\cos(\theta)\sin(\psi) & \cos(\theta)\cos(\psi) \end{bmatrix}, \\
 E_d &= \begin{bmatrix} \cos(\theta)\cos(\phi) & -\cos(\theta)\sin(\phi) & \sin(\theta) \\ \sin(\phi) & \cos(\phi) & 0 \\ 0 & 0 & 1 \end{bmatrix}, \tag{B.4}
 \end{aligned}$$

and

$$\begin{aligned}\mathbf{G}_p &= \begin{bmatrix} 1 & \sin(\psi)\tan(\theta) & -\cos(\psi)\tan(\theta) \\ 0 & \cos(\psi) & \sin(\psi) \\ 0 & -\sec(\theta)\sin(\psi) & \sec(\theta)\cos(\psi) \end{bmatrix}, \\ \mathbf{G}_d &= \begin{bmatrix} \sec(\theta)\cos(\phi) & \sec(\theta)\sin(\phi) & 0 \\ \sin(\phi) & \cos(\phi) & 0 \\ -\tan(\theta)\cos(\phi) & \tan(\theta)\sin(\phi) & 1 \end{bmatrix}. \end{aligned} \quad (\text{B.5})$$

The second Euler angle needs to be restricted to $\theta \in (-\frac{\pi}{2}, \frac{\pi}{2})$. We also note the identities:

$$\mathbf{E}_d = \mathbf{E}_p \mathbf{R}, \quad \mathbf{G}_d (\mathbf{E}_d)^{-1} = \mathbf{G}_p (\mathbf{E}_p)^{-1},$$

$$\mathbf{G}_d = (\mathbf{E}_d)^{-T} = \mathbf{G}_p \mathbf{R}^T, \quad \mathbf{G}_p = (\mathbf{E}_p)^{-T} = \mathbf{G}_d \mathbf{R}. \quad (\text{B.6})$$

These identities can be used to establish the following relationships:

$$\begin{aligned}\begin{bmatrix} \mathbf{g}^1 \\ \mathbf{g}^2 \\ \mathbf{g}^3 \end{bmatrix} &= \sec^2(\theta) \begin{bmatrix} 1 & 0 & -\sin(\theta) \\ 0 & \cos^2(\theta) & 0 \\ -\sin(\theta) & 0 & 1 \end{bmatrix} \begin{bmatrix} \mathbf{g}_1 \\ \mathbf{g}_2 \\ \mathbf{g}_3 \end{bmatrix}, \\ \begin{bmatrix} \mathbf{g}_1 \\ \mathbf{g}_2 \\ \mathbf{g}_3 \end{bmatrix} &= \begin{bmatrix} 1 & 0 & \sin(\theta) \\ 0 & 1 & 0 \\ \sin(\theta) & 0 & 1 \end{bmatrix} \begin{bmatrix} \mathbf{g}^1 \\ \mathbf{g}^2 \\ \mathbf{g}^3 \end{bmatrix}. \end{aligned} \quad (\text{B.7})$$

To illuminate the relations (B.3), it is convenient to consider graphical representations of the various basis vectors. These representations, first with respect to the distal basis, and then with respect to the proximal basis are shown in Figure B.1, respectively. Referring to

Figure B.1, we observe a pair of cones of semi-angle θ whose axes of symmetry are defined by \mathbf{g}_1 and \mathbf{g}_3 , respectively. For a fixed value of θ the cones can be considered to spin (ψ) and precess (ϕ).

B.0.2 Angular Velocity and Displacements

The angular velocity vector $\boldsymbol{\omega}$ associated with the 1-2-3 Euler angles has several equivalent representations

$$\begin{aligned}\boldsymbol{\omega} &= \dot{\psi}\mathbf{g}_1 + \dot{\theta}\mathbf{g}_2 + \dot{\phi}\mathbf{g}_3 \\ &= \omega_1\mathbf{d}_1 + \omega_2\mathbf{d}_2 + \omega_3\mathbf{d}_3 \\ &= \Omega_1\mathbf{p}_1 + \Omega_2\mathbf{p}_2 + \Omega_3\mathbf{p}_3.\end{aligned}\tag{B.8}$$

Using (B.3), it follows that

$$\begin{bmatrix} \omega_1 \\ \omega_2 \\ \omega_3 \end{bmatrix} = (\mathbf{E}_d)^T \begin{bmatrix} \dot{\psi} \\ \dot{\theta} \\ \dot{\phi} \end{bmatrix}, \quad \begin{bmatrix} \omega_1 \\ \omega_2 \\ \omega_3 \end{bmatrix} = \mathbf{R} \begin{bmatrix} \Omega_1 \\ \Omega_2 \\ \Omega_3 \end{bmatrix}.\tag{B.9}$$

These results are used to relate incremental rotations of the tibia (ω_i) and femur (Ω_i) to changes in the Euler angles and vice versa.

Appendix C

Mechanical Pivot Shift Device: Supplemental Figures

Other Work

MPSD design requirements	manual	C.P.M.	robot	valgus-IT
test-retest reliability	●	●	●	●
inter-rater reliability	○	-	-	-
quantitative kinematics	●	●	●	○
known knee loads	○	○	●	●
dynamic test	●	●	○	○
accessibility	●	●	○	●

● good
 ○ fair
 ○ poor

Lopomo et al. Musahl et al. Kanamori et al. Markolf et al.

Figure C.1: Comparison of other pivot-shift devices

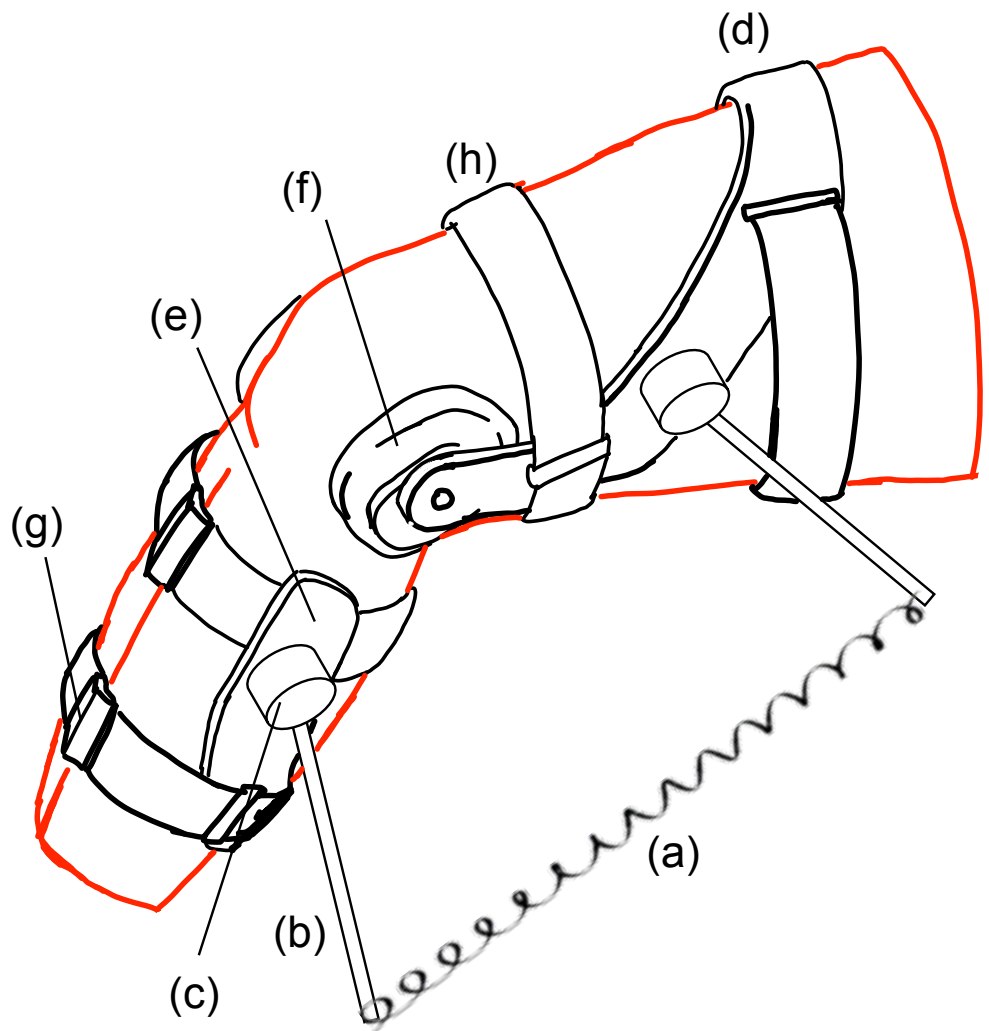


Figure C.2: a) tension-applying spring, b) spring-positioning rods, c) rod-positioning hub, d) femoral rigid frame, e) tibial rigid frame, f) femoral epicondyle stabilizer, g) tibial ridge stabilizer, h) fastening strap

Appendix D

Marker-based Kinect Motion Capture: Supplemental Figures

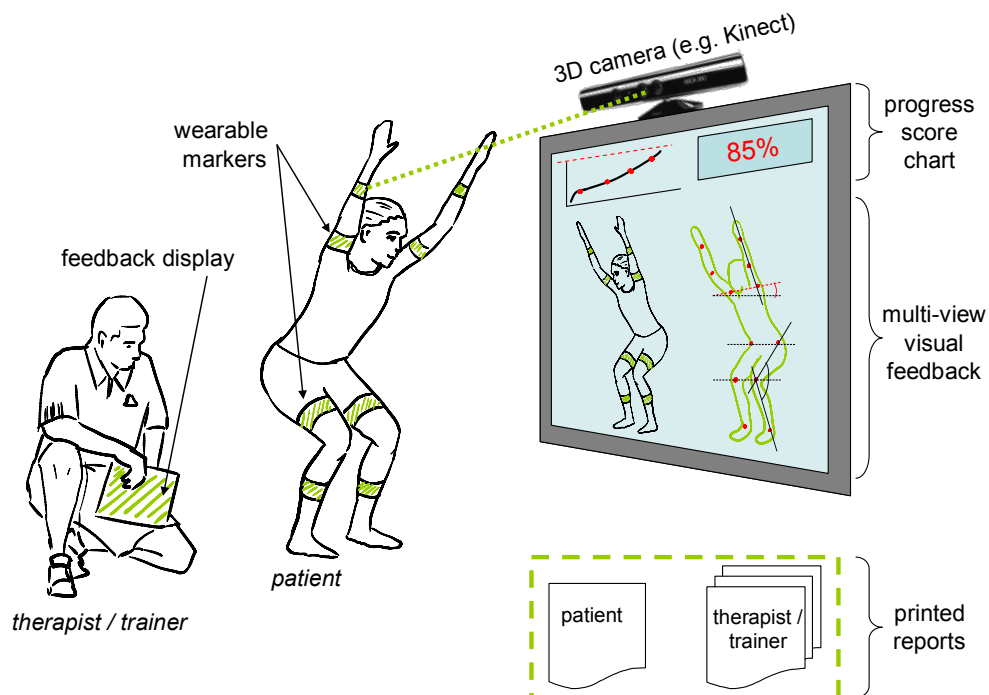


Figure D.1: Proposed clinical setup for Kinect motion capture

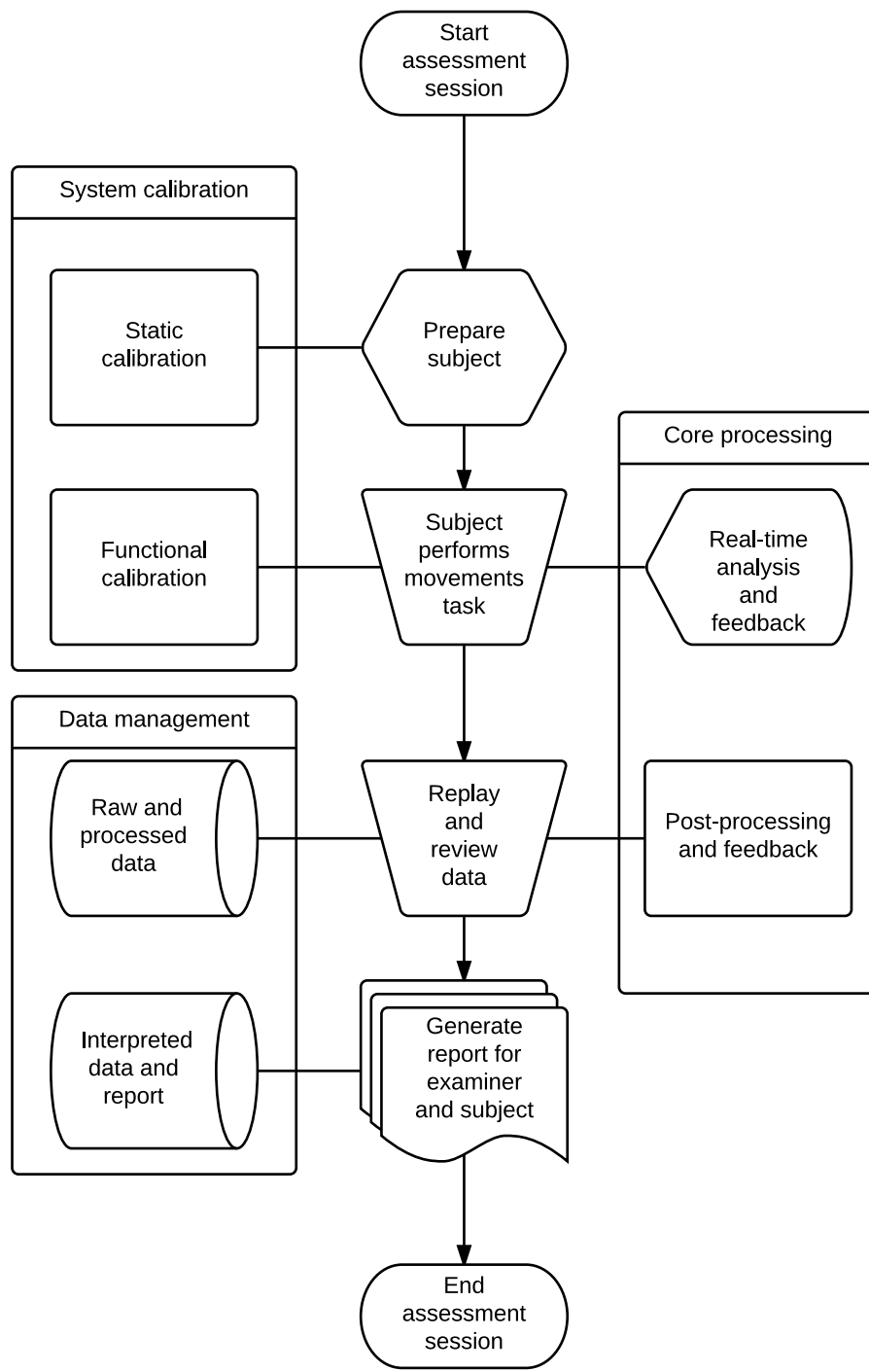


Figure D.2: Flowchart for Kinect-based motion capture

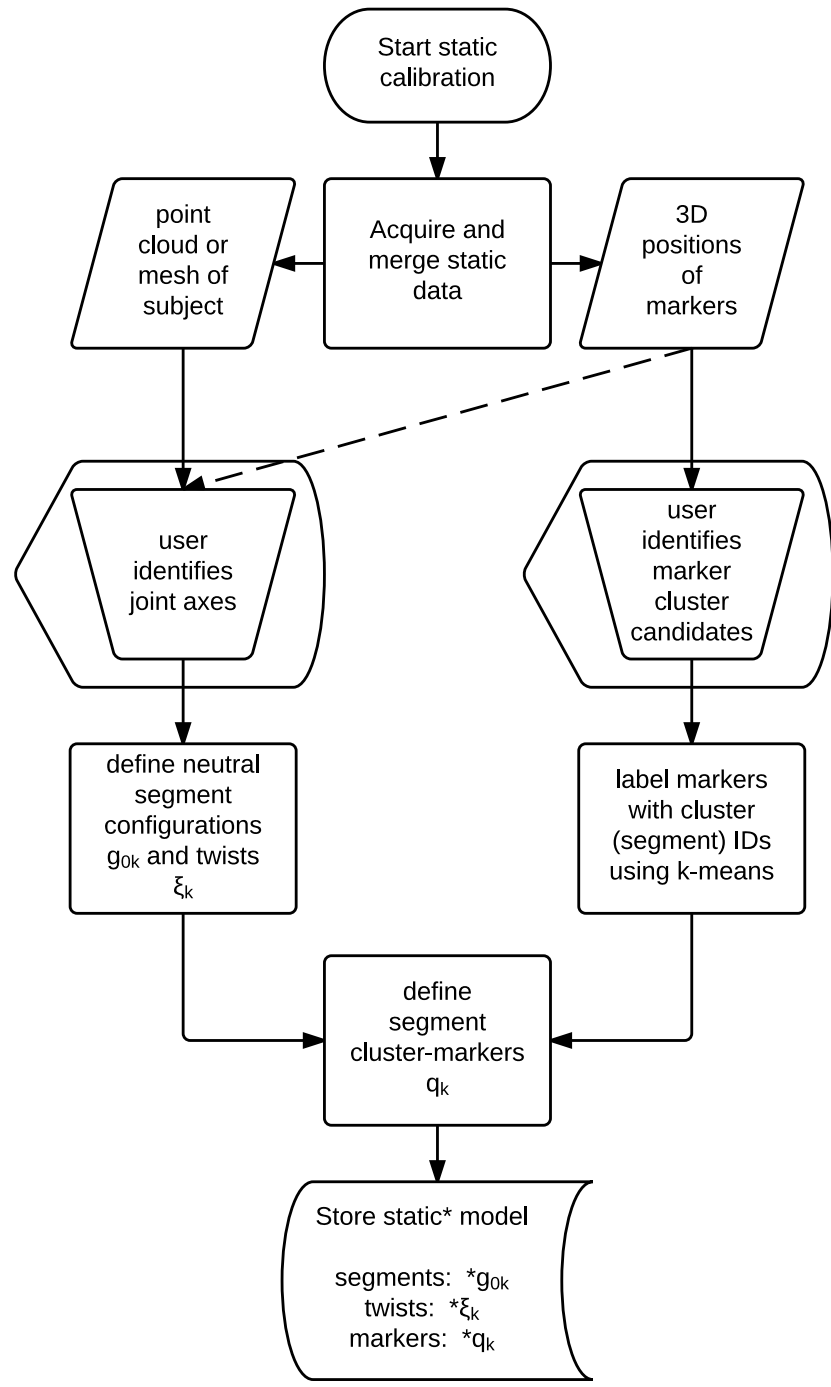


Figure D.3: Proposed method for static rigid body calibration

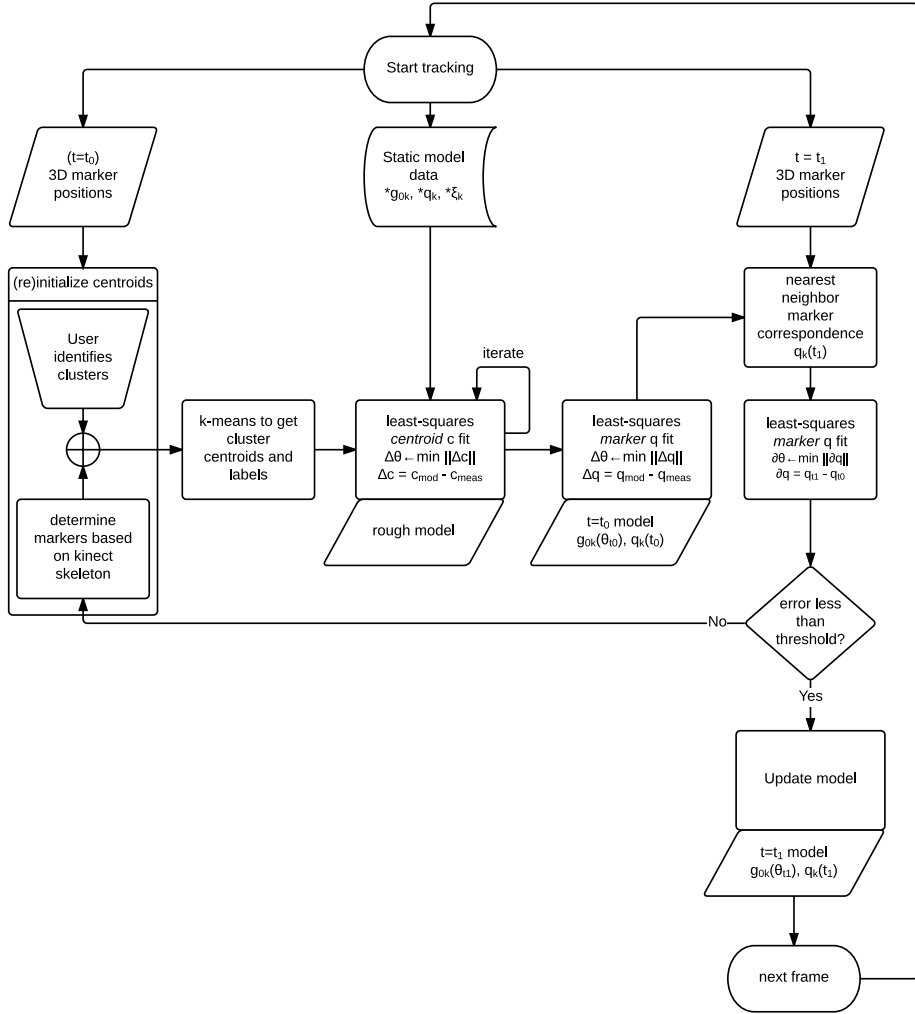


Figure D.4: Proposed method for twist-based rigid body tracking

Bibliography

[Ahldn *et al.*, 2012] Mattias Ahldn, Paulo Araujo, Yuichi Hoshino, Kristian Samuelsson, Kellie K. Middleton, Kouki Nagamune, Jn Karlsson, and Volker Musahl. Clinical grading of the pivot shift test correlates best with tibial acceleration. *Knee Surgery, Sports Traumatology, Arthroscopy*, 20(4):708–712, 2012.

[Allum *et al.*, 1984] R. Allum, D. Jones, M. A. Mowbray, and H. R. Galway. Triaxial electrogoniometric examination of the pivot shift sign for rotatory instability of the knee. *Clinical Orthopaedics and Related Research*, (183):144–146, 1984.

[Anderson, 2003] Allen F. Anderson. Transepiphyseal replacement of the anterior cruciate ligament in skeletally immature patients. *The Journal of Bone & Joint Surgery*, 85(7):1255–1263, 2003.

[Andrews *et al.*, 1994] M. Andrews, F. R. Noyes, and S. D. Barber-Westin. Anterior cruciate ligament allograft reconstruction in the skeletally immature athlete. *The American Journal of Sports Medicine*, 22(1):48–54, 1994.

[Asano *et al.*, 2005] T. Asano, M. Akagi, and T. Nakamura. The functional flexion-extension axis of the knee corresponds to the surgical epicondylar axis: In vivo analysis using a biplanar image-matching technique. *The Journal of Arthroplasty*, 20(8):1060–1067, 2005.

- [Attygalle *et al.*, 2008] S. Attygalle, M. Duff, T. Rikakis, and Jiping He. Low-cost, at-home assessment system with Wii remote based motion capture. In *Virtual Rehabilitation, 2008*, pages 168–174, 2008.
- [Ayeni *et al.*, 2012] Olufemi R. Ayeni, Manraj Chahal, Michael N. Tran, and Sheila Sprague. Pivot shift as an outcome measure for acl reconstruction: a systematic review. *Knee Surgery, Sports Traumatology, Arthroscopy*, 20(4):767–777, 2012.
- [Bach *et al.*, 1988] B. R. Bach, R. F. Warren, and T. L. Wickiewicz. The pivot shift phenomenon: results and description of a modified clinical test for anterior cruciate ligament insufficiency. *The American Journal of Sports Medicine*, 16(6):571–576, 1988.
- [Bartel *et al.*, 2006] Donald L. Bartel, Dwight T. Davy, and Tony M. Keaveny. *Orthopaedic Biomechanics: Mechanics and Design in Musculoskeletal Systems*. Prentice Hall, Upper Saddle River, N.J, 1 edition edition, 2006.
- [Bedi *et al.*, 2011] Asheesh Bedi, Volker Musahl, Volker Steuber, Daniel Kendoff, Dan Choi, Answorth A. Allen, Andrew D. Pearle, and David W. Altchek. Transtibial versus anteromedial portal reaming in anterior cruciate ligament reconstruction: An anatomic and biomechanical evaluation of surgical technique. *Arthroscopy: The Journal of Arthroscopic & Related Surgery*, 27(3):380–390, 2011.
- [Benjaminse *et al.*, 2006] Anne Benjaminse, Alli Gokeler, and Cees P. van der Schans. Clinical diagnosis of an anterior cruciate ligament rupture: a meta-analysis. *The Journal of Orthopaedic and Sports Physical Therapy*, 36(5):267–288, 2006.
- [Bland and Altman, 1999] J M Bland and D G Altman. Measuring agreement in method comparison studies. *Statistical methods in medical research*, 8(2):135–160, 1999.

- [Bois, 1902] Augustus Jay Du Bois. *Kinematics, statics, kinetics, statics of rigid bodies and of elastic solids*. Wiley, 1902.
- [Bull and Amis, 1998a] A. M. J. Bull and A. A. Amis. Knee joint motion: Description and measurement. *Proceedings of the Institution of Mechanical Engineers, Part H: Journal of Engineering in Medicine*, 212(5):357–372, 1998.
- [Bull and Amis, 1998b] Anthony M. J. Bull and Andrew A. Amis. The pivot-shift phenomenon: a clinical and biomechanical perspective. *The Knee*, 5(3):141–158, 1998.
- [Bull *et al.*, 1999] A. M. Bull, H. N. Andersen, O. Basso, J. Targett, and A. A. Amis. Incidence and mechanism of the pivot shift. an in vitro study. *Clinical Orthopaedics and Related Research*, (363):219–231, 1999.
- [Bull *et al.*, 2002] A. M. J. Bull, P. H. Earnshaw, A. Smith, M. V. Katchburian, A. N. A. Hassan, and A. A. Amis. Intraoperative measurement of knee kinematics in reconstruction of the anterior cruciate ligament. *The Journal of Bone and Joint Surgery. British Volume*, 84(7):1075–1081, 2002.
- [Burdick *et al.*, 2005] Richard K. Burdick, Connie M. Borror, and Douglas C. Montgomery. *Design and Analysis of Gauge R and R Studies: Making Decisions with Confidence Intervals in Random and Mixed ANOVA Models*. SIAM, 2005.
- [Cammarata and Dhaher, 2008] M. L. Cammarata and Y. Y. Dhaher. The differential effects of gender, anthropometry, and prior hormonal state on frontal plane knee joint stiffness. *Clinical Biomechanics*, 23(7):937 – 945, 2008.
- [Churchill *et al.*, 1998] D. L. Churchill, S. J. Incavo, C. C. Johnson, and B. D. Beynnon. The transepicondylar axis approximates the optimal flexion axis of the knee. *Clinical Orthopaedics and Related Research*, 356:111–118, 1998.

- [Clark *et al.*, 2012] Ross A. Clark, Yong-Hao Pua, Karine Fortin, Callan Ritchie, Kate E. Webster, Linda Denehy, and Adam L. Bryant. Validity of the Microsoft Kinect for assessment of postural control. *Gait & Posture*, 36(3):372–377, 2012.
- [Davis, 1988] R. B. Davis. Clinical gait analysis. *IEEE engineering in medicine and biology magazine: the quarterly magazine of the Engineering in Medicine & Biology Society*, 7(3):35–40, 1988.
- [Desroches *et al.*, 2010] G. Desroches, L. Chèze, and R. Dumas. Expression of joint moment in the joint coordinate system. *Journal of Biomechanical Engineering*, 132(11):114503, 2010.
- [Donaldson *et al.*, 1985] W. F. Donaldson, R. F. Warren, and T. Wickiewicz. A comparison of acute anterior cruciate ligament examinations. initial versus examination under anesthesia. *The American Journal of Sports Medicine*, 13(1):5–10, 1985.
- [Dumont *et al.*, 2012] Guillaume D. Dumont, Grant D. Hogue, Jeffrey R. Padalecki, Ngozi Okoro, and Philip L. Wilson. Meniscal and chondral injuries associated with pediatric anterior cruciate ligament tears relationship of treatment time and patient-specific factors. *The American Journal of Sports Medicine*, 40(9):2128–2133, 2012.
- [Ehrig *et al.*, 2007] R. M. Ehrig, W. R. Taylor, G. N. Duda, and M. O. Heller. A survey of formal methods for determining functional joint axes. *Journal of Biomechanics*, 40(10):2150–2157, 2007.
- [Frobell *et al.*, 2013] R. B. Frobell, H. P. Roos, E. M. Roos, F. W. Roemer, J. Ranstam, and L. S. Lohmander. Treatment for acute anterior cruciate ligament tear: five year outcome of randomised trial. *BMJ*, 346(jan24 1):f232–f232, 2013.

- [Fujie *et al.*, 1996a] H. Fujie, G. A. Livesay, M. Fujita, and S. L. Woo. Forces and moments in six-dof at the human knee joint: mathematical description for control. *Journal of Biomechanics*, 29(12):1577–1585, 1996.
- [Fujie *et al.*, 1996b] H. Fujie, G. A. Livesay, M. Fujita, and S. L.-Y. Woo. Forces and moment in six-DOF at the human knee joint: Mathematical description for control. *Journal of Biomechanics*, 29(12):1577–1585, 1996.
- [Galway and MacIntosh, 1980] H. R. Galway and D. L. MacIntosh. The lateral pivot shift: a symptom and sign of anterior cruciate ligament insufficiency. *Clinical Orthopaedics and Related Research*, (147):45–50, 1980.
- [Graf *et al.*, 1992] Ben K. Graf, Richard H. Lange, C. Keith Fujisaki, Gregory L. Landry, and R. K. Saluja. Anterior cruciate ligament tears in skeletally immature patients: Meniscal pathology at presentation and after attempted conservative treatment. *Arthroscopy: The Journal of Arthroscopic & Related Surgery*, 8(2):229–233, 1992.
- [Grood and Suntay, 1983a] E. S. Grood and W. J. Suntay. A joint coordinate system for the clinical description of three-dimensional motions: Application to the knee. *Journal of Biomechanical Engineering*, 105(2):136–144, 1983.
- [Grood and Suntay, 1983b] E. S. Grood and W. J. Suntay. A joint coordinate system for the clinical description of three-dimensional motions: application to the knee. *Journal of Biomechanical Engineering*, 105(2):136–144, 1983.
- [Han *et al.*, 2013] Jungong Han, Ling Shao, Dong Xu, and J. Shotton. Enhanced computer vision with Microsoft Kinect sensor: A review. *IEEE Transactions on Cybernetics*, 43(5):1318–1334, 2013.

[Hettrich and Spindler, 2013] Carolyn M. Hettrich and Kurt P. Spindler. Acl clinical outcomes. In Martha M. Murray, Patrick Vavken, and Braden Fleming, editors, *The ACL Handbook*, pages 29–40. Springer New York, 2013.

[Hollister *et al.*, 1993] A. M. Hollister, S. Jatana, A. K. Singh, W. W. Sullivan, and A. G. Lupichuk. Rotation of the knee. *Clinical Orthopaedics and Related Research*, 290:159–268, 1993.

[Hoshino *et al.*, 2012] Yuichi Hoshino, Paulo Araujo, Mattias Ahlden, Charity G. Moore, Ryosuke Kuroda, Stefano Zaffagnini, Jon Karlsson, Freddie H. Fu, and Volker Musahl. Standardized pivot shift test improves measurement accuracy. *Knee surgery, sports traumatology, arthroscopy: official journal of the ESSKA*, 20(4):732–736, 2012.

[Hoshino *et al.*, 2013] Yuichi Hoshino, Paulo Araujo, Mattias Ahldn, Kristian Samuelsson, Bart Muller, Marcus Hofbauer, Megan R. Wolf, James J. Irrgang, Freddie H. Fu, and Volker Musahl. Quantitative evaluation of the pivot shift by image analysis using the ipad. *Knee Surgery, Sports Traumatology, Arthroscopy*, 21(4):975–980, 2013.

[Howard *et al.*, 1998] S. Howard, M. Žefran, and V. Kumar. On the 6×6 Cartesian stiffness matrix for three-dimensional motions. *Mechanism and Machine Theory*, 33(4):389–408, 1998.

[Hsu *et al.*, 2006] W.-H. Hsu, J. A. Fisk, Y. Yamamoto, R. E. Debski, and S. L-Y. Woo. Differences in torsional joint stiffness of the knee between genders. *The American Journal of Sports Medicine*, 34(5):765–770, 2006.

[Jakob *et al.*, 1987] R. P. Jakob, H. U. Staubli, and J. T. Deland. Grading the pivot shift. objective tests with implications for treatment. *Journal of Bone & Joint Surgery, British Volume*, 69-B(2):294–299, 1987.

[Jonsson *et al.*, 2004] Hkan Jonsson, Katrine Riklund-Ahlstrm, and Jonas Lind. Positive pivot shift after acl reconstruction predicts later osteoarthritis: 63 patients followed 5-9 years after surgery. *Acta Orthopaedica Scandinavica*, 75(5):594–599, 2004.

[Jrvel *et al.*, 2001] T. Jrvel, T. Paakkala, P. Kannus, and M. Jrvinen. The incidence of patellofemoral osteoarthritis and associated findings 7 years after anterior cruciate ligament reconstruction with a bone-patellar tendon-bone autograft. *The American Journal of Sports Medicine*, 29(1):18–24, 2001.

[Kanamori *et al.*, 2000] A. Kanamori, S. L. Woo, C. B. Ma, J. Zeminski, T. W. Rudy, G. Li, and G. A. Livesay. The forces in the anterior cruciate ligament and knee kinematics during a simulated pivot shift test: A human cadaveric study using robotic technology. *Arthroscopy: The Journal of Arthroscopic & Related Surgery: Official Publication of the Arthroscopy Association of North America and the International Arthroscopy Association*, 16(6):633–639, 2000.

[Kennedy *et al.*, 2011] Abbey Kennedy, Dezba G. Coughlin, Melodie F. Metzger, Ronald Tang, Andrew D. Pearle, Jeffrey C. Lotz, and Brian T. Feeley. Biomechanical evaluation of pediatric anterior cruciate ligament reconstruction techniques. *The American Journal of Sports Medicine*, 39(5):964–971, 2011.

[Kim *et al.*, 1999] Seung-Ho Kim, Kwon-Ick Ha, Jin-Hwan Ahn, and Dong-Kook Chang. Anterior cruciate ligament reconstruction in the young patient without violation of the epiphyseal plate. *Arthroscopy: The Journal of Arthroscopic & Related Surgery*, 15(7):792–795, 1999.

[Kim *et al.*, 2011a] Myung-Ku Kim, Byung-Cheol Lee, and Joo-Hyun Park. Anatomic single bundle anterior cruciate ligament reconstruction by the two anteromedial portal

method: The comparison of transportal and transtibial techniques. *Knee Surgery & Related Research*, 23(4):213–219, 2011.

[Kim *et al.*, 2011b] Sunny Kim, Jose Bosque, John P. Meehan, Amir Jamali, and Richard Marder. Increase in outpatient knee arthroscopy in the united states: A comparison of national surveys of ambulatory surgery, 1996 and 2006. *The Journal of Bone & Joint Surgery*, 93(11):994–1000, 2011.

[Kocher *et al.*, 2002] Mininder S. Kocher, Hillary S. Saxon, W. David Hovis, and Richard J. Hawkins. Management and complications of anterior cruciate ligament injuries in skeletally immature patients: survey of the herodius society and the ACL study group. *Journal of Pediatric Orthopedics*, 22(4):452–457, 2002.

[Kocher *et al.*, 2004] Mininder S. Kocher, J. Richard Steadman, Karen K. Briggs, William I. Sterett, and Richard J. Hawkins. Relationships between objective assessment of ligament stability and subjective assessment of symptoms and function after anterior cruciate ligament reconstruction. *The American Journal of Sports Medicine*, 32(3):629–634, 2004.

[Kocher *et al.*, 2005] Mininder S. Kocher, Sumeet Garg, and Lyle J. Micheli. Physeal sparing reconstruction of the anterior cruciate ligament in skeletally immature prepubescent children and adolescents. *The Journal of Bone & Joint Surgery*, 87(11):2371–2379, 2005.

[Kroon, 2011] Dirk-Jan Kroon. Kinect matlab, 2011.

[Kubo *et al.*, 2007] Seiji Kubo, Hirotugu Muratsu, Shinichi Yoshiya, Kiyonori Mizuno, and Masahiro Kurosaka. Reliability and usefulness of a new in vivo measurement system of the pivot shift. *Clinical Orthopaedics and Related Research*, 454:54–58, 2007.

[Kuroda *et al.*, 2012] Ryosuke Kuroda, Yuichi Hoshino, Daisuke Araki, Yuichiro Nishizawa, Kouki Nagamune, Tomoyuki Matsumoto, Seiji Kubo, Takehiko Matsushita, and Masahiro

Kurosaka. Quantitative measurement of the pivot shift, reliability, and clinical applications. *Knee surgery, sports traumatology, arthroscopy: official journal of the ESSKA*, 20(4):686–691, 2012.

[Kurtz *et al.*, 2014] Steven M. Kurtz, Kevin L. Ong, Edmund Lau, and Kevin J. Bozic. Impact of the economic downturn on total joint replacement demand in the united states. *The Journal of Bone & Joint Surgery*, 96(8):624–630, 2014.

[Labbe *et al.*, 2010] David R. Labbe, Jacques A de Guise, Neila Mezghani, Vronique Godbout, Guy Grimard, David Baillargeon, Patrick Lavigne, Julio Fernandes, Pierre Ranger, and Nicola Hagemeister. Feature selection using a principal component analysis of the kinematics of the pivot shift phenomenon. *Journal of Biomechanics*, 43(16):3080–3084, 2010.

[Labbe *et al.*, 2011a] David R. Labbe, Jacques A. de Guise, Vronique Godbout, Guy Grimard, David Baillargeon, Patrick Lavigne, Julio Fernandes, Vincent Mass, Pierre Ranger, and Nicola Hagemeister. Accounting for velocity of the pivot shift test manoeuvre decreases kinematic variability. *The Knee*, 18(2):88–93, 2011.

[Labbe *et al.*, 2011b] David R. Labbe, Jacques A. de Guise, Neila Mezghani, Vronique Godbout, Guy Grimard, David Baillargeon, Patrick Lavigne, Julio Fernandes, Pierre Ranger, and Nicola Hagemeister. Objective grading of the pivot shift phenomenon using a support vector machine approach. *Journal of Biomechanics*, 44(1):1–5, 2011.

[Labb *et al.*, 2014] David R. Labb, Di Li, Guy Grimard, Jacques A. de Guise, and Nicola Hagemeister. Quantitative pivot shift assessment using combined inertial and magnetic sensing. *Knee surgery, sports traumatology, arthroscopy: official journal of the ESSKA*, 2014.

[Lane *et al.*, 2008a] Clayton G. Lane, Russell Warren, and Andrew D. Pearle. The pivot shift. *The Journal of the American Academy of Orthopaedic Surgeons*, 16(12):679–688, 2008.

[Lane *et al.*, 2008b] Clayton G. Lane, Russell F. Warren, Fatima C. Stanford, Daniel Kendoff, and Andrew D. Pearle. In vivo analysis of the pivot shift phenomenon during computer navigated ACL reconstruction. *Knee Surgery, Sports Traumatology, Arthroscopy*, 16(5):487–492, 2008.

[Lawrence *et al.*, 2011] J. Todd R. Lawrence, Nina Argawal, and Theodore J. Ganley. Degeneration of the knee joint in skeletally immature patients with a diagnosis of an anterior cruciate ligament tear is there harm in delay of treatment? *The American Journal of Sports Medicine*, 39(12):2582–2587, 2011.

[Leitze *et al.*, 2005] Zachary Leitze, Ron E. Losee, Peter Jokl, Thomas R. Johnson, and John A. Feagin. Implications of the pivot shift in the ACL-deficient knee. *Clinical Orthopaedics and Related Research*, (436):229–236, 2005.

[Lie *et al.*, 2007] Denny T. T. Lie, Anthony M. J. Bull, and Andrew A. Amis. Persistence of the mini pivot shift after anatomically placed anterior cruciate ligament reconstruction. *Clinical Orthopaedics and Related Research*, 457:203–209, 2007.

[Lopomo *et al.*, 2010] Nicola Lopomo, Stefano Zaffagnini, Simone Bignozzi, Andrea Visani, and Maurilio Marcacci. Pivot-shift test: Analysis and quantification of knee laxity parameters using a navigation system. *Journal of Orthopaedic Research*, 28(2):164–169, 2010.

[Markolf *et al.*, 2008] Keith L. Markolf, Samuel Park, Steven R. Jackson, and David R. McAllister. Simulated pivot-shift testing with single and double-bundle anterior cruciate

ligament reconstructions. *The Journal of Bone and Joint Surgery. American Volume*, 90(8):1681–1689, 2008.

[Markolf *et al.*, 2010a] Keith L. Markolf, Steven R. Jackson, and David R. McAllister. A comparison of 11 o'clock versus oblique femoral tunnels in the anterior cruciate ligament-reconstructed knee knee kinematics during a simulated pivot test. *The American Journal of Sports Medicine*, 38(5):912–917, 2010.

[Markolf *et al.*, 2010b] Keith L. Markolf, Steven R. Jackson, and David R. McAllister. Relationship between the pivot shift and lachman tests. *The Journal of Bone & Joint Surgery*, 92(11):2067–2075, 2010.

[Matsumoto, 1990] H. Matsumoto. Mechanism of the pivot shift. *Journal of Bone & Joint Surgery, British Volume*, 72-B(5):816–821, 1990.

[Metzger *et al.*, 2010] M. F. Metzger, N. A. Faruk Senan, and O. M. O'Reilly. On Cartesian stiffness matrices in rigid body dynamics: An energetic perspective. *Multibody Syst. Dyn.*, 44(4):441–472, 2010.

[Millett *et al.*, 2002] Peter J. Millett, Andrew A. Willis, and Russell F. Warren. Associated injuries in pediatric and adolescent anterior cruciate ligament tears: Does a delay in treatment increase the risk of meniscal tear? *Arthroscopy: The Journal of Arthroscopic & Related Surgery*, 18(9):955–959, 2002.

[Mohtadi and Grant, 2006] Nick Mohtadi and John Grant. Managing anterior cruciate ligament deficiency in the skeletally immature individual: A systematic review of the literature. [miscellaneous article]. *Journal of Sport Medicine November 2006*, 16(6):457–464, 2006.

[Moksnes *et al.*, 2012] Hvard Moksnes, Lars Engebretsen, and May Arna Risberg. Management of anterior cruciate ligament injuries in skeletally immature individuals. *The Journal of Orthopaedic and Sports Physical Therapy*, 42(3):172–183, 2012.

[Most *et al.*, 2004] E. Most, J. Axe, H. Rubash, and G. Li. Sensitivity of the knee joint kinematics calculation to selection of flexion axes. *Journal of Biomechanics*, 37(11):1743 – 1748, 2004.

[Murray *et al.*, 1994] Richard M. Murray, Zexiang Li, S. Shankar Sastry, and S. Shankara Sastry. *A Mathematical Introduction to Robotic Manipulation*. CRC Press, 1994.

[Musahl *et al.*, 2010a] Volker Musahl, Olufemi R. Ayeni, Musa Citak, James J. Irrgang, Andrew D. Pearle, and Thomas L. Wickiewicz. The influence of bony morphology on the magnitude of the pivot shift. *Knee Surgery, Sports Traumatology, Arthroscopy*, 18(9):1232–1238, 2010.

[Musahl *et al.*, 2010b] Volker Musahl, Musa Citak, Padhraig F. O'Loughlin, Daniel Choi, Asheesh Bedi, and Andrew D. Pearle. The effect of medial versus lateral meniscectomy on the stability of the anterior cruciate ligament-deficient knee. *The American Journal of Sports Medicine*, 38(8):1591–1597, 2010.

[Musahl *et al.*, 2010c] Volker Musahl, James Voos, Padhraig F. O'Loughlin, Volker Stueber, Daniel Kendoff, and Andrew D. Pearle. Mechanized pivot shift test achieves greater accuracy than manual pivot shift test. *Knee Surgery, Sports Traumatology, Arthroscopy*, 18(9):1208–1213, 2010.

[Musahl *et al.*, 2011] Volker Musahl, Asheesh Bedi, Musa Citak, Padhraig O'Loughlin, Daniel Choi, and Andrew D. Pearle. Effect of single-bundle and double-bundle anterior cruciate ligament reconstructions on pivot-shift kinematics in anterior cruciate ligament-

and meniscus-deficient knees. *The American Journal of Sports Medicine*, 39(2):289–295, 2011.

[Musahl *et al.*, 2012a] Volker Musahl, Yuichi Hoshino, Mattias Ahlden, Paulo Araujo, James J. Irrgang, Stefano Zaffagnini, Jon Karlsson, and Freddie H. Fu. The pivot shift: a global user guide. *Knee surgery, sports traumatology, arthroscopy: official journal of the ESSKA*, 20(4):724–731, 2012.

[Musahl *et al.*, 2012b] Volker Musahl, Romain Seil, Stefano Zaffagnini, Scott Tashman, and Jon Karlsson. The role of static and dynamic rotatory laxity testing in evaluating acl injury. *Knee surgery, sports traumatology, arthroscopy: official journal of the ESSKA*, 20(4):603–612, 2012.

[Neuman *et al.*, 2009] P. Neuman, I. Kostogiannis, T. Fridn, H. Roos, L. E. Dahlberg, and M. Englund. Patellofemoral osteoarthritis 15 years after anterior cruciate ligament injury—a prospective cohort study. *Osteoarthritis and cartilage / OARS, Osteoarthritis Research Society*, 17(3):284–290, 2009.

[Noyes *et al.*, 1980] F. R. Noyes, E. S. Grood, D. L. Butler, and M. Malek. Clinical laxity tests and functional stability of the knee: biomechanical concepts. *Clinical Orthopaedics and Related Research*, (146):84–89, 1980.

[Noyes *et al.*, 1991] F. R. Noyes, E. S. Grood, J. F. Cummings, and R. R. Wroble. An analysis of the pivot shift phenomenon. the knee motions and subluxations induced by different examiners. *The American Journal of Sports Medicine*, 19(2):148–155, 1991.

[Obdrzalek *et al.*, 2012] S. Obdrzalek, G. Kurillo, F. Ofli, R. Bajcsy, E. Seto, H. Jimison, and M. Pavel. Accuracy and robustness of kinect pose estimation in the context of coaching

of elderly population. In *2012 Annual International Conference of the IEEE Engineering in Medicine and Biology Society (EMBC)*, pages 1188–1193, 2012.

[Ochiai *et al.*, 2012] Satoshi Ochiai, Tetsuo Hagino, Shinya Senga, Masanori Saito, and Hirotaka Haro. Prospective evaluation of patients with anterior cruciate ligament reconstruction using a patient-based health-related survey: comparison of single-bundle and anatomical double-bundle techniques. *Archives of Orthopaedic and Trauma Surgery*, 132(3):393–398, 2012.

[O'Reilly *et al.*, 2013] Oliver M. O'Reilly, Mark P. Sena, Brian T. Feeley, and Jeffrey C. Lotz. On representations for joint moments using a joint coordinate system. *Journal of Biomechanical Engineering*, 135(11):114504–114504, 2013.

[O'Reilly, 2007] O. M. O'Reilly. The dual Euler basis: constraints, potentials, and Lagrange's equations in rigid body dynamics. *ASME Journal of Applied Mechanics*, 74(2):1–10, 2007.

[O'Reilly, 2008] O. M. O'Reilly. *Intermediate Dynamics for Engineers: A Unified Treatment of Newton-Euler and Lagrangian Mechanics*. Cambridge University Press, Cambridge, 2008.

[Panjabi, 1992] M. M. Panjabi. The stabilizing system of the spine. part i. function, dysfunction, adaptation, and enhancement. *Journal of Spinal Disorders*, 5(4):383–389; discussion 397, 1992.

[Pearle *et al.*, 2009] Andrew D. Pearle, Daniel Kendoff, Volker Musahl, and Russell F. Warren. The pivot-shift phenomenon during computer-assisted anterior cruciate ligament reconstruction. *The Journal of Bone and Joint Surgery. American Volume*, 91 Suppl 1:115–118, 2009.

[Peters *et al.*, 2010] Alana Peters, Brook Galna, Morgan Sangeux, Meg Morris, and Richard Baker. Quantification of soft tissue artifact in lower limb human motion analysis: A systematic review. *Gait & Posture*, 31(1):1–8, 2010.

[Petrigliano *et al.*, 2012] Frank A. Petrigliano, Clayton G. Lane, Eduardo M. Suero, Answorth A. Allen, and Andrew D. Pearle. Posterior cruciate ligament and posterolateral corner deficiency results in a reverse pivot shift. *Clinical Orthopaedics and Related Research*, 470(3):815–823, 2012.

[Reichl *et al.*, 2010] I. Reichl, W. Auzinger, H.-B. Schmiedmayer, and E. Weinmüller. Reconstructing the knee joint mechanism from kinematic data. *Mathematical and Computer Modelling of Dynamical Systems*, 16(5):403–415, 2010.

[Sena *et al.*, 2011] Mark Sena, Dezba Coughlin, Jeffrey Lotz, and Brian Feeley. Quantitative evaluation of rotational knee joint stability using a mechanical pivot shift device. Long Beach, CA, 2011.

[Sena *et al.*, 2013] Mark Sena, James Chen, Ryan Dellamaggiora, Dezba G. Coughlin, Jeffrey C. Lotz, and Brian T. Feeley. Dynamic evaluation of pivot-shift kinematics in physeal-sparing pediatric anterior cruciate ligament reconstruction techniques. *The American Journal of Sports Medicine*, 41(4):826–834, 2013.

[Simmonds, 1994] J. G. Simmonds. *A Brief on Tensor Analysis*. Springer-Verlag, New York, second edition, 1994.

[Sohn and Garrett, 2009] David H. Sohn and William E. Garrett. Transitioning to anatomic anterior cruciate ligament graft placement. *The Journal of Knee Surgery*, 22(2):155–160, 2009.

[Stone and Skubic, 2011] Erik Stone and Marjorie Skubic. Evaluation of an inexpensive depth camera for in-home gait assessment. *J. Ambient Intell. Smart Environ.*, 3(4):349–361, 2011.

[Stonestreet *et al.*, 2012] Matthew J. Stonestreet, Kerwyn C. Jones, Marcus S. Kirkpatrick, Kushal S. Shah, Caroline E. Frampton, Melanie A. Morscher, and John J. Elias. All-epiphyseal ACL reconstruction improves tibiofemoral contact: An in vitro study. *Journal of Pediatric Orthopaedics*, 32(1):15–20, 2012.

[Vavken and Murray, 2013] Patrick Vavken and Martha M. Murray. Acl injury epidemiology. In Martha M. Murray, Patrick Vavken, and Braden Fleming, editors, *The ACL Handbook*, pages 3–17. Springer New York, 2013.

[Vaz *et al.*, 2013] Sharmila Vaz, Torbjrn Falkmer, Anne Elizabeth Passmore, Richard Parsons, and Pantelis Andreou. The case for using the repeatability coefficient when calculating test-retest reliability. *PLoS ONE*, 8(9):e73990, 2013.

[Žefran and Kumar, 2002] M. Žefran and V. Kumar. A geometrical approach to the study of the Cartesian stiffness matrix. *ASME Journal of Mechanical Design*, 124(1):30–38, 2002.

[Wren *et al.*, 2011a] Tishya A. L. Wren, George E. Gorton, Sylvia unpuu, and Carole A. Tucker. Efficacy of clinical gait analysis: A systematic review. *Gait & Posture*, 34(2):149–153, 2011.

[Wren *et al.*, 2011b] Tishya A. L. Wren, Norman Y. Otsuka, Richard E. Bowen, Anthony A. Scaduto, Linda S. Chan, Minya Sheng, Reiko Hara, and Robert M. Kay. Influence of gait analysis on decision-making for lower extremity orthopaedic surgery: Baseline data from a randomized controlled trial. *Gait & Posture*, 34(3):364–369, 2011.

[Yamamoto *et al.*, 2010] Yuji Yamamoto, Yasuyuki Ishibashi, Eiichi Tsuda, Harehiko Tsukada, Shugo Maeda, and Satoshi Toh. Comparison between clinical grading and navigation data of knee laxity in ACL-deficient knees. *BMC Sports Science, Medicine and Rehabilitation*, 2(1):27, 2010.

Publishing Agreement

It is the policy of the University to encourage the distribution of all theses, dissertations, and manuscripts. Copies of all UCSF theses, dissertations, and manuscripts will be routed to the library via the Graduate Division. The library will make all theses, dissertations, and manuscripts accessible to the public and will preserve these to the best of their abilities, in perpetuity.

Please sign the following statement:

I hereby grant permission to the Graduate Division of the University of California, San Francisco to release copies of my thesis, dissertation, or manuscript to the Campus Library to provide access and preservation, in whole or in part, in perpetuity.



Author Signature



Date